To the Graduate Council:

I am submitting herewith a dissertation written by Khaled Meftah entitled "Experimental Study of the Effect of Void Reactivity Feedback on the Behavior of the Scaled Model Boiling Water Reactor". I have examined the final copy of this dissertation for form and content and recommend that it will be accepted in partial fulfillment of the requirements for the degree of Doctor of Philosophy , with a major in Nuclear Engineering.

Dr. A. E. Ruggles, Major Professor

We have read this dissertation
and recommend its acceptance.

Belle R Upadhyaya

Accepted for the council:

Associate Vice Chancellor and
Dean of the Graduate School

EXPERIMENTAL STUDY OF THE EFFECT OF VOID REACTIVITY FEEDBACK ON THE BEHAVIOR OF THE SCALED MODEL BOILING WATER REACTOR

A Dissertation
Presented for the
Doctoral of Philosophy Degree
The University of Tennessee, Knoxville

Khaled Meftah
August 1997

ACKNOWLEDGMENTS

I would like to express my sincere thanks to my advisor, Dr. Arthur. E. Ruggles for his guidance, advice and encouragement during the course of this research. I would also thank my dissertation committee members, Dr. Roger Parsons of Mechanical and Aerospace Engineering, Dr. H. Lee Dodds, and Dr. Belle. R. Upadhyaya of the Nuclear Engineering Department. Many thanks to the Head of the Nuclear Engineering Department, Dr. H. Lee Dodds for his comments and guidance.

Throughout my dissertation study, I was funded by the Tennessee Valley Authority (TVA). I hereby acknowledge the TVA for their invaluable research funding.

In the pursuit of this research, I benefited from technical help of several scientists. In particular Dr. Mounir Laroussi of the Electrical Engineering Department. His comments and suggestions were invaluable in this research. My special thanks also to Dr. Kok of Delft Institute in Netherlands.

In the pursuit of this degree, I benefited from the discussions with my fellow graduate students. In particular, I would like to thank Aucyone A. Dasilva, Ugur Mertyurek, David Kenna, Hanna Moussa, Paulo Brasko, Ali S. Erbay and Karani Gulec.

Finally, I would like to dedicate this work to my late father Abderrahman, who taught me the basics of this life. This work is also dedicated to my mother cherifa Belkhiria, my beautiful wife Amina Abdellatif Zrigue, and my little daughter Fatima Ezzahra.

ABSTRACT

A Scaled Model Boiling Water Reactor (SMBWR) model uses low pressure (i.e., 0.095 MPa) water in a heated channel 0.5 meters in length with four electrically heated fuel simulator rods. The axial void profile in the channel is measured using conductivity probes and the power to the heaters is modulated according to the void fraction to simulate void reactivity feedback. The steam from the heated channel is passed through a valve that reduces the pressure to 0.012 MPa where the steam is condensed in conditions similar to those found in a conventional BWR condenser. The feedwater flow rate, heater power, and instrumentation in the facility are controlled and monitored through a Quadra 950 computer running LabVIEW software. The void fraction signals are analyzed to identify the different flow regimes and determine the vapor velocity in the SMBWR channel using features of the probability density function and power spectral density. The void coefficient of reactivity is modified in the BWR scale model through the LabVIEW interface and the effect on the behavior of the channel is directly observed. The system response is reported for abrupt stepwise pressure changes and abrupt stepwise power changes. The response is typical of that expected for a BWR. The void reactivity feedback effect is also examined by analyzing the frequency response of the channel void fraction at steady state.

TABLE OF CONTENTS

LIST OF TABLES

LIST OF FIGURES

CHAPTER 1

INTRODUCTION

1.1 Motivation for this Study

The design and construction of the Scaled Model Boiling Water Reactor (SMBWR) provides a unique opportunity and a platform to explore BWR stability and two-phase flow characteristics in the boiling water reactor channel. The implementation of a void fraction sensor in the heated channel allows quantitative examination of the two-phase flow behavior in the reactor channel. This type of data is rare for flow boiling situations. Further, the void fraction measurement in the reactor channel is employed to couple the power kinetics with the channel thermalhydraulics via void reactivity feedback. This allows quantitative investigation of the effect of the void reactivity on the boiling channel behavior. The quantitative study of the channel thermalhydraulics in the presence of void-reactivity feedback is an original contribution of this work.

1.2 Statement of the Problem

The objective of this dissertation is to study the two-phase flow characteristics in the heated channel of the SMBWR. These include two-phase regimes and vapor velocity in the reactor channel. This study is accomplished by analyzing the output of several axial void probes. Also, the channel thermalhydraulics is coupled with the heater power via void reactivity feedback. In this part the channel average void fraction is utilized to modulate the power using a simple point kinetic model. The boiling channel behavior is investigated by performing transients with different void reactivity coefficients.

1.3 Contributions of this Work

The following are the original contributions of this work:

1. The study of two-phase flow characteristics is usually conducted in air-water systems with co-current flow. In the present study, void probe sensors are installed in a heated channel which exhibits more complex behavior than that of air-water sections.

2. The experimental investigation of the coupling of the power with the channel thermalhydraulics is accomplished for the first time in a thermalhydraulic loop. This study allows delineation of the main differences between the simple heated channel and that with void reactivity feedback. In this study different coefficients of reactivity are employed in order to see their effects on the system behavior.

3. An improved design of a void fraction sensor that considers the physical features of the Scaled Model Boiling Water Reactor and implements in-situ referencing to single phase liquid conductivity.

CHAPTER 2

LITERATURE REVIEW

2.1 Introduction

The study of two-phase flow instabilities is relevant to the design and operation of many industrial systems such as boiling water reactors, thermosiphon boilers, and various chemical plants. Flow oscillations are undesirable in these systems because they can induce equipment vibration, thermal stress in the heated wall and in the cladding, and also can cause transient burnout [1]. This issue of stability and nonlinear dynamic behavior, especially in boiling water reactors, has drawn a lot of attention after the Lasalle-2 boiling water nuclear reactor underwent a transient from a stable operating point to an oscillatory behavior, which is believed to be the result of the effect of the coupling between the neutron kinetics and thermal hydraulics in the reactor core [2,3].

In general a two-phase flow system is stable if when flow parameters such as pressure or power are perturbed, the new operating condition tends to converge asymptotically to its initial operating point. On the other hand if the perturbation causes the system to diverge from its operating point, the system is said to be unstable. There are static and dynamic flow instabilities, categorized by the nature of the equations required to establish the stability limit [4].

In static instability the perturbed system departs from a stable operating point to a new operating point, which can be either stable or unstable. This type of instability includes flow excursion (Ledinegg instability), and flow regime transition. The stability limits for static instability can be established from examination of the steady (i.e., static) flow equations.

Dynamic instabilities are motivated by the transport times and feedback phenomena that exist in two-phase systems. One of the most common dynamic instabilities is the density-wave oscillation, which arises primarily from the interaction between flow rate, vapor generation and pressure drop [1]. For example, a small reduction in the inlet velocity will induce a reduction in flow resistance first in the single phase liquid region. Later the flow resistance will increase in the two-phase region due to an increase in the vapor generation. The pressure drop in the liquid phase can be out of phase with that of the two-phase region of the system due to fluid transport times, allowing the external pressure boundary condition to be constant in time. Density wave oscillations may diverge or become sustained oscillations, giving rise to so-called limit cycles. In addition to density wave oscillations, a two-phase flow system can experience pressure-drop oscillations, which occur when operating on the negative-slope region of the pressure drop versus mass flow characteristic [5]. Finally, the coupling between neutronics and channel thermal hydraulics can cause oscillatory behavior due to feedback between reactivity, power and steam volume in the core.

2.2 Thermalhydraulic Stability in the Boiling Water Reactor

Studies of the fuel cooling channel thermalhydraulics in boiling water reactors is usually conducted through investigation of the dynamic behavior of single and parallel heated channels, which are known to have rich nonlinear dynamics [3]. These experimental and numerical studies have been carried out over the past fifty years. Density wave oscillations, pressure-drop oscillations, Ledinegg instabilities and acoustic instabilities all have been investigated [4]. Recently, Whitfield and Roy [6] have experimentally studied dynamic instability in a rod-bundle at low mass flow rates. They have shown that the system exhibits quasi periodic oscillations. Experimental stability tests were also performed by Van Der Hagen [7] on the Dodewaard reactor in the Netherlands. In the Doodeward reactor three different types of stability were investigated. These include reactor kinetic stability, thermalhydraulic stability and total plant stability. The reactor-kinetic stability is caused by the interaction of neutron dynamics and the thermalhydraulic feedback mechanism. The thermalhydraulic stability deals with two-phase flow dynamics in the heated channel. Next, the total plant stability is induced by the reactor response to pressure changes caused by the movement of the control valve. Furthermore, Rizwan-uddin and Dorning [8], have numerically shown that by imposing different pressure boundary conditions on the heated channel, the system exhibits different types of nonlinear dynamic behavior. For the constant pressure boundary condition, which corresponds to a constant inlet mass flow rate, the heated loop experiences a Hopf bifurcation and it departs from a stable fixed operating point to a stable limit cycle. On the other hand, for periodic pump oscillations, Rizwan-uddin and Dorning observed that depending on the oscillation frequency, the system can evolve to either a stable N-limit cycle or to aperiodic behavior. In addition, frequency domain analysis has been utilized in studying the system stability around fixed operating points. This has resulted in developing marginal stable boundaries, MSB, which divide the multidimensional parameter space into stable and unstable regions.

2.3 Effect of Neutronics on the Channel Stability

The coupling between neutronics and channel thermalhydraulics is known to have an important effect on the stability of boiling water reactors. This type of instability is called global instability and it arises primarily from the dependence of the reactor power on the moderator (i.e., liquid fraction) in the core. This instability was demonstrated by March-Leuba [9] in his reduced nonlinear model, which consists of the point kinetics equations, fuel equation and a second order linear differential equation that relates the void reactivity with the reactor power. The void reactivity equation is derived by linearizing the energy and continuity equations, respectively. Even though the nonlinear terms existed only in the point kinetics equations, the reduced model presented the main stability features in the boiling water reactor. By varying the feedback gain, the system behavior shifts from a stable to an oscillatory stable system. By further increasing the feedback gain, the system experiences a cascade of period doubling which leads to chaotic behavior.

The effect of neutron kinetics on the channel thermalhydraulic stability was also investigated by Bergdhal et al. [10], who studied the stability of the Forsmark boiling water reactor during start up operation. This system has exhibited a power oscillation during high power and low flow conditions that occur during start-up. In their analysis, Bergdall et al. found that the system oscillations were mainly due to the dynamic coupling between neutronics and thermalhydraulics via void reactivity feedback. Next, Podowski [1] stressed the importance of the coupling between the channel thermalhydraulics and neutronics in terms of varying the coefficients of reactivity. For example, if the magnitude of the coefficient of reactivity becomes too large in the negative side, the system may experience self sustained oscillations as observed in the stability tests performed on the CAORSO (Italy) boiling water reactor. Rizwan uddin and Dorning [3] have numerically investigated the effect of neutron kinetics on core stability. In their analysis, Rizwan-uddin and Dorning found that the dynamics is similar to those exhibited by isolated channels. This was manifested by Hopf bifurcations from a stable fixed point to stable limit cycles.

2.4 Importance of Void Fraction Measurement

The coupling between the channel thermalhydraulics and the power kinetics in the Scaled Boiling Water Reactor via void reactivity feedback requires knowledge of the channel void fraction. This measurement provides useful information about the behavior of the two-phase flow characteristics in the boiling channel. In a commercial boiling water reactor core, the measurement of void fraction is very difficult due to the complexity of the internal structure and the operating environment.

Several techniques are currently employed to measure void fraction. These include photon, neutron or gamma radiation absorption methods, quick closing valves, optical and impedance methods [11]. All these methods exploit differences in the thermo-physical properties of the liquid and the vapor phase. The selection of any particular method depends on the particular application. For example, the quick closing valve method is best suited for volumetric measurement in adiabatic flows, whereas the impedance and the radiative techniques are best suited for chordal and local measurements in heated or adiabatic flow.

Void fraction measurement can provide useful information on the channel thermalhydraulic behavior. Recently, Whitfield and Roy [7] utilized the impedance techniques to measure the local vapor fraction of freon in their scaled model. This measurement was used to determine the void fraction distribution in the channel. Void fraction was also measured in an air-water system by Micaelli and Tournaire [12,13] to study void wave propagation at low void fraction (< 40%). In their studies the impedance method was employed. Tournaire has compared the performance of a two-electrode sensor with that of a six-electrode sensor, which uses a rotating electrical field to measure the axial void fraction. Tournaire found that a two-electrode sensor is more sensitive to void distribution than that of a sensor with six electrodes. In the Netherlands, Kok [14] studied the feasibility of using the capacitive measurement technique for void fraction measurement in freon in a rod bundle geometry. The technique, used by Kok to measure void fraction, was originally developed by Hereens [15] for measuring very small distance variations in air. Kok has validated the sensor performance using an air-oil test section. The oil was used here because it has a dielectric constant comparable with that of freon-12, used as the working fluid in the Dodewaard scale model. In Kok's study, however, there is still a question of how this capacitance technique can be implemented in the scaled model where metal heater structure can greatly increase the parasitic effects acting on the capacitance measurement. Van Der Hagen [8] has also measured void fraction in the Dodewaard reactor to determine the in-core coolant velocity used to study the reactor stability. In this study neutron gamma detectors were utilized to measure void fraction in the reactor channel. The void velocity was determined using the cross correlation function, auto- and cross-power spectral density. These signal processing techniques were tested by Van Der Hagen in an air water test loop. In this loop ultra violet light sources were used to excite a fluorescent powder, dissolved in the water, to emit visible light, which is captured by photo-transistor sensor. This sensor was designed to model the neutron gamma detector.

CHAPTER 3

EXPERIMENTAL APPARATUS AND PROCEDURE

This chapter discusses the experimental apparatus and procedure used in the present investigation. A description of the Scaled Model Boiling Water Reactor (SMBWR) is presented. The instrumentation and data acquisition system is explained. Different void fraction measurement techniques are outlined and each technique is reviewed in terms of application and limitation. The theory of the impedance technique used in this work to measure void fraction is described and the design criterion and calibration of the void fraction sensor are discussed.

3.1 Description of the Scaled Model Boiling Water Reactor

The Scaled Model Boiling Water Reactor (SMBWR) is sponsored by the Tennessee Valley Authority (TVA) to provide practical training for nuclear engineering students and reactor operators in the function and operation of conventional boiling water reactors. In the early stage of this project, a conceptual design [16] was developed and reviewed by a steering committee in order to verify the model met the objectives of the sponsor and the department.

The scaling analysis of the boiling water reactor model suggested that the best working fluid is a refrigerant (HCFC123). However, because of the concern over safety, regulations and expense, this choice was abandoned and water was chosen as the working fluid for the model. The scaled model provides flow visualization in the reactor core, steam separator and condenser. This is accomplished by the extensive usage of clear pressure boundaries or pressure boundaries fitted with windows. Further, this model incorporates void reactivity feedback, which is an important characteristic of a boiling water reactor. The channel average void fraction is measured with conductivity probes and coupled with the power via a simple power kinetic model. This allows the SMBWR to be used as a research tool to investigate system stability issues that arise from the coupling between neutronics and channel thermalhydraulics in Boiling Water Reactors. The model design parameters are presented in Table 3.1. In addition, the model details and construction design features are further discussed by Kenna [17].

The Scaled Model Boiling Water Reactor, shown in Figure 3.1, is composed of a boiling channel, steam separator, manual control valve, condenser and a feed water pump. Figure 3.2 shows a picture of the reactor model.

The boiling channel is made of 7740-Pyrex glass with an outer diameter of 50 mm, an inside diameter of 46 mm and a length of 508

Table 3.1 : Design Core Parameters of the Scaled Model Boiling Water Reactor

Parameter	Value
Channel diameter (mm)	45.97
Heater diameter (mm)	8.00
Pitch distance (mm)	6.35
Channel height (mm)	457.20
Upper plenum diameter (mm)	60.96
Heater height (mm)	419.10
Number of heaters	4
Nominal power (kW)	0.75
Operating pressure (MPa)	0.095
Feed water Flow rate (kg/s)	3.16E-4
Feed water inlet temperature (^{o}C)	90.0
Feed water outlet temperature (^{o}C)	100.0
Total channel flow rate (kg/s)	3.16E-2
Heat Flux (kW/m2)	70.8

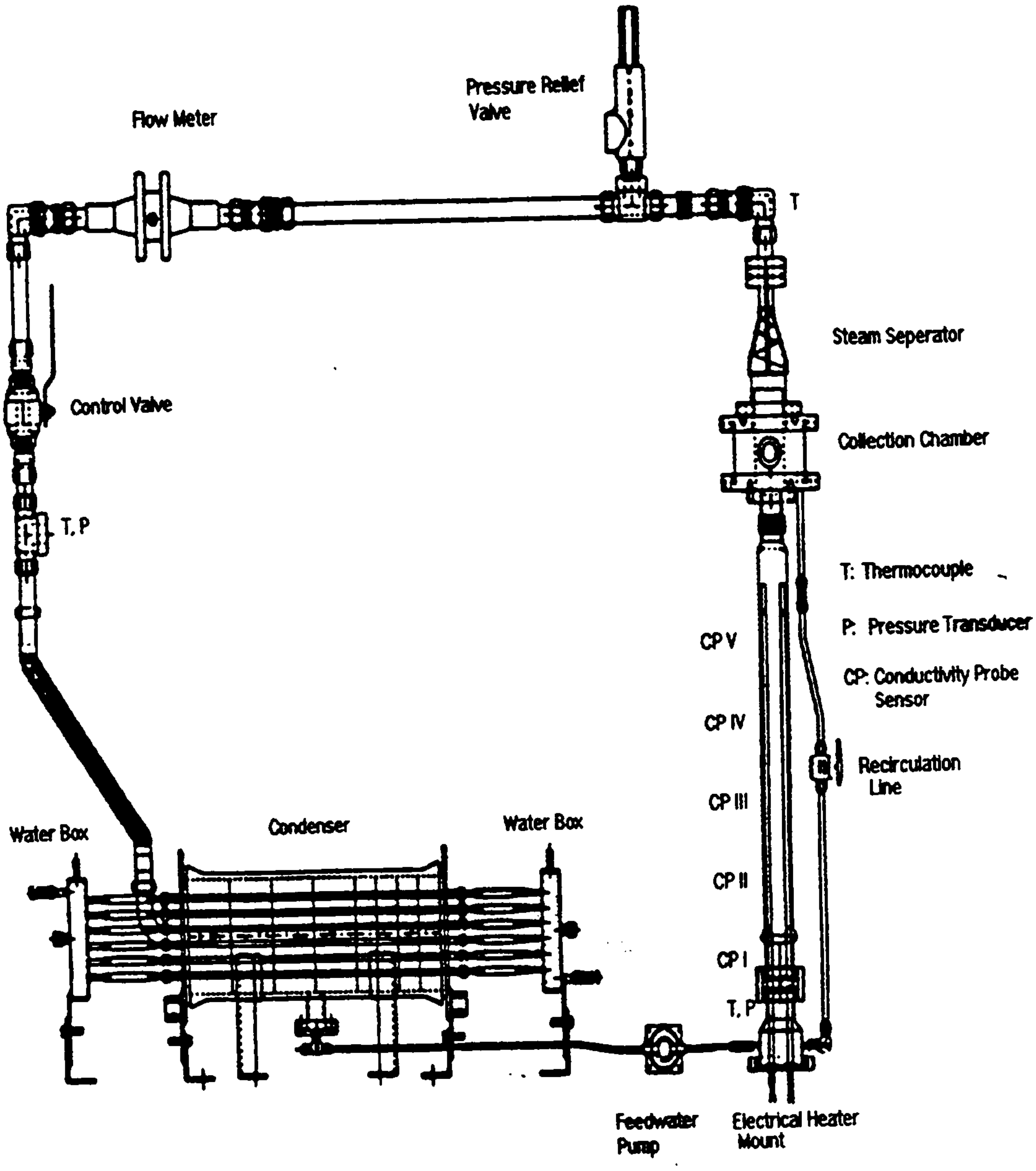

Figure 3.1: General Schematic of the Scaled Model Boiling Water Reactor Facility.

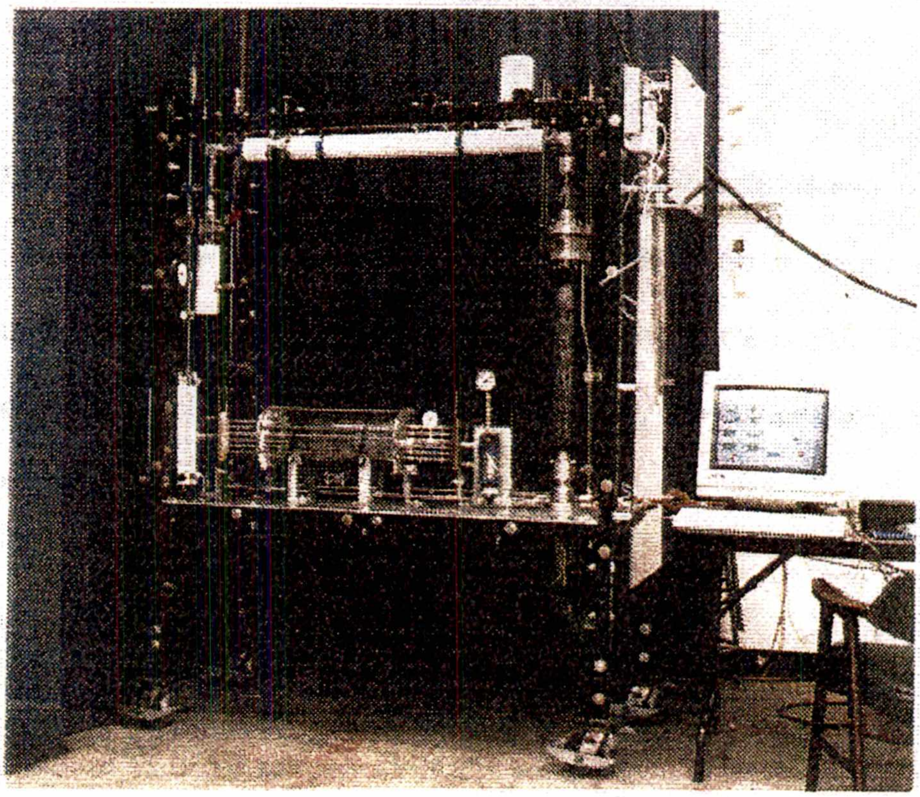

Figure 3.2: Picture of the SMBWR Facility

mm. The Pyrex glass allows visualization of the two-phase flow. The glass channel houses four electrical heaters, arranged in a square lattice with a pitch distance of 6.35 mm. Each heater has an approximate length of 419 mm and a diameter of 8 mm. The heater sheath is constructed from incoloy and it is filled with magnesium oxide insulation. The position of the heaters is maintained using two stainless steel spacers, which are also utilized to support the void probes in the channel.

The steam-water mixture generated in the boiling channel passes through a steam separator. The separated liquid is collected in the upper plenum and recirculated to the lower plenum through a recirculation line. After exiting the steam separator the vapor mass flow is measured by an orifice flow meter. A manual control valve is employed to drop the steam pressure from the nominal 0.095 MPa to the condenser inlet pressure of 0.013 MPa. The condensate water is fed to the boiling channel through a positive displacement feed water pump that also measures the feedwater flow.

3.2 Instrumentation and Data Acquisition System

The SMBWR has 15 sensors, used for system operation and control. These sensors are composed of thermocouples (5), pressure transducers (5) and void fraction sensors (5). Table 3.2 gives a list of the different sensors employed in the SMBWR. Next, the power and the feedwater flow rate are controlled using output signals generated

Table 3.2 : Listing of the Input and Output Signals of the SMBWR Facility

Input Signals
1. Core inlet water temperature
2. Core inlet Water Pressure
3. Vapor core outlet temperature
4. Up stream vapor pressure
5. Down stream vapor pressure
6. Condenser inlet vapor temperature
7. Condenser inlet vapor pressure
8. Condenser inlet water temperature
9. Condenser inlet water pressure
10. Condenser outlet water temperature
11. Condenser outlet water pressure
12. Vapor fraction (five sensors)
Output Signals
1. Heater power
2. Inlet water flow rate

from the data acquisition board MIO-16L, which has 14 input channels and two output channels. The data acquisition board has a processing frequency of 100 KHz. For signals that need conditioning because of low voltage values and their sensitivity to noise (e.g., thermocouples), analog conditioning modules are employed. These modules increase the gain of the signal and reduce the noise. The connector block (CB-50 series) is employed to log the signals which do not need conditioning directly to the data acquisition board, which digitizes these signals and passes them for further processing to the LabIEW program. Figure 3.3 shows a general schematic of the data acquisition system.

3.2.1 Description of the LabVIEW Program

LabVIEW is a general development program, which serves the same purpose as other development program systems such as FORTRAN and BASIC. LabVIEW [18] uses a graphical programming language, G, to develop programs. This is in contrast to other programming systems which utilize text-based language to create lines of code. LabVIEW has extensive libraries of functions, which are suitable for data acquisition, instrument controls, data analysis, storage and presentation. In LabVIEW, each program is called a virtual instrument because it simulates and imitates actual operating instruments. The steps in the development of any virtual instrument (VI) follow.

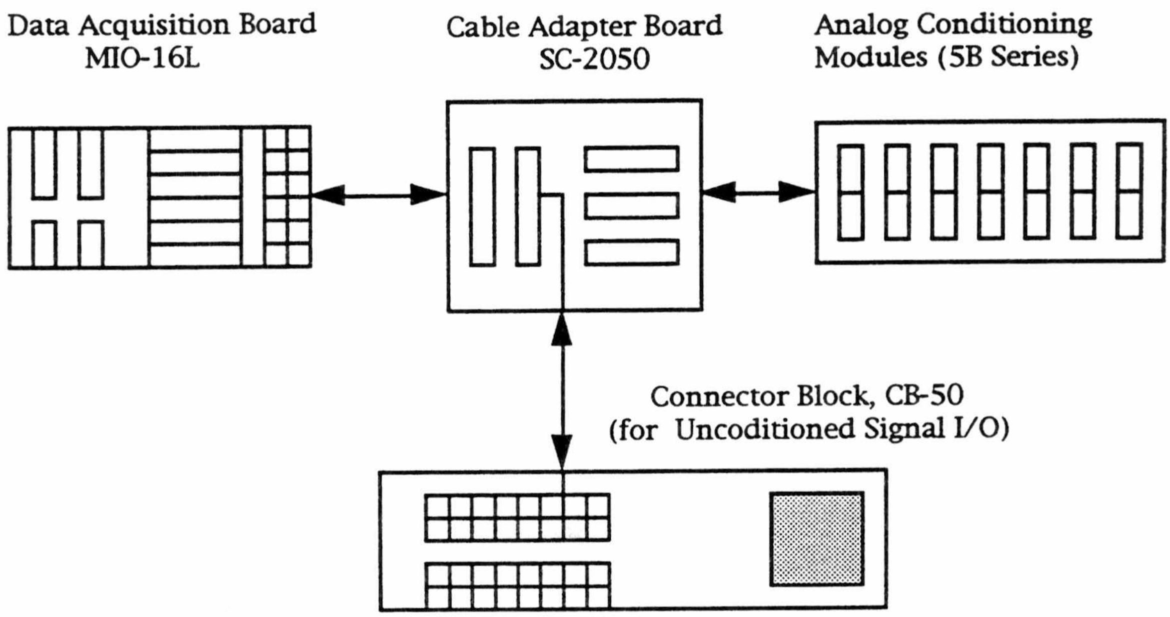

Figure 3.3: General Schematic of the Data Acquisition System

3.2.1.1 Front Panel

The user interface is called the front panel where one can develop the virtual instrument using Knobs, push buttons, wave form graphs and other instrument controls, which simulate the real instrument. Figure 3.4 shows a simple front panel, used to read temperature. This front panel is constructed by selecting controls and indicators from the Control menu in the front panel. In addition, the front panel can set the initial conditions and passes data to the simulated instrument.

3.2.1.2 Block Diagram

The constructed VI in the front panel receives instructions from the block diagram which is developed using the graphical language (G). The block diagram is analogous to source code for the VI. Figure 3.5 shows the block diagram of the front panel shown in Figure 3.4. The block diagram is constructed by wiring objects together to send or receive data and also to perform specific functions.

The VI Programs are hierarchical and a VI can be used as a subVI in another VI. These sub VIs can be executed independently from the main VI, which makes debugging easier. The sub VI corresponds to the so-called subroutines in standard programming languages (C or BASIC).

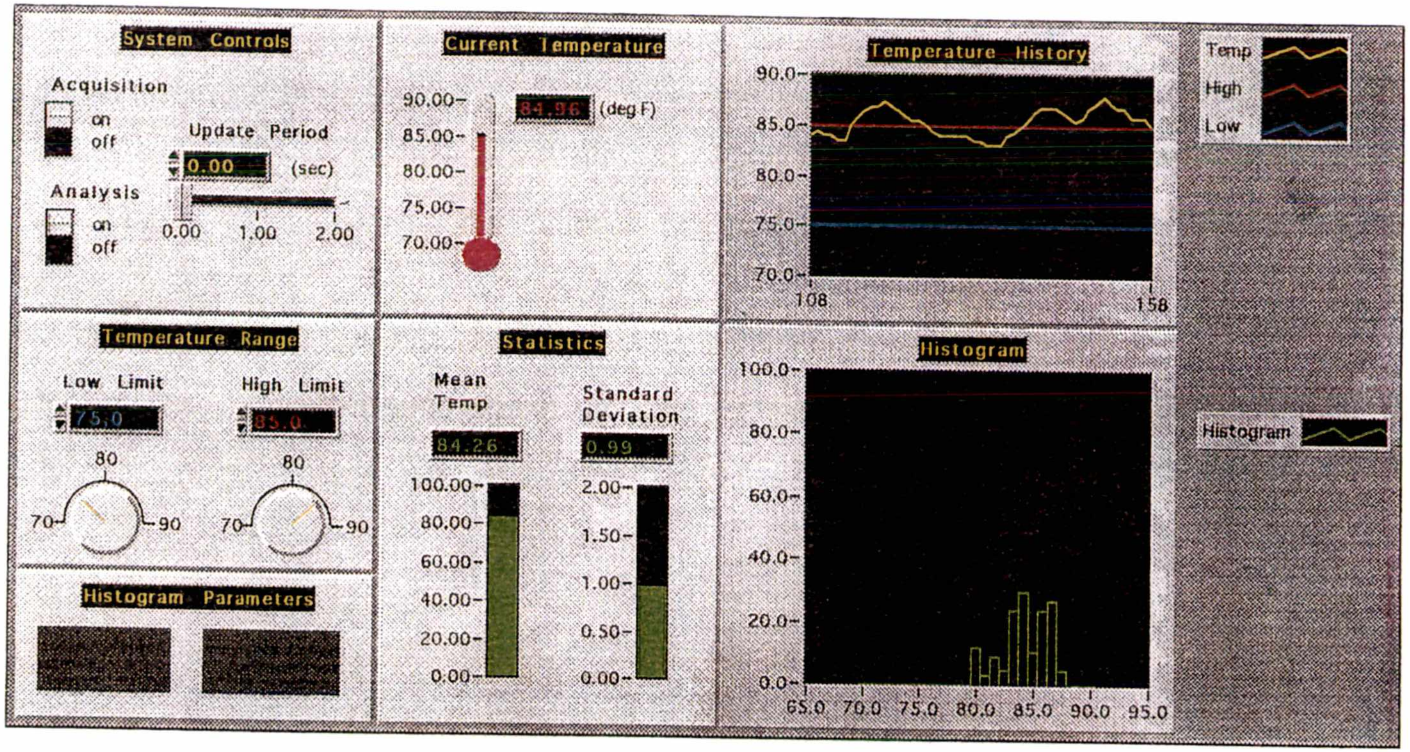

Figure 3.4: LabVIEW Front Panel for a Temperature Reading Instrument [18].

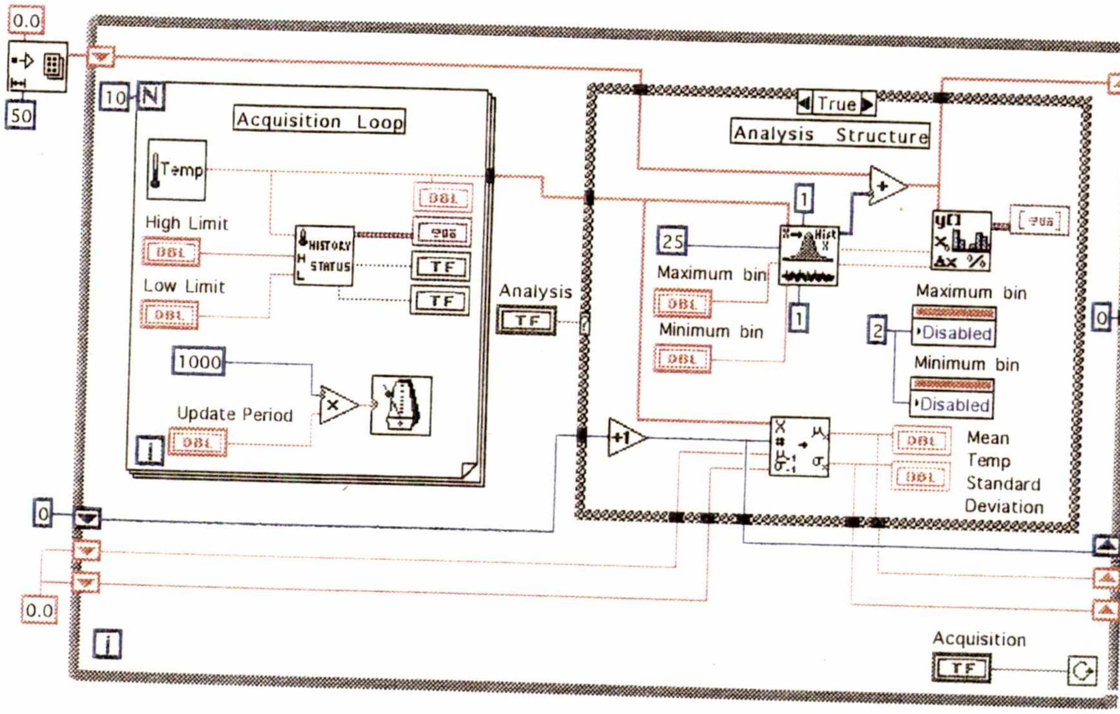

Figure 3.5: LabVIEW Block Diagram for a Temperature Reading Instrument [18].

3.2.2 High-Speed Camera

A Hycam model K2004E-115 16 mm motion picture camera is employed to observe the two-phase flow characteristics in the heated boiling channel and to determine the flow regime and the void velocity in SMBWR. When the camera is used, data are collected simultaneously using the LabVIEW program. This allows for data correlation with the filming event.

3.3 Void Fraction Measurement Techniques

There are different techniques to measure vapor fraction, which is defined as the ratio of the vapor volume to the total volume of the two phase flow system. These techniques include volumetric, electrical, optical and radiative measurements, whose suitability depends on the particular application [19].

3.3.1 Quick Closing Valve Method

This method is used for sensor calibration and it consists of valves at the beginning and at the end of the test section. During a test run, the two valves are closed simultaneously to trap the liquid and vapor or gas in the channel. Then the liquid is drained and measured. This allows the channel average void fraction to be determined when the total volume of the channel is known.

3.3.2 Radiative Techniques

A beam of gamma rays or X-rays is attenuated by passing through a certain material. In a two-phase flow system, The absorption takes place in the liquid phase. This absorption is measured by passing a collimated beam of gamma or X-rays with intensity I_0 through the channel. The attenuated beam is then described by an exponential decay law of the form:

$$I = I_o \exp(-\mu d) \tag{3.1}$$

Where, μ is the linear attenuation coefficient and d is the distance traveled through the two-phase region. The radiative method gives an axial measurement of the void fraction. The main problem with this method is related to safety and regulation issues. In addition, this method is bounded by the statistical nature of the radioactive decay of the element that has created the Gamma rays and these effects may limit the frequency response [14,19].

3.3.3 Acoustic Method

Since the speed of sound varies differently in the liquid and vapor phase, The vapor fraction can be measured through the variation of the sound speed. The void distribution in the channel greatly effects this type of measurement. In addition, the internal structure of the boiling channel (e.g. fuel rods) can complicate the measurement.

3.3.4 Impedance Method

The impedance method is widely used in measuring void fraction because of its simplicity, fast response, and its low cost. The impedance method uses the difference in electrical properties of liquid and water vapor. Vapor fraction can be measured either through the dielectric or the resistivity of the two phase media. In general, for a non-electrolytic liquid such as freon, the method of capacitance is utilized to determine the dielectric of the two-phase flow, whereas in a conductive liquid such as water, it is preferred to determine the resistivity of the two-phase media [20]. There are some difficulties that need to be addressed in order to produce a reliable measurement. For example, the void distribution, electrode geometry, operating frequency and liquid temperature can greatly influence the measurement results. These factors are discussed in the next sections. In this work, the impedance method is adopted and implemented to measure the channel void fraction.

3.4 Theory of Operation of the Impedance Method

For a two-phase flow medium, placed between two electrode plates and subjected to a potential voltage (Figure 3.6.a), the

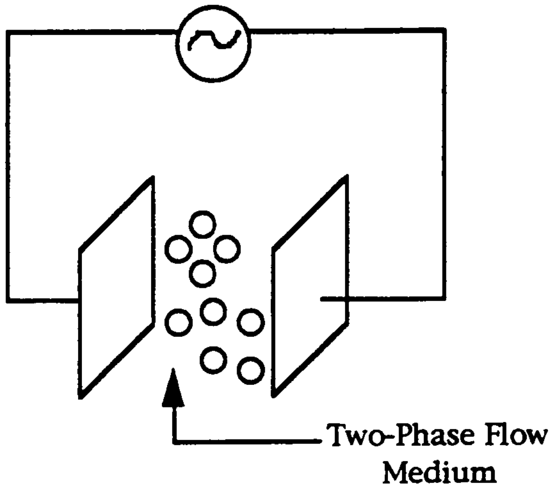

(a)

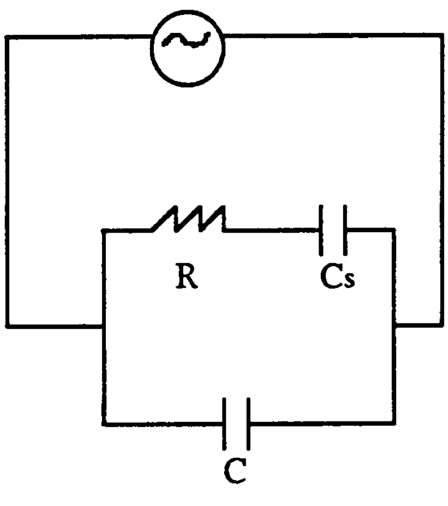

(b)

Figure 3.6: Void Fraction Measurement Using the Impedance Technique: (a) Two-Phase Flow Medium; (b) Electrical Representation of the Flow Field

equivalent impedance can be represented by a resistance R in series with capacitance C and in parallel with C_s, as can be seen in Figure 3.6.b. Thus, the equivalent impedance can be written as [12]:

$$Z = \left\{ \frac{1}{R + \frac{1}{i\omega C_s}} + i\omega C \right\}^{-1} \tag{3.2}$$

where R can be defined as the fluid resistivity, C_s is the capacitance caused by molecular polarization near the electrode plate; and C is the fluid capacitance. The fluid resistivity, R, can be written as:

$$R = \frac{d}{K \times B} \tag{3.3}$$

Where, B is the electrode area, d is the distance between the electrodes and K is the fluid conductivity. In addition, the fluid capacitance can be written in terms of the fluid dielectric constant as:

$$C = \frac{\varepsilon \times B}{d} \tag{3.4}$$

where ε is the dielectric constant of the fluid. Equation 3.2 indicates that the resistivity or the capacitance of the fluid can be determined for a known frequency. For a conductivity measurement, Z=R, it is necessary to have the following condition :

$$R << \frac{1}{2\pi f C} \quad \text{and} \quad R >> \frac{1}{2\pi f C_s} \tag{3.5}$$

Michaelli [12] has found that for resistivity measurement, the operating frequency should be in the range of :

$$2 \times 10^3 \leq f \leq 7 \times 10^6 \text{ Hz} \tag{3.6}$$

For high operating frequency, f, one can neglect the conductivity effect and determine the capacitance (dielectric constant) of the two-phase flow medium. However, there are many difficulties associated with the application of the capacitance method which requires a proper cable shielding because of the effect of the parasitic capacitances resulting from the connecting cables between the sensor probes, measuring instrument, and the metallic structure of the flow channel which is characterized by a very complex structure. Therefore, the capacitance effect is eliminated by operating at a low frequency and the resistivity of the two-phase flow media is determined.

3.4.1 Factors Affecting The Void Fraction Measurement

Four different factors influencing the void measurement are discussed in this section with their importance to the implementation of the void sensor in SMBWR.

3.4.1.1 Operating Frequency

The sensor operating frequency is important to the void fraction measurement. In this study the conductivity method is preferred over the capacitance method. Therefore, the operating frequency was set to 10 KHz, which is low enough to eliminate the capacitance effect [12].

3.4.1.2 Operating Temperature of the Fluid

The increase of the water temperature changes the conductivity and ionization levels. Figure 3.7 shows how water temperature varies with the ionization and conductivity of the liquid [21]. Therefore, it is necessary to place a reference probe in the liquid region in order to monitor these changes and adjust the calibration curve *in-situ*.

3.4.1.3 Void Distribution

The void distribution in the boiling channel can influence the measurement because of the electrical representation of the flow regimes which can have different flow patterns such as bubbly, churn, slug and annular. For coaxial electrodes it was found that a slug regime can be electrically represented by two phases (resistances) in parallel. Similarly, the annular regime can be represented as two phases in series [22]. In addition, there are

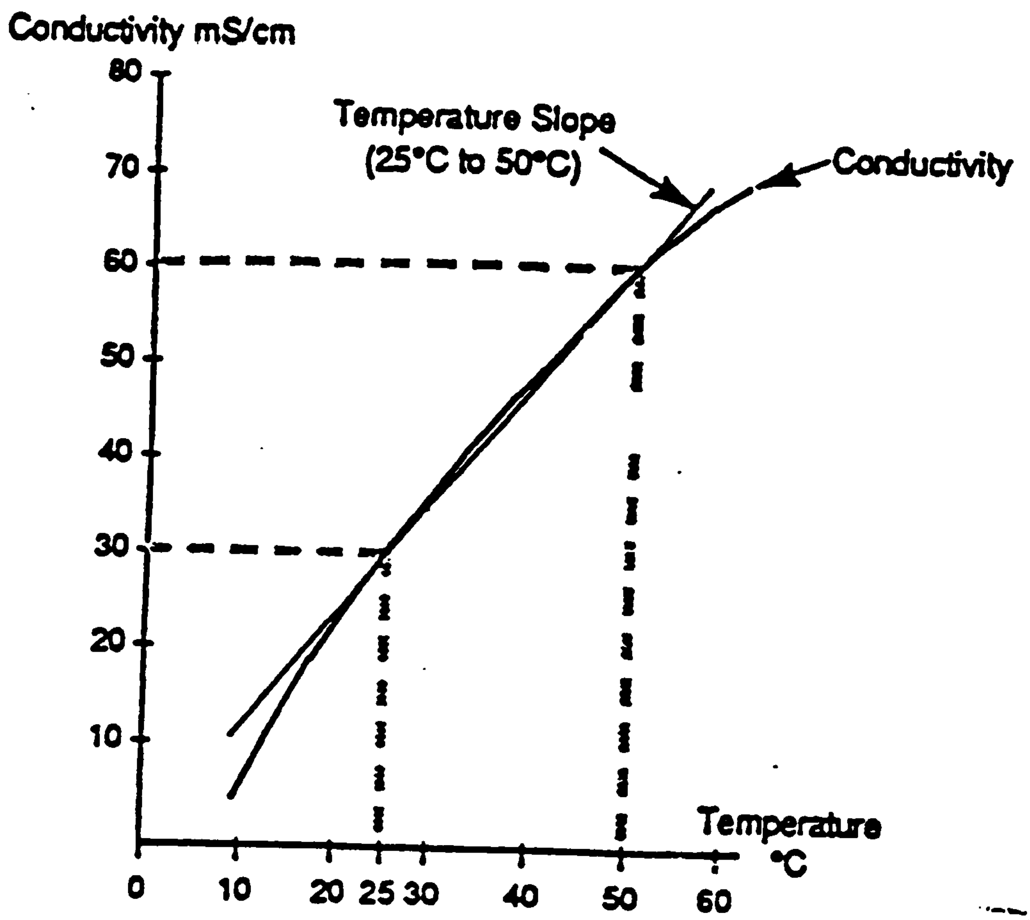

Figure 3.7 : Effect of Temperature on the Water Conductivity [21]

several studies [13] of the bubbly regime. These have included the effect of the bubbles' distributions and geometry on the relative resistance of the medium. The first of these studies was carried out by Maxwell [23] who investigated the conductivity effect of small spherical bubbles in an electrical infinite homogenous medium, in which no interactions between bubbles occur. In his study Maxwell found out that the void fraction can be related to the relative admittance of the medium by:

$$\frac{K_\alpha - K_L}{K_\alpha + 2K_L} = \alpha \frac{K_G - K_L}{K_G + 2K_L} \tag{3.7}$$

where K_L is the liquid phase conductivity, K_G is the vapor phase conductivity, K_α is the two-phase conductivity and α is the void fraction. This formula, however is valid only for a low void fraction region(< 20%). In another study, Burgemann [24] investigated the effect of spherical bubbles with different geometry and distributions. In this study, Burgemann found that the relative conductivity of the media can be related to the void fraction by :

$$\left[\frac{K_G - K_\alpha}{K_G - K_L}\right]\left[\frac{K_L}{K_\alpha}\right]^{1/3} = 1 - \alpha \tag{3.8}$$

For interacting bubbles, Jeffrey[25] has used a probabilistic approach to take into account the possibility of a bubble interacting with its neighbor. This has resulted in the following relation between K/K_L and α:

$$\frac{K_\alpha - K_L}{K_\alpha + u} = \alpha \frac{K_G - K_L}{K_G + u} \tag{3.9}$$

where u is a function of the shape and distribution of the bubbles in the two phase region.

3.5 Design Specifications and Calibration of the Void Fraction Sensor

This section discusses the design criteria for the void fraction sensor. The electronic circuit of the sensor is described. The calibration of the sensor in an air-water test section whose structure resembles that of the SMBWR is given and the implementation of the void sensor in the actual boiling reactor model is presented.

3.5.1 Design Criterion of the Void Fraction Sensor

The design of the conductivity sensor depends on the application and there are several criterion that should be considered. First, The conductivity sensor should be placed in a way that will not disturb the flow field, which can result in the distortion of the void distribution along the boiling channel. Second, the channel structure, especially the heaters, should not interfere with the electrical potential field established between the plates of the sensor. Third, the response of the sensor should be fast enough to allow realistic reactivity feedback simulation.

3.5.2 Description of the Void Sensor

3.5.2.1 Description of the Electronic Circuit

The electronic circuit, used to process the resistance signal is based on the work of Michaelli and Tournaire [12,13], who studied the wave propagation of void and pressure in an air-water test section. Figure 3.8 shows a general schematic of the circuit, which is composed of four different stages. In the first stage, the sinusoidal signal input from the signal generator (4 V peak to peak) is modulated by the void fraction fluctuation and then converted from a voltage to conductance value. Next, this signal is rectified and demodulated in stages 3 and 4, respectively. In the last stage, The void signal is passed through a low pass-filter of 40 Hz to cut high frequency noise such as that of the power controller. Further processing of the signal is done using Lab-View according to the particular application, which is discussed later.

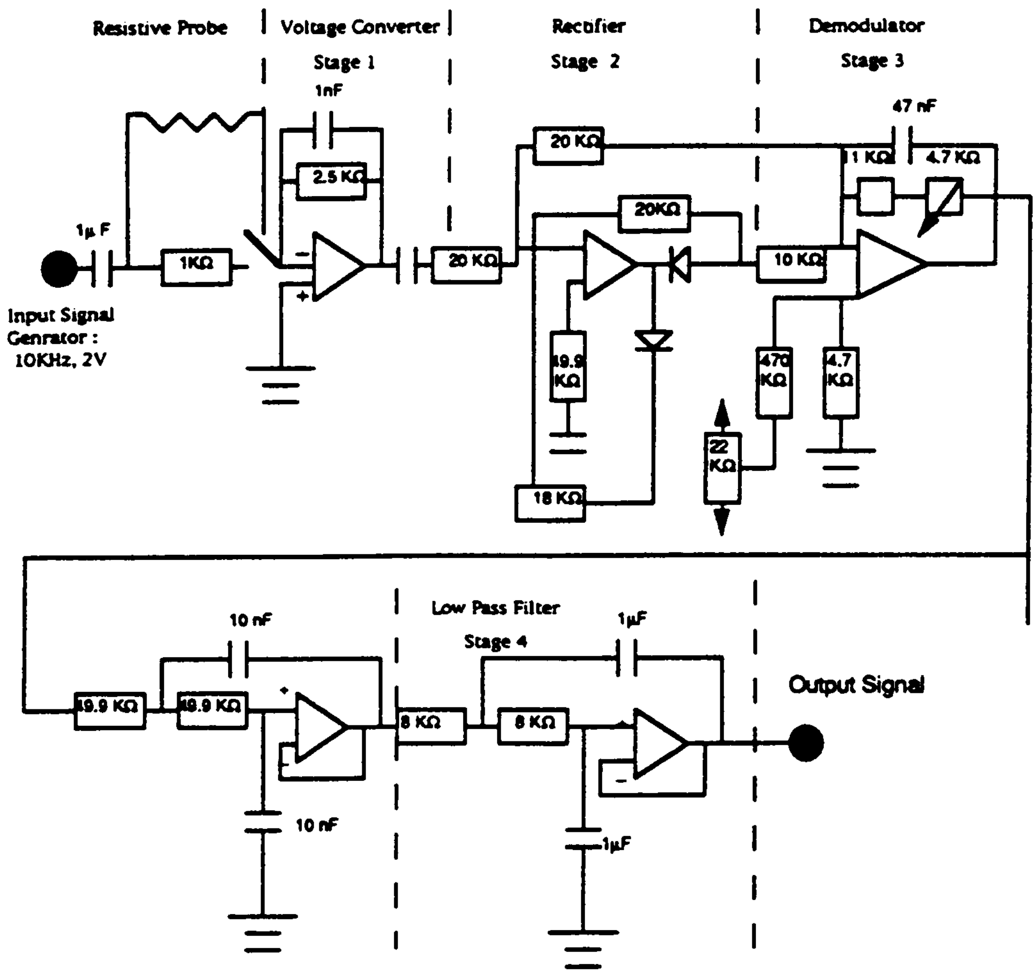

Figure 3.8 : General Schematic of the Sensor Electronics.

3.5.2.3 Electrode Plates

Each conductivity probe consists of two parallel stainless steel plates 20 mm in length and 10 mm in width; separated by a distance of 20 mm. In the boiling channel there are 5 probes, positioned at 5 axial positions. The lowest probe is used as reference probe and it is placed in the liquid phase in order to monitor the changes in the liquid temperature and ionization levels. The conductivity probes are installed along a Teflon strip in order to provide insulation from the heaters. The outer sheath of the heaters are grounded to help confine the electrical field between the probes.

3.5.3 Calibration of the Void Fraction Sensor

Before implementing the void fraction sensor in the SMBWR, the void sensor is tested and validated using a simple air-water test section, which has the same geometry and materials as that of the SMBWR. In addition, the air-water section allows study of the effect of the initial conductivity on the void fraction measurement.

3.5.3.1 Description of the Air Water Section

The air-water test section is constructed to test the void fraction sensor and to obtain a reliable calibration curve, which is used to determine the void fraction in the boiling water reactor channel. The test section consists of a Plexiglas cylinder with four internal rods to simulate the presence of the heaters. Each probe consists of two parallel plates installed along a Teflon strip. There are three sensors installed in the channel. Figure 3.9 shows a simple schematic of the air-water test section.

The variation of the void fraction in the channel is measured using an inverted manometer, which is basically an inverted U tube, connected to the test section through two ports, placed in the water channel separated by vertical distance H_p, as seen in Figure 3.9. When there is no air injection in the water channel, the water column in the inverted U tube is at the same level on both sides. The height difference in the inverted U tube is proportional to the void fraction between the probes in the water channel when the liquid flow rate is near zero. This relation can be determined by establishing a pressure balance using a simple schematic of the inverted manometer system, shown in Figure 3.10. Therefore, at level A the pressure balance can be written as:

$$p_1 + (z_2 - z_1)g\rho_w + (z_4 - z_2)g\rho_w = p_2 + (z_3 - z_2)g\rho_w + (z_4 - z_3)g\rho_a \quad (3.10)$$

Where $\rho's$ and $z's$ are the densities and the distances, defined in Figure 3.10. Equation 3.10 can be rearranged as:

$$p_1 - p_2 = g(z_4 - z_3)(\rho_w - \rho_a) + g\rho_c(z_2 - z_1) \quad (3.11)$$

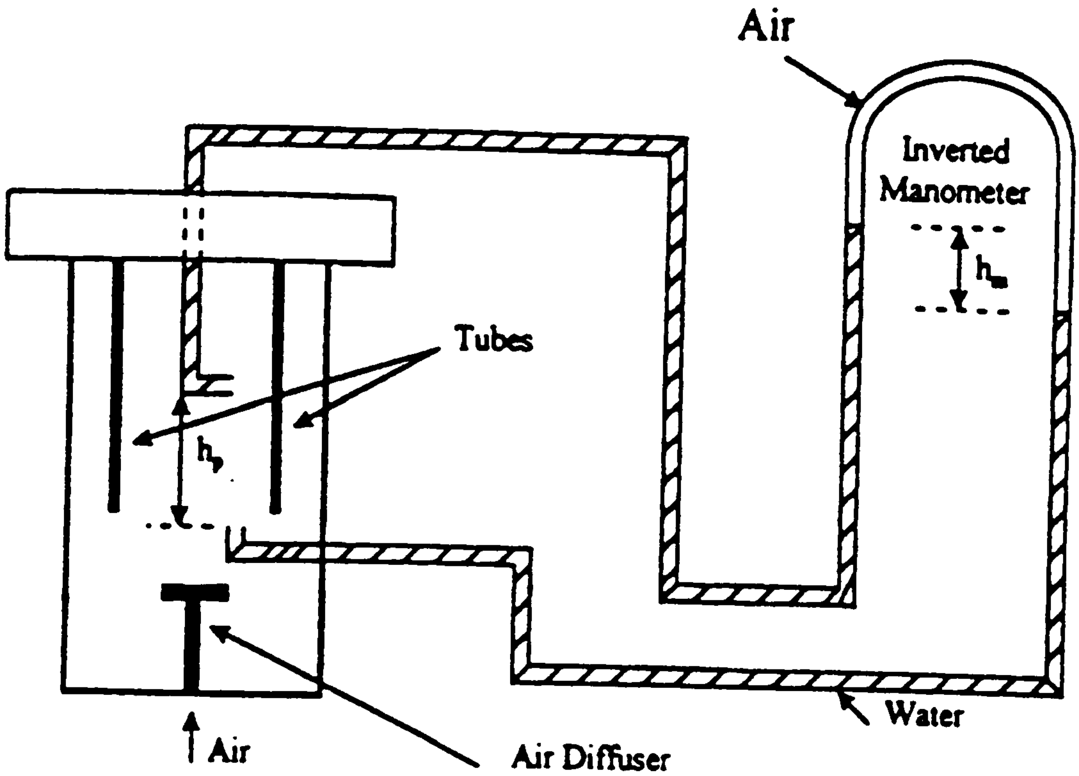

Figure 3.9: Simple Schematic of the Air-Water Test Section

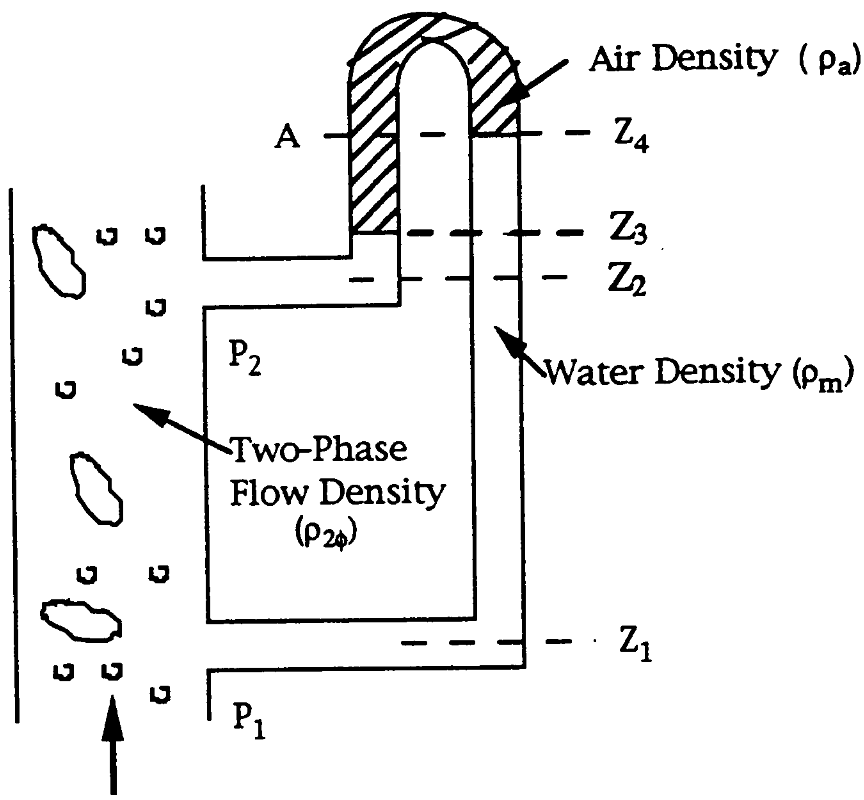

Figure 3.10: Simple Schematic of the Inverted Manometer

Next, the pressure difference between the two pressure ports is written in terms of the two-phase flow density as:

$$p_1 - p_2 = g\rho_{2\Phi}(z_2 - z_1) \tag{3.12}$$

where $\rho_{2\Phi}$ is the two-phase flow density and can be written in terms of the void fraction, α, as:

$$\rho_{2\phi} = \alpha\rho_a + (1-\alpha)\rho_w \tag{3.13}$$

By equating Equation 3.11 and 3.12 one can obtain the following relation accepting that $\rho_a << \rho_w$ for the conditions of interest here:

$$\alpha = \frac{z_4 - z_3}{z_2 - z_1} = \frac{H_m}{H_p} \tag{3.14}$$

Where H_m and H_p are defined in Figure 3.9.

3.5.3.2 Experimental Procedures and Analysis

By introducing air into the water channel through the bubble diffuser, bubbles are generated and convected up along the channel. When bubbles pass by the electrode plates, the voltage potential established between the plates is modulated by the change in void fraction, which is processed by the electronic circuit to give an output voltage proportional to the void fraction. The time average voltage output is measured using a digital voltmeter (Keithly 197). This instrument is capable of storing data, which can be retrieved later for data analysis.

In each test run, the inlet air flowrate is fixed and the voltage data are recorded for a period of a 30 seconds. In addition, the variation in the height of the inverted manometer is recorded. This procedure is repeated two to three times to test data repeatability. The initial ionization is varied by using tap water, distilled water and salt water in order to study the effect of the initial conductivity on the void fraction measurement. The average of the voltage output was plotted against the ratio of H_m/H_p, which is proportional to the channel void fraction. These experimental plots are compared with the theoretical curve of Maxwell, who studied the electrical effect of spherical bubbles on an infinite homogenous media.

3.5.3.3 Results and discussion

This section presents results obtained from the air-water test section. This includes a general review of the void fraction behavior in the air-water channel and the effect of the initial conductivity is highlighted.

3.5.3.3.1 General Observations

By injecting air the to water channel, bubbles start rising along the channel. An air diffuser at the air inlet creates uniform and spherical bubbles. The passage of these bubbles between the sensor void probes creates a change in the voltage potential field which is recorded in the voltmeter. For low air flowrate, the bubbles are nearly spherical and their velocities are relatively small. This can be classified as a bubbly flow regime. Next, the increase of the inlet air flow rate causes more interaction between the bubbles, which start coalescing and forming bigger bubbles. This changes the flow regime to a churn regime, which is characterized by chaotic behavior.

A typical calibration curve is shown in Figure 3.11, which is a plot of the ratio of the conductivity K/Kl versus the void fraction in the water channel using tap water. The Maxwell theoretical curve is also shown. For low void fraction (bubbly regime), the experimental data correlates well with the Maxwell curve as expected. Agreement with the Maxwell curve persists to 20%, which is consistent with many previous works [12,13,22,26]. As the void fraction increases in the channel, the calibration curve deviates remarkably from the Maxwell curve due to the transition from bubbly to churn flow regimes. The increase in the channel void fraction is also characterized by the increase in the fluctuations in both the sensor output and in the reading of the water column height of the inverted manometer.

The uncertainty in the present results comes mainly from the uncertainty in the reading of the void meter and the height of the water column. Figures 3.12., 3.13 and 3.14 show the outputs of the three probes (conductivity ratio) as a function of the void fraction. In

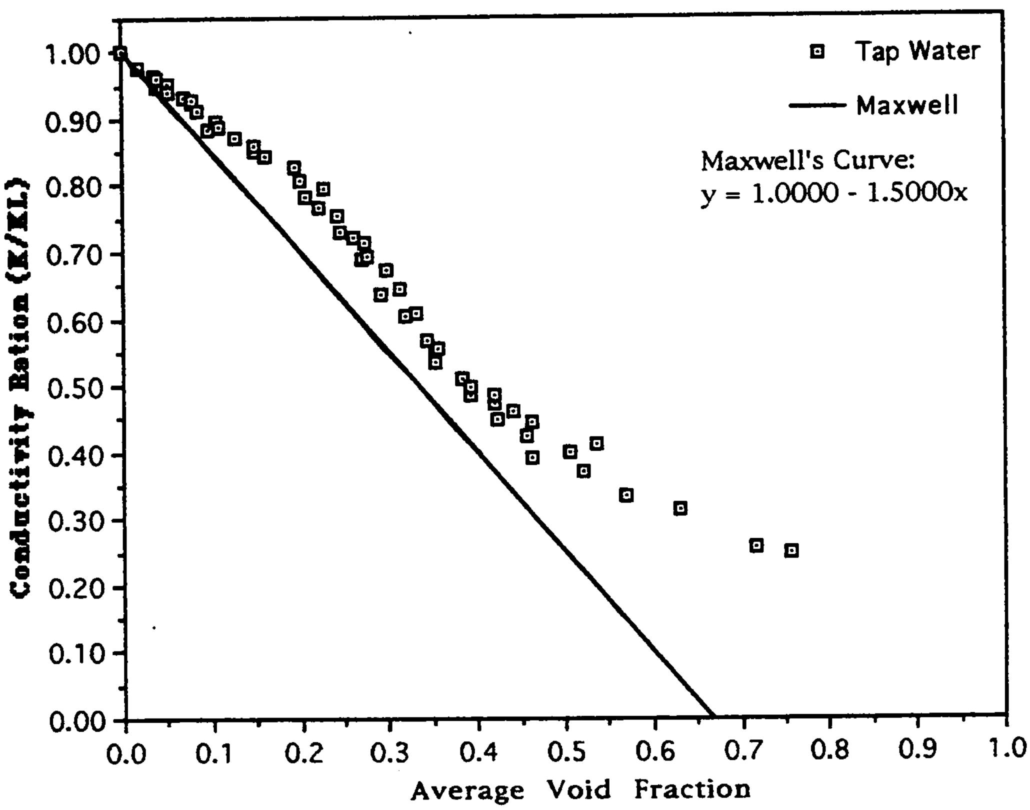

Figure 3.11: Void Fraction Measurement Using Tap Water

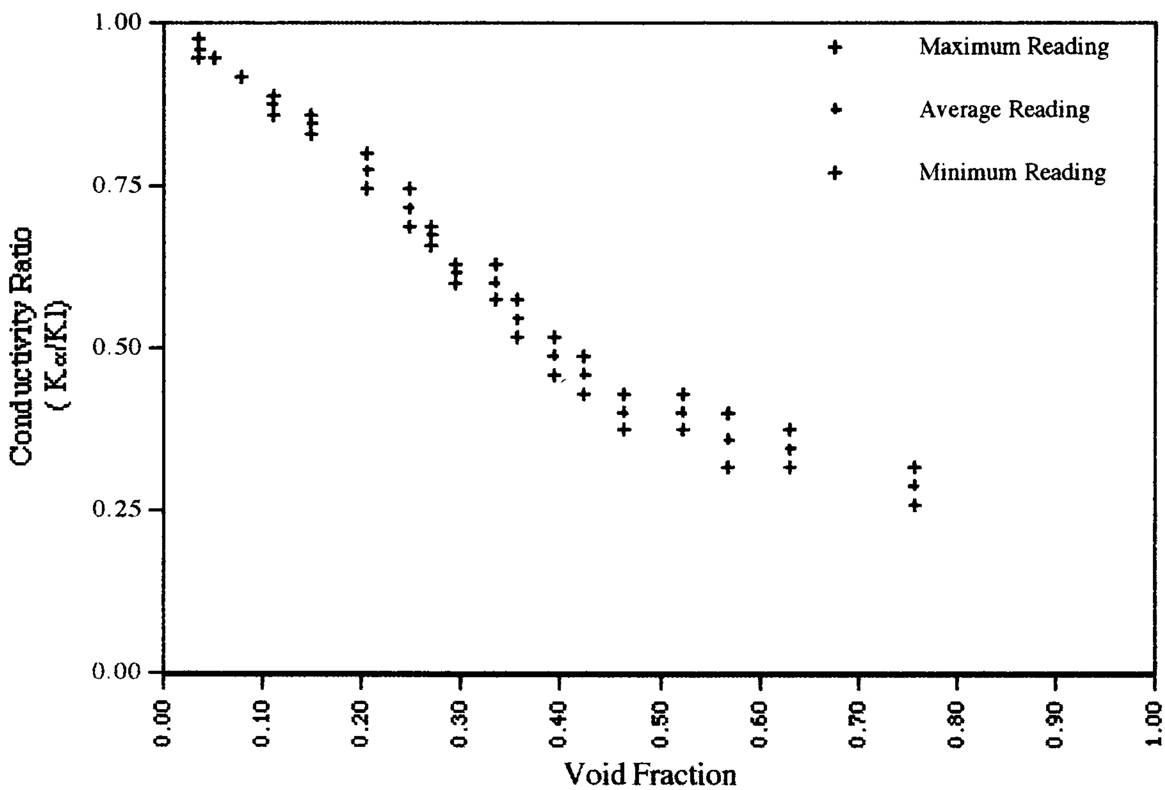

Figure 3.12 : Measurement Uncertainty in Probe I

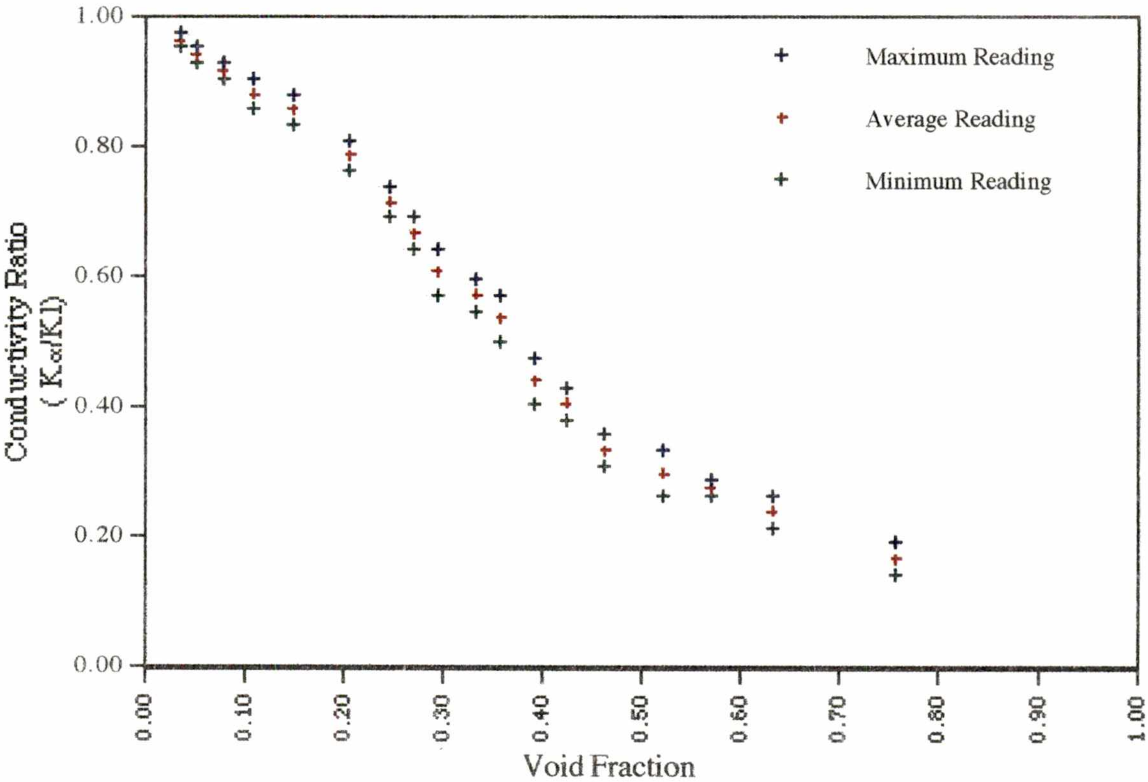

Figure 13: Measurement Uncertainty in Probe II

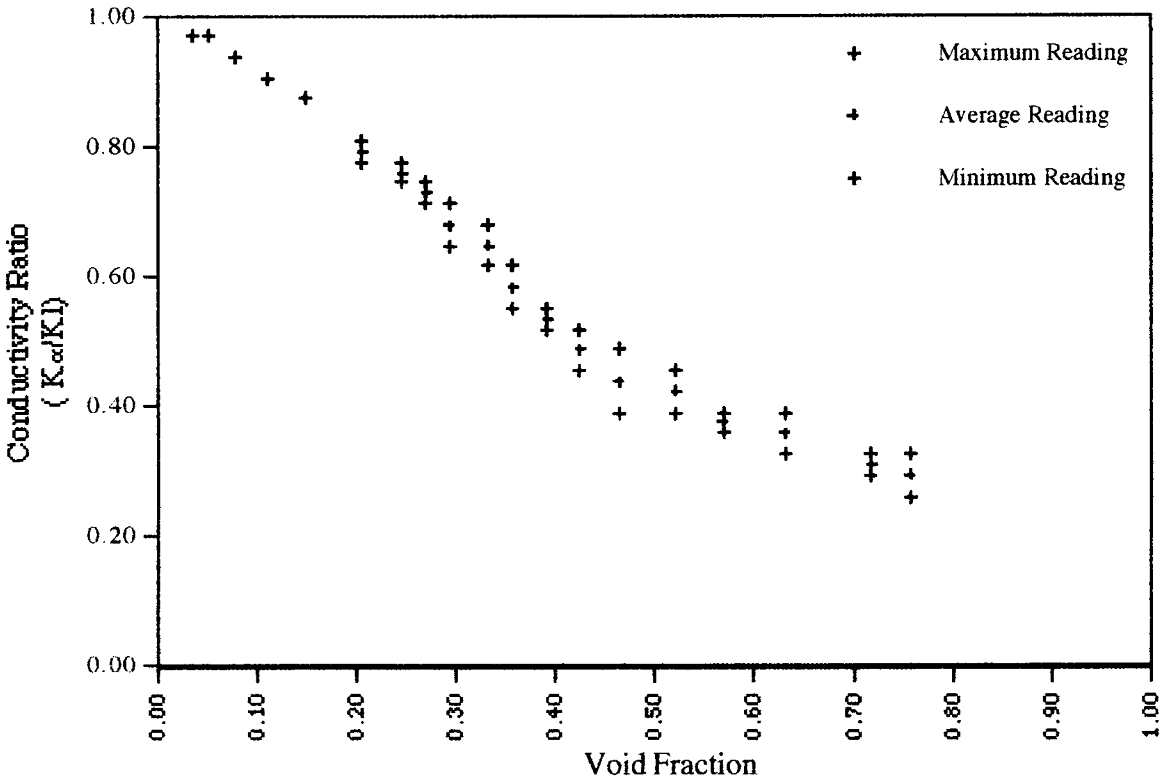

Figure 3.14: Measurement Uncertainty in Probe III

each figure the maximum, the minimum and the average values of the sensor output is shown. At low void fraction (e.g., low air flow rate) the fluctuation is very small. On the other hand, the increase in the void fraction increases the uncertainty. This is due to the fluctuating nature the void fraction in the air-water channel, especially at high void fraction where the churn flow dominates.

3.5.3.3.2 Effect of the Initial Conductivity

In the heated boiling water reactor channel, the liquid saturation temperature of the water is a function of the system operating conditions. This temperature change will directly affect the liquid conductivity and ionization. Therefore, it is necessary to investigate the effect of the liquid conductivity on the void fraction measurement in order to obtain a good estimate of the void fraction at different conditions. In the air water system the liquid conductivity is varied by mixing tap water with salt to increase the water conductivity, or with distilled water to decrease the conductivity level. Next, the water conductivity is measured as a function of the voltage output of the sensor circuit. In this study the water has four different conductivity values, which are: 0.803 V, 0.532 V, 0.403 V, 0.309 V. Four different calibration curves are obtained and compared with Maxwell's curve.

Figure 3.15 shows four different void fraction measurement curves with different liquid conductivities. For low void fraction

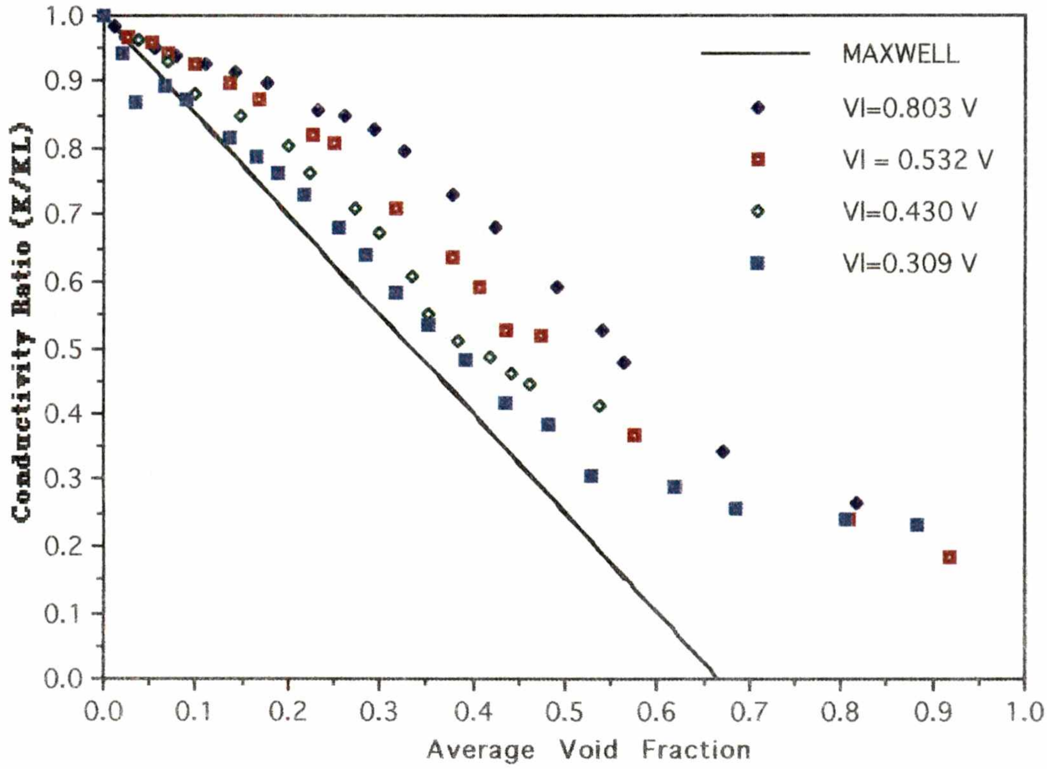

Figure 3.15: Effect of the Initial Conductivity on the Void Fraction Measurement

(< 10%), the four curves nearly agree with the Maxwell curve, which is a good representation for low void fraction measurement. As the void fraction increases, these curves start drifting apart; and as the liquid conductivity increases, the calibration curve over predicts the Maxwell curve. This can be seen for void fraction between 10 and 65%. Next, for void fraction higher than 65%, these four calibration curves again converge to one single curve.

From this study it is recommended that the initial water conductivity should be kept as low as possible, which can be achieved by both using distilled water with small addition of tap water and changing the water of the channel core and the condenser regularly.

CHAPTER 4

VOID SIGNAL PROCESSING AND SENSOR PERFORMANCE

4.1 Introduction

The installation of the void measurement probes in the Scaled Model Boiling Water Reactor (SMBWR) allows the study of the spatial and temporal void fraction fluctuations in addition to providing an indication of the channel average void fraction. Analysis of the void probe output can determine the vapor velocity and flow patterns in the boiling water channel. The sensor performance in the heated channel is also evaluated.

This chapter is divided into three sections. The first section discusses data acquisition and procedures. This includes data collection, preparation and storage. Next, an overview of signal processing techniques is given in order to provide the necessary tools to analyze the void fraction signal. Finally, results and discussions of the void signal processing and performance are presented.

4.2 Data Collection and Procedure

The sensor voltage output signal is digitized by the data acquisition board and passed to Lab-View where data processing is performed. Figure 4.1 shows the front panel and the block diagram of the Lab-View program utilized to acquire data from the void sensor. The front panel is used to set the rate of data acquisition and the number of points to acquire per second. In this study the sampling rate is 100 data samples per second since the sensor circuit has a maximum frequency response of 40 Hz. This satisfies the Nyquist criterion which states that for a given signal to be sampled without the loss of information, the sampling rate must be at least twice the maximum frequency contained in the signal.

4.2.1 Effect of the Power Controller on the Void Signal

The SRC power controller, used to control the heater power is a single phase angle controller [27]. The load voltage is controlled by turning on the SRC controller in each half cycle. For example, for a 50% power delivery, the SRC chops half of the original electrical cycle as shown in Figure 4.2. The power controller responds to the actual load by appropriately rectifying the original signal. A sudden and abrupt change in the sensor voltage output occurs as a result of the heater power controller response. The sensor circuit has a low pass filter of 40 Hz, intended to suppress the 60 Hz component; however, the heater power effect is still exhibited by the void probe output. Fortunately, the change occurs abruptly and persists for a small percentage of the total time as can be seen in Figure 4.3. In addition, the void sensor exhibits this noise as a very high negative voltage.

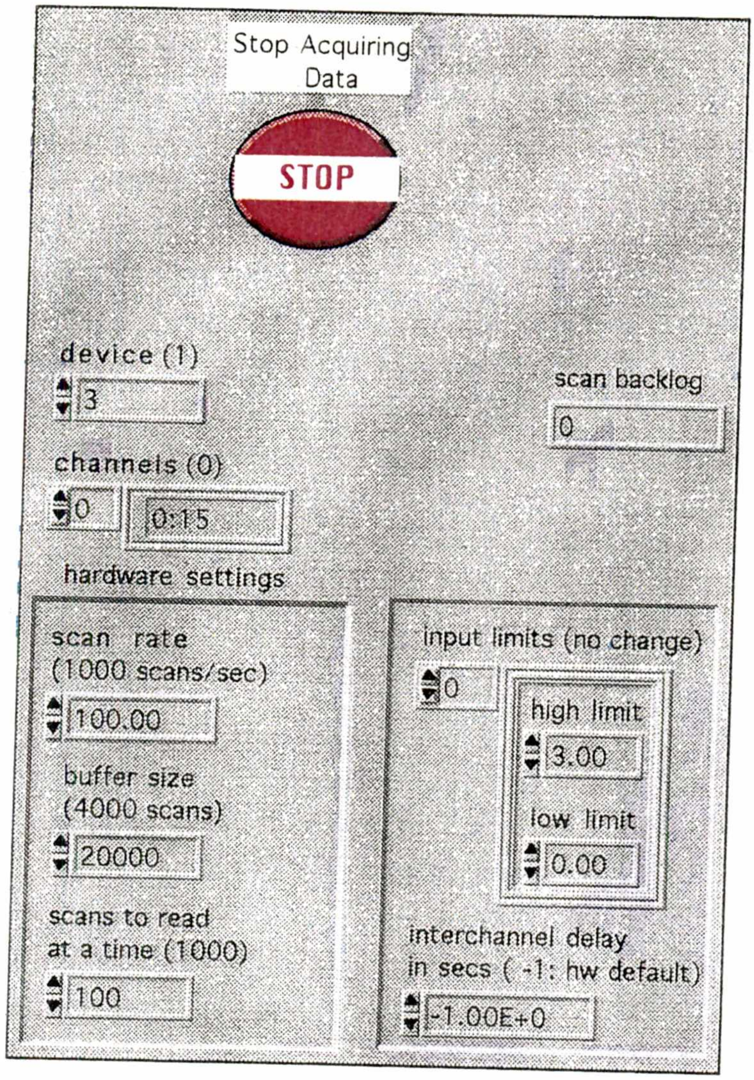

(a)

Figure 4.1: LabVIEW Program For Data Acquisition and Processing: (a) Front Panel, (b) Block Diagram.

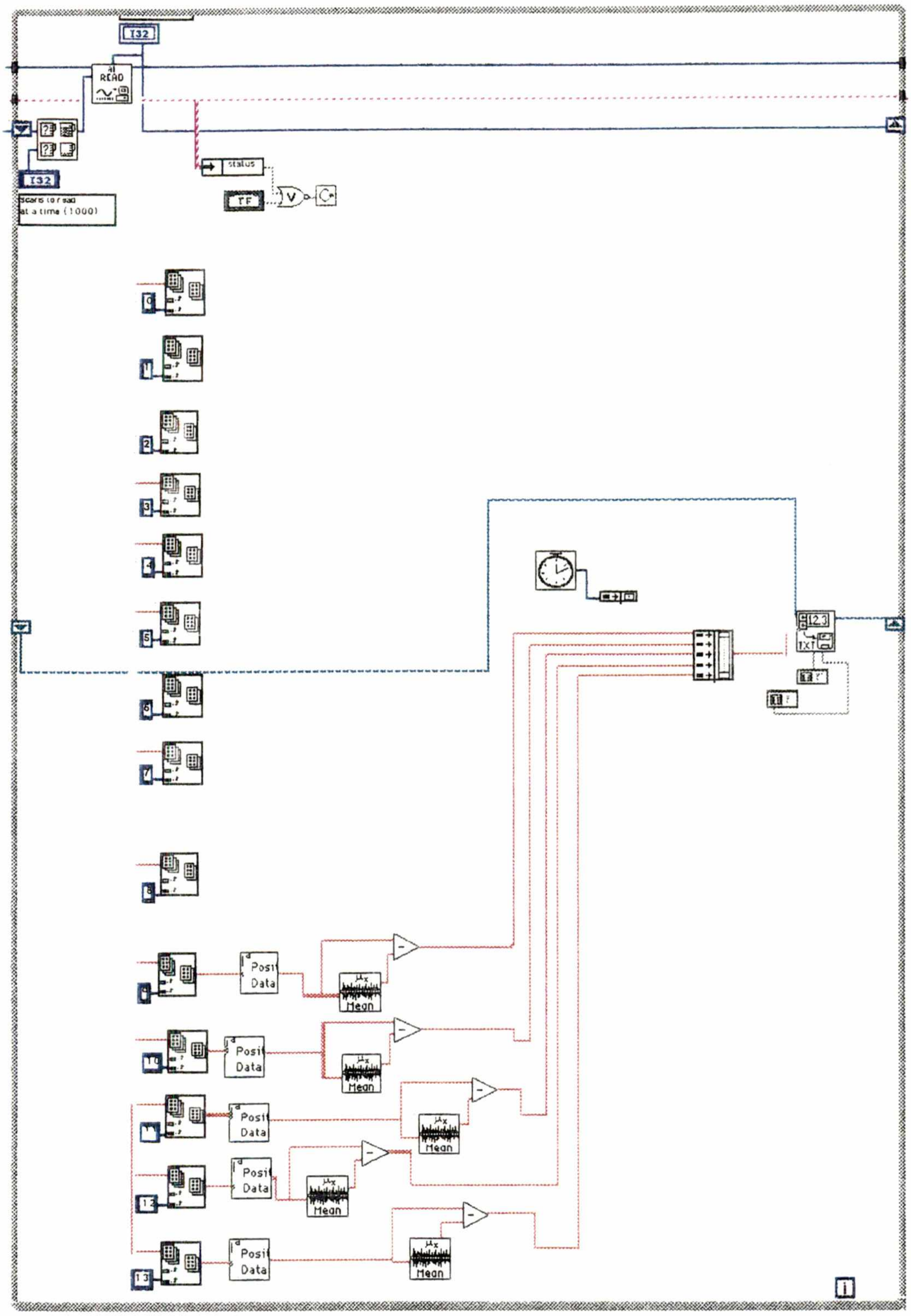

(b)

Figure 4.1: (Continued)

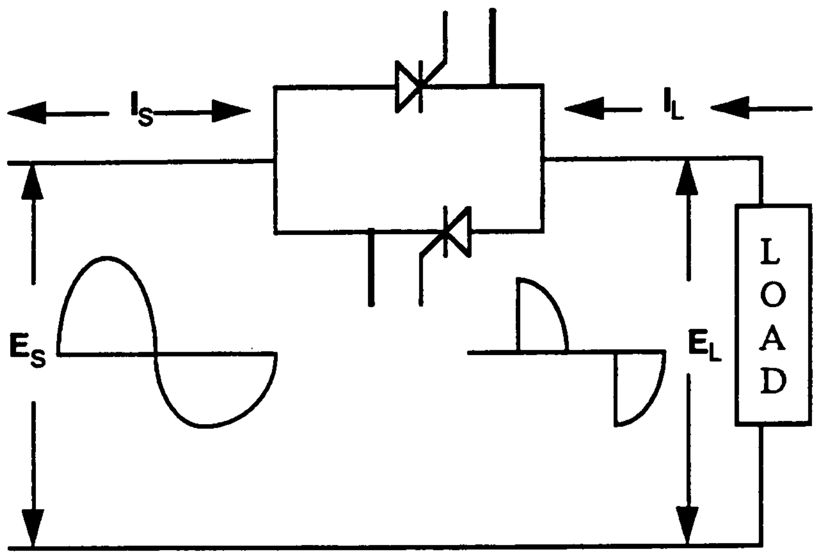

Figure 4.2 : Phase Angle Control at 50% Power Delivery [27].

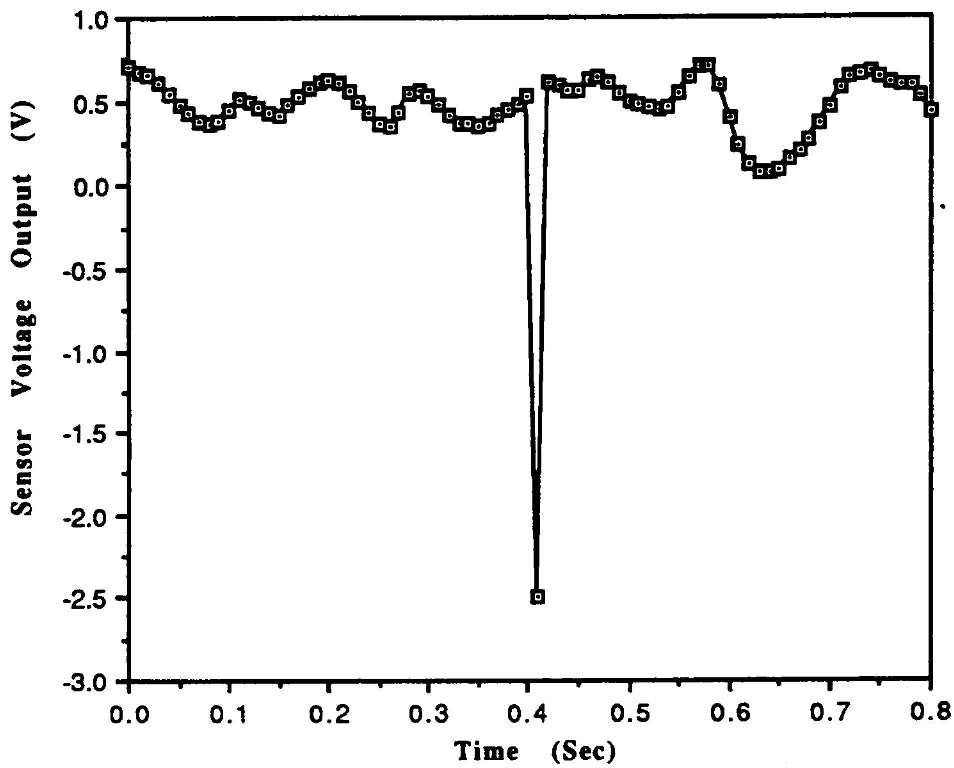

Figure 4.3 : Effect of the Power Controller on the Sensor Voltage Output.

Therefore, this noise can be remedied by eliminating the negative value from the signal allowing only positive values to pass. A Sub VI, called Positive Data, is implemented in the block diagram, shown in Figure 4.1 to defeat the spurious power supply noise

4.2.2 Data Preparation

The void signal acquired from the sensor is comprised of AC and DC components. The void fluctuation (AC component) is of primary importance for signal analysis. Therefore, the DC component is subtracted from the original signal for each acquisition. In each collected 100 data points, the mean is calculated and subtracted from the signal. This is accomplished by adding a Sub-VI to the block diagram as shown in Figure 4.1. The fluctuating component of the signal is saved in a spread sheet file, which can be retrieved later for further processing and analysis. The DC signal is used for void reactivity/power control, as discussed later.

4.3 Signal Processing Techniques

The analysis of the void fraction signal can provide a wide range of information about the void fraction behavior in the boiling channel. This includes void velocity, void wave propagation and flow regime. As a part of investigating the sensor performance, the void velocity and flow regimes are determined in the Scaled Model Boiling Water Reactor.

4.3.1 Time Domain Signature

The analysis of any signal can be performed either in the time domain or in the frequency domain in order to provide useful information [28,29,30]. In the time domain, several characteristics of the stationary signal can be determined to provide an estimate of the signal in terms of its mean, variance, correlation and probability distribution.

4.3.1.1 Mean Value

For a given set of samples of $\alpha(t)$ with a time length of T, the mean value can be determined as:

$$\alpha(t) = \frac{1}{T}\int_{0}^{T} \alpha(t)dt \tag{4.1}$$

Numerically the mean of a signal can be estimated as :

$$\alpha(t) = \frac{1}{N}\sum_{k=0}^{k=N} \alpha_k(t) \tag{4.2}$$

Where N is the number of samples in $\alpha(t)$. Both space and time averages of the void fraction signal are performed to facilitate simulation of the void-reactivity feedback as discussed in the next chapter

4.3.1.2 Probability Density Function

The time series of a stationary random signal is described by its probability density function, which can be considered as the histogram of the signal. In this section the main concept of the probability density function is explained along with its application in identifying some of the two-phase flow characteristics.

For a given void fraction signal, $\alpha(t)$, the probability that the void fraction lies within a specified range of $[\alpha - \frac{\Delta\alpha}{2}, \alpha + \frac{\Delta\alpha}{2}]$ is given by :

$$\hat{P}[\alpha, \Delta\alpha] = \text{Prob}[(\alpha - \Delta\alpha) \le \alpha(t) \le (\alpha - \Delta\alpha)] \tag{4.3}$$

where $\Delta\alpha$ is a specified length of $\alpha(t)$ as can be seen in Figure 4.4. The probability, $\hat{P}[\alpha, \Delta\alpha]$, can also be written as:

$$\hat{P}[\alpha, \Delta\alpha] = \frac{1}{T} \sum_{i=1}^{K} \Delta t_i = \frac{T_\alpha}{T} \tag{4.4}$$

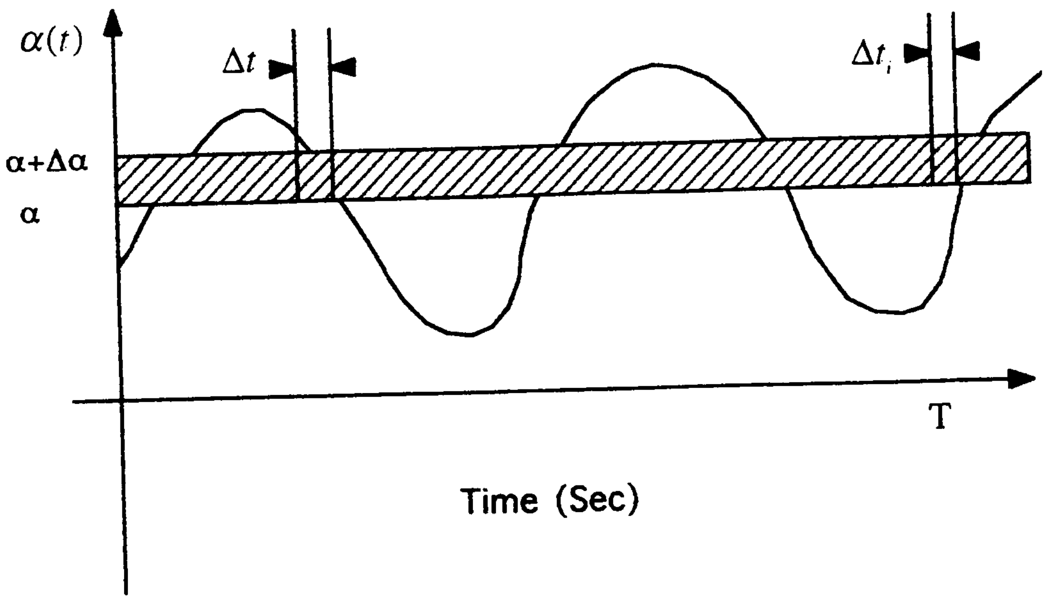

Figure 4.4: Computation of the Probability Functiom Distribution

where Δt_i' s are the time intervals at which the signal has resided in the amplitude range of $[\alpha - \frac{\Delta\alpha}{2}, \alpha + \frac{\Delta\alpha}{2}]$. For a long time history the probability, $\hat{P}[\alpha, \Delta\alpha]$, reaches the true probability $P[\alpha, \Delta\alpha]$ [30]. Next, the probability density function can then be defined as:

$$P(\alpha) = \lim_{\Delta\alpha \to 0} \frac{P[\alpha, \Delta\alpha]}{\Delta\alpha} = \lim_{\substack{\Delta\alpha \to 0 \\ T \to \infty}} \frac{\hat{P}[\alpha, \Delta\alpha]}{\Delta\alpha} = \lim_{\substack{\Delta\alpha \to 0 \\ T \to \infty}} \hat{P}(\alpha) \tag{4.5}$$

where $\hat{P}(\alpha) = \frac{T_\alpha}{T\Delta\alpha}$. As one can see the probability density function represents the probability, per unit void fraction, that the void fraction lies in the interval range $[\alpha - \frac{\Delta\alpha}{2}, \alpha + \frac{\Delta\alpha}{2}]$. By using the probability density function, one can identify the different flow regimes in a two-phase flow system.

4.3.1.3 Correlation Functions

The auto correlation function of a signal $\alpha_i(t)$ and cross correlation between two signals $\alpha_i(t)$ and $\alpha_j(t)$ can provide some information on the relationship for one or two signals when they are separated by a time displacement [29,30]. For example, The auto correlation of a stationary signal gives the general time dependence of the signal values separated by a time lag τ. The autocorrelation function, $R_{\alpha_i\alpha_i}(\tau)$, can be written as:

$$R_{\alpha_i\alpha_i}(\tau) = E[\alpha_i(t)\alpha_i(t+\tau)] = \lim_{T\to\infty}\frac{1}{T}\int_0^T \alpha_i(t)\alpha_i(t+\tau)dt \tag{4.6}$$

The autocorrelation can also provide useful information on the signal periodicity. For a discrete sample of data N, the auto correlation can be written as:

$$R_{\alpha_i\alpha_i}(k) = \frac{1}{N}\sum_{i=1}^{N-k}(\alpha_i - m_\alpha)(\alpha_{i+k} - m_\alpha) \tag{4.7}$$

The cross correlation function of two signals $\alpha_i(t)$ and $\alpha_j(t)$ also describes the general dependence of one set of data on the other. This cross correlation can be written as:

$$R_{\alpha_i\alpha_j}(\tau) = E[\alpha_i(t)\alpha_j(t+\tau)] = \lim_{T\to\infty}\frac{1}{T}\int_0^T \alpha_i(t)\alpha_j(t+\tau)dt \tag{4.8}$$

Numerically, the cross correlation at lag, $\tau = k\Delta t$, can be computed as:

$$R_{\alpha_i\alpha_l}(k) = \frac{1}{N}\sum_{j=1}^{N-k}(\alpha_{ij} - m_{\alpha_i})((\alpha_l)_{j+k} - m_{\alpha_l}) \tag{4.9}$$

The cross correlation function can be utilized to measure delay time and detect noise in stationary signals [29].

4.3.1.4 Delay Time Measurement

The cross correlation is of particular interest in this study since it allows measurement of the vapor velocity in the boiling channel.

This can be obtained by determining the delay time, associated with the passage of a vapor bubble through two successive probes in the boiling water channel, as shown in Figure 4.5. For a given two output void signals $\alpha_i(t)$ and $\alpha_j(t)$ from sensors i and j respectively, the signal $\alpha_j(t)$ can be written in term of $\alpha_i(t)$ as :

$$\alpha_j(t) = \lambda \alpha_i(t - \tau_o) + n(t) \tag{4.10}$$

Where λ is an attenuation factor and n(t) represents a zero mean value noise (see figure 4.5). The cross correlation of signal $\alpha_i(t)$ and $\alpha_j(t)$ is then written as:

$$R_{\alpha_i\alpha_j}(\tau) = E[\alpha_i(t) \times \alpha_j(t+\tau)] = E[\alpha_i(t) \times \{\lambda \alpha_i(t+\tau-\tau_o) + n(t+\tau)\}$$

$$= \lambda E[\alpha_i(t)\alpha_i(t+\tau-\tau_o) = \lambda R_{\alpha_i\alpha_i}(\tau - \tau_o) \tag{4.11}$$

Therefore, $R_{\alpha_i\alpha_j}(\tau)$ can be written as the autocorrelation $R_{\alpha_i\alpha_i}(\tau)$ with a lag time τ_o and multiplied by the attenuation factor λ. Thus the peak value for $R_{\alpha_i\alpha_i}(\tau)$ occurs at $\tau = \tau_o$, where the two signals are correlated; and it represents the time delay for the signal to go from probe i to probe j. this can be written as:

$$R_{\alpha_i\alpha_j}(\tau)_{peak} = R_{\alpha_i\alpha_j}(\tau_o) = \lambda R_{\alpha_i\alpha_i}(0) = \lambda \sigma_{\alpha_i}{}^2 \tag{4.12}$$

Knowledge of the distance between the two probes can be used to determine the mean void velocity as:

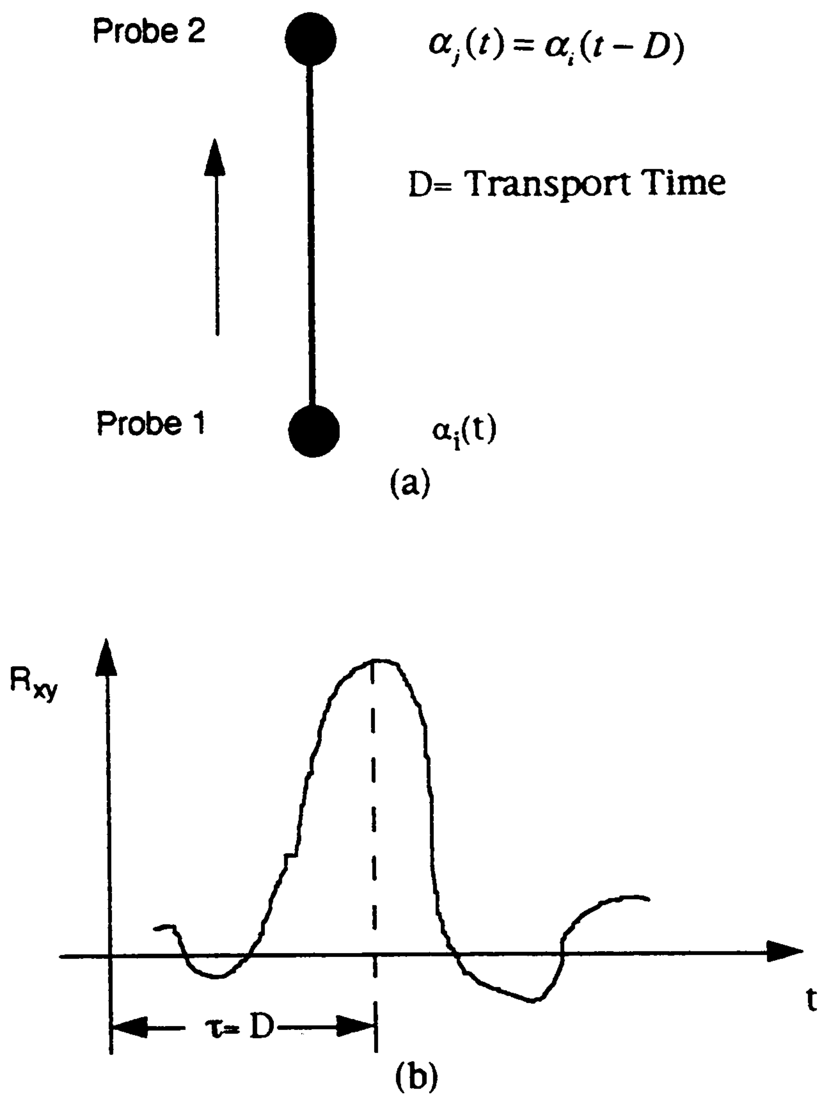

Figure 4.5 : Measurement of the Delay Time Using Cross Correlation Function: (a) Physical Representation of the Delay Time, (b) Correlation Function of the Two Detectors.

$$V = \frac{d}{\tau_o} \tag{4.13}$$

4.3.2 Frequency Domain Analysis

The signal time series can also be analyzed in the frequency domain to provide further details on the signal behavior. In the frequency domain one can determine the signal energy at certain frequencies. In this section the power spectral density of a signal $\alpha_i(t)$ and the cross power spectral density of two signals $\alpha_i(t)$ and $\alpha_{i+1}(t)$ are employed to analyze the main characteristics of the void signal; and also to determine the vapor velocity in the boiling water channel.

4.3.2.1 Spectral Density Estimation

For given stationary signals $\alpha_i(t)$, measured in an interval [0, T] the Fourier transform is determined as:

$$X(f,T) = \int_0^T \alpha_i(t) e^{-j2\pi ft} dt \tag{4.14}$$

From the Fourier transform the spectral density is written as:

$$S_{\alpha_i\alpha_i}(f,T) = \frac{1}{T} |X(f,T)|^2 \tag{4.15}$$

For large period of T, the spectral density is given in term of the correlation function as:

$$S_{\alpha_i\alpha_i}(f) = \lim_{T\to\infty} S_{\alpha_i\alpha_i}(f,T) = \int_{-\infty}^{\infty} R_{\alpha_i\alpha_i}(\tau)e^{-j2\pi f\tau}d\tau \tag{4.16}$$

Likewise, the cross power spectral density is written as:

$$S_{\alpha_i\alpha_{i+1}}(f) = \lim_{T\to\infty} S_{\alpha_i\alpha_{i+1}}(f,T) = \int_{-\infty}^{\infty} R_{\alpha_i\alpha_{i+1}}(\tau)e^{-j2\pi f\tau}d\tau \tag{4.17}$$

The spectral density and cross power spectral density provide information on the coherence of the signal, defined as:

$$\gamma_{\alpha_i\alpha_{i+1}}(f)^2 = \frac{\left|S_{\alpha_i\alpha_{i+1}}(f)\right|^2}{S_{\alpha_i\alpha_i}(f)S_{\alpha_{i+1}\alpha_{i+1}}(f)} \tag{4.18}$$

Because of measurement noise and signal attenuation, as discussed earlier, the coherence function is usually between 0 and 1. For perfect correlation, γ is equal to 1. If the two signals are uncorrelated, γ is equal to 0.

4.3.2.2 Delay Time Measurement Using Cross Power Spectral Density

The cross power spectrum is utilized to determine the delay time between two adjacent sensors. This method is also used to double check the vapor velocity that is determined from the cross-correlation function, discussed earlier. The delay time measurement using the cross power spectral density is determined by substituting Equation 4.11 into Equation 4.17 to give the two-sided cross power spectral density, which is written as :

$$S_{\alpha_i\alpha_j} = \lambda \int_{-\infty}^{+\infty} R_{\alpha_i\alpha_i}(\tau - \tau_o) e^{-j2\pi f\tau} d\tau \tag{4.19}$$

the one-sided cross-power spectral density is written as:

$$G_{\alpha_i\alpha_j}(f) = \lambda G_{ii}(f) e^{-j2\pi f\tau_o} \tag{4.20}$$

The cross power spectral density is a complex number and it can be represented by a magnitude and a phase, which are written as:

$$\left|G_{\alpha_i\alpha_j}(f)\right| = \lambda G_{\alpha_i\alpha_i}(f) \tag{4.21}$$

and

$$\theta_{\alpha_i\alpha_j}(f) = 2\pi f\tau_0 \tag{4.22}$$

The phase is a function of the frequency, f, with a local slope of $2\pi\tau_0$, which physically represents the transport time of the vapor bubble from sensor i to sensor i+1. Therefore, by knowing the distance between the two probes, the vapor velocity can be determined using Equation 4.13.

4.4 Two-Phase Flow Pattern Identification

The identification of the flow regime is relevant in the study of two-phase flow systems. For example, in a well-defined flow pattern one can apply the appropriate correlations in order to determine heat transfer rate, pressure drop and void fraction. In industrial applications the knowledge of the flow regime can be used to select the models that best represent the process. In the petroleum industry, gas or air is usually used to excavate petroleum from underground. This requires flow regime control in order to extract the maximum liquid petroleum per unit energy spent to circulate the air in the underground [31]. In addition, the flow regime is controlled to give the minimum pressure loss in the transport of gaseous and liquid petroleum components in a single pipe. Knowledge of flow regime and flow regime control are also important in chemical reactors where interfacial area and residence times are critical to process control.

4.4.1 Overview of the Two-Phase Flow Patterns

The channel void distribution depends on the channel geometry, orientation and also on the flow parameters such as operating pressure, inlet gas and liquid flow rates [32]. In nuclear reactors there are mainly vertical (e.g., fuel assembly in a BWR) and horizontal flows.

In vertical co-current flow, there are bubbly, slug, churn and annular flow regimes. These four regimes are shown in Figure 4.6.a. In a bubbly regime, vapor is dispersed in the liquid matrix, and the bubbles are relatively small and can vary in size and shape. Generally, the bubbly regime is characterized by the vapor size less than the characteristic length of the channel cross section. In contrast to the bubbly regime, the slug regime is characterized by gas plugs that fill the cross section. These gas plugs can also vary in shape and size. The churn flow has the same characteristics as the slug regime in terms of the bubble size, but the vapor distribution in the channel is random and chaotic. For the annular regime the vapor is confined in the central zone of the channel core with a thick liquid film on the wall. Many sets of rules have been proposed to predict transition between flow regimes based on geometry and flow parameters [33].

For horizontal flow, one can observe the same patterns as those of the vertical flow; however, the effect of gravity on the fluids with different densities makes the horizontal flow non-symmetrical and causes the fluid to stratify, which adds two flow patterns, called

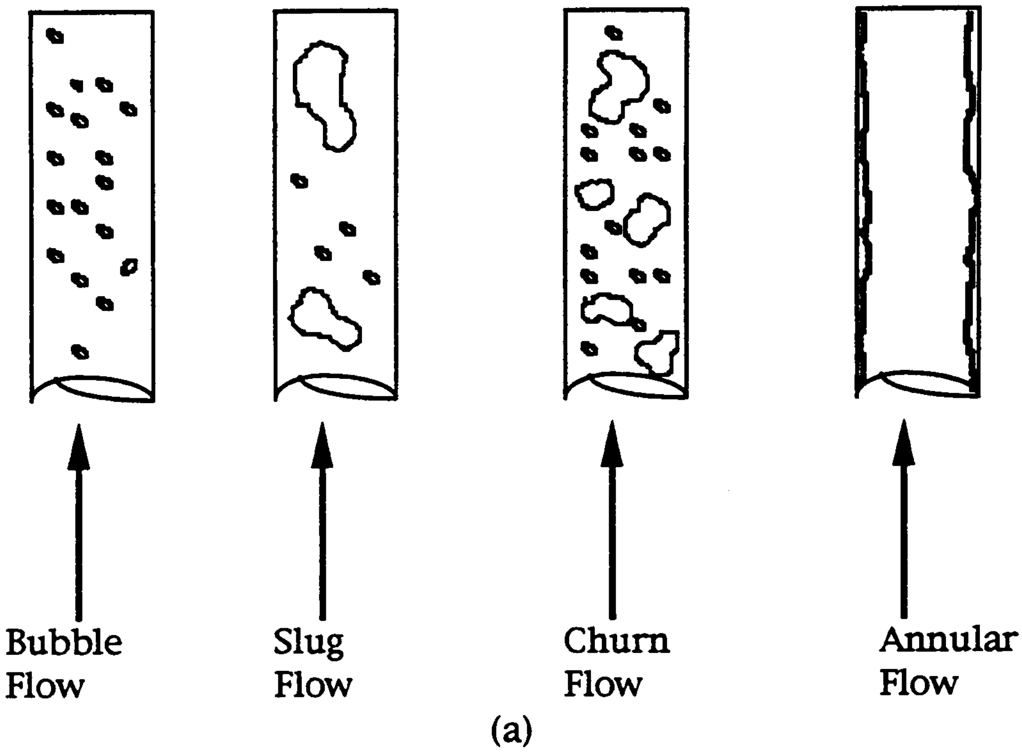

Figure 4.6: Illustration of the Two-Phase Flow Regimes: (a) Vertical Flow, (b) Horizontal Flow.

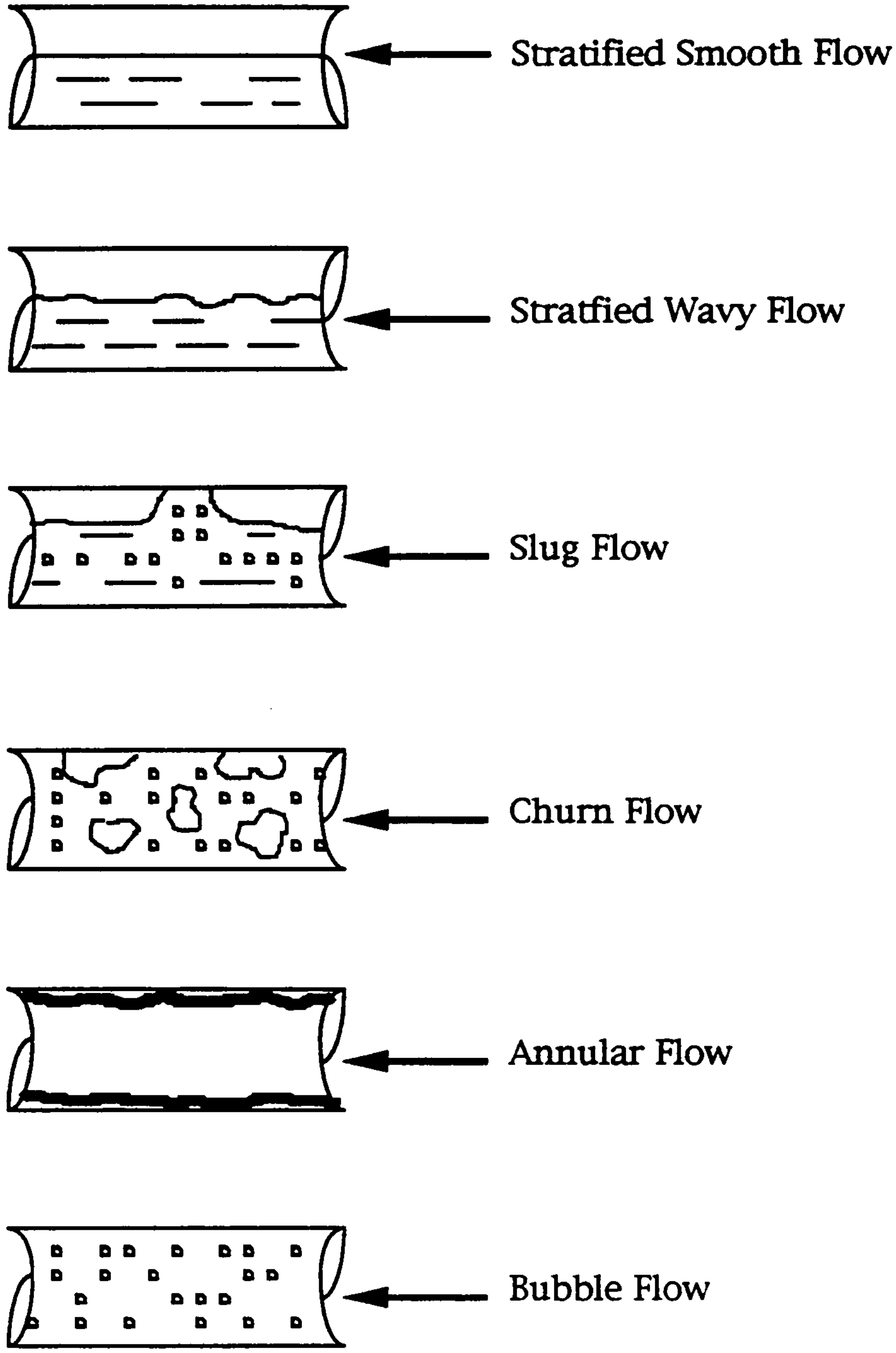

(b)

Figure 4.6 (Continued)

stratified smooth flow and stratified wavy flow, as shown in Figure 4.6.b. For a stratified smooth flow pattern, the gas flow rate is much less than that of the stratified wavy flow in which the friction between the liquid and vapor interface becomes dominant.

4.4.2 Flow Regime Identification Techniques

There are several techniques that have been employed over the past several years to identify flow regimes in two-phase flow systems. In their review of two-phase flow patterns, Rouhani and Souhal [31] classified these identification techniques as direct and indirect methods, which are briefly discussed in the following sections:

4.4.2.1 Direct Method

This method involves direct observation of the two-phase flow regimes through a transparent channel or a window fitted in the channel wall. These observations are done either visually or with a high speed camera, which allows formulation of still pictures of the two-phase flow patterns. Furthermore, X-ray attenuation pictures are also used to overcome the effect of light refraction in the liquid-gas interface. The main disadvantage of the direct method is the fact that the observer is subjective of the flow when the data is collected. Therefore, flow regime may be observer dependent.

4.4.2.2 Indirect Method

This method consists of determining the two-phase flow patterns through a statistical analysis of the two-phase flow fluctuations in pressure or void fraction. This method is also called 'Flow regime signature' [31]. The statistical analysis used to identify the flow regimes can be classified into the following categories:

4.4.2.2.1 Probability Density Function Analysis

The definition of the probability density function is explained in section 4.3. This signal processing method was used by Jones and Zuber [34] to classify flow patterns in an air-water channel based on time domain signals from X-ray sensors. Jones and Zuber used high-speed motion pictures to correlate with the PDF distribution. In their analysis Jones and Zuber found that void fluctuation in different flow regimes give probability density distributions with different features. Figure 4.7 shows different flow regimes with their respective probability distributions. For the bubbly regime, the void fraction undergoes only a minor fluctuation around its average. This is exhibited by the sharp center at the mean void fraction. The slug flow is characterized by the passage of gas plugs, surrounded by small vapor bubbles. This behavior is clearly represented by the existence of two peaks, indicating that the slug flow is a combination of the annular and bubbly regimes. Next, the annular flow regime is

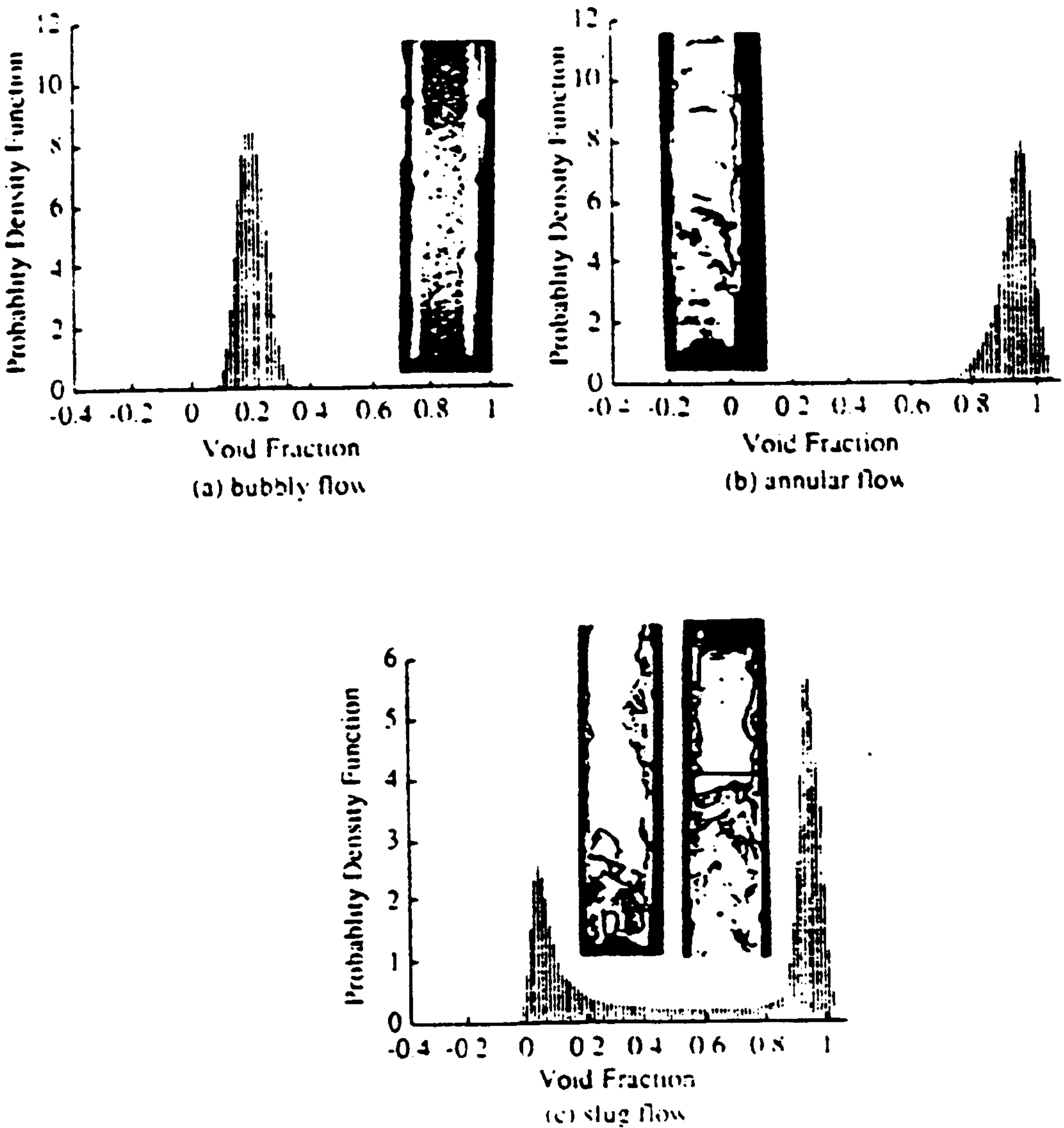

Figure 4.7 . Flow Regimes and Their PDF Distributions [34].

characterized by a high void fraction, represented by a high peak in the PDF distribution.

4.4.2.2.2 High Frequency Contribution Fraction

This method is recently developed by Wang et al. [35,36] to classify flow regimes in two-phase flow systems. This method consists basically of computing the power spectral density of the void signal and then examining the high frequency content:

$$HFCF = \frac{\sum_{K=S}^{N/2-1} PSD(k)}{\sum_{K=0}^{N/2-1} PSD(k)} \tag{4.23}$$

Where N is the number of points of each block in which the power spectral density is computed. In addition, Wang et al. have also used visual observations and the power spectral density characteristics to set some criterion for flow regime identification. The High Frequency Contribution Fraction method is verified by analyzing the void signal from three different sensors (fission chamber, light sensor and impedance sensor) in an air-water system. In their analysis, Wong et al. found that the power spectral density of the different flow regimes have the following characteristics:

- Wide frequency range for the bubbly regime
- A unique spectral peak at lower frequency for the slug regime
- Multiple peaks in the low frequency range for the churn flow.

Next, Wang et al. have classified the flow regimes according to the variation of the HFCF ratio. This criterion, however, depends on the void signal and how it is acquired. This can be seen in the different HFCF criteria that Wang et al. have obtained for the three different sensors. For example, the HFCF criterion for the churn was found to be between 0.03 and 0.15 when the optical sensor was used. On the other hand, by using the impedance probe with arc type electrodes, the HFCF criterion was found to be between 0.01 and 0.03 for the churn flow regime.

4.4.2.2.1 Noise Analysis

This method is customarily used to model the fluctuation of a signal in order to extract useful information about the behavior of the system. By using a time series model one can determine the transfer function of a system and its response to any given input, and also one can forecast future values of the time series model from current and past values [37]. This method has been extensively employed by many authors to model reactor neutron noise, pressure and temperature fluctuations. These time series model include auto regressive model (AR), moving average model (MR) and auto regressive moving average model (ARMA).

This noise analysis method is also utilized by several authors [38,39] to model the pressure fluctuations in two-phase flow in order to identify the flow regimes using the dynamic signature ratio, which is defined as the ratio of the variance of the original pressure signal to the residual variance of ARMA model.

4.5 Flow Pattern Identification in the Scaled Model Boiling Water Reactor

The objective of this section is to determine the flow regimes in the SMBWR, which gives a unique opportunity to analyze data from a boiling heated channel rather than from an air-water test section. The flow regimes are identified using visual observation, high speed camera and time series analysis of the void fraction fluctuations using the probability density function (PDF) and the High Frequency Contribution Fraction (HFCF) technique. In addition, the power spectral density of each flow regime is examined.

4.5.1 Test Conditions and Signal Processing

Before collecting data, the reactor model is brought to a steady state condition, discussed in detail in section 5.6. For each test run while the flow regime is visually observed through the glass channel, the void fraction signal is recorded at a rate of 100 Hz. The high speed camera is also used on some test runs to further analyze the recorded data.

The analysis of the probability density function is performed using a computer program written in MATLAB and listed in appendix

A. This program implements the basic concept of computing the probability density function, which is given earlier in section 4.3. For the HFCF and power spectral analysis the void signal data are analyzed using a signal processing tool called GLOBAL [40]. In each analysis the sample size of each test is 10000 samples. In addition, the block size for the Fourier transform computation was fixed at 1024 points per block.

4.5.2 General Observation of the Flow Regimes

The heated channel of the Scaled Model Boiling Water Reactor exhibits different flow regimes. These regimes vary along the channel and are described according to the sensor probe locations.

4.5.2.1 Probe I

This probe is intentionally placed in the liquid phase to monitor the changes in the liquid conductivity and ionization level. This probe is also used as a reference to determine the axial void fraction at the upper four probes. The changes in the liquid voltage depend on several factors such as increase in the operating temperature.

4.5.2.2 Probe II

This probe is near the start of the boiling length and it is in the bubbly regime in most operating conditions. At this location the bubbles size are small and their convected velocities are relatively slow. These vapor bubbles look spherical in shape and range in diameters from 5 mm to 8 mm.

4.5.2.3 Probe III

At this probe the bubbly regime still persists but the bubble size has remarkably increased along with the bubble velocity. This is due mainly to bubbles coalescing and forming bigger bubbles. The shape of these bubbles has been distorted from the spherical shape.

4.5.2.4 Probe IV

At this level the vapor bubble diameters have increased to 18 mm and they form gas plugs. In addition, smaller vapor bubbles are observed but their velocity is much faster than those of probe I and II. The vapor bubble size and distribution are irregular and chaotic in nature. In addition, occasional flow reversals are observed at this probe. These irregularity are clearly seen in the high speed camera film.

4.5.2.5 Probe V

At this probe the churn flow is dominant and vapor plugs are frequent. Sometimes the vapor engulfs probe IV and V at the same time. At this probe occasional flow reversals are also observed and it adds to the chaotic nature of the two-phase flow in this region. The flow reversal is also observed using the high speed camera. The flow reversal is due mainly to the abrupt change in the cross sectional area inside the channel at the end of the heaters.

4.5.3 Analysis of the Flow Regimes

The bubbly and the churn flows are observed in the heated channel of the Scaled Model Boiling Water Reactor. The main characteristics of these regimes are discussed in the following sections using three different techniques: the probability density function (PDF), the High Frequency Contribution Fraction (HFCF), and the spectral density analysis. The slug regime, which is not detected in the heated channel, is identified in the air-water system in order to further investigate the performance of the void fraction sensor.

4.5.3.1 Probability Density Function

The use of the probability density function to identify the flow regime has proved to be adequate by many authors [34,41] who utilized either the fluctuations of the void fraction or the pressure to delineate between the different flow regimes. However, these analyses were all performed in air-water test sections, which exhibit less complexity than that of a heated channel. The present study presents the PDF analysis with void fraction fluctuations of a boiling water channel.

In the bubbly regime, seen at probe II, the void fraction exhibits small fluctuation about its mean. This is shown in Figure 4.8.a, which presents the void fraction time series. The probability density function distribution is shown in Figure 4.8.b, which shows a sharp peak at a high value of the void fraction. The PDF then decreases appreciably as the void fraction increases. The bubbly regime is also frequently noticed at probe III where the vapor bubble velocity and size have increased. Figure 4.9.a shows the time series of the void fraction at probe III. The PDF distribution (Figure 4.9.b) shows some differences from that of probe II. First, the PDF at probe III is broadened and covers a higher void fraction area than that of probe II. Second, the PDF peak is less pronounced than that of probe II.

The churn flow is most obvious at probe V, where the void fraction behaves in a chaotic way in terms of its size and distribution. The time series of the churn flow is presented in Figure 4.10.a. This figure shows high amplitude fluctuation of the void fraction. The PDF distribution is also shown in Figure 4.10.b, and the PDF covers a wide range of void fraction, which verifies the irregularities in the bubble size that have been observed in the heated channel. Probe VI exhibits also churn regime behavior. The time series of the void fraction and its respective PDF distribution are shown in Figures 4.11.a and 4.11.b, respectively.

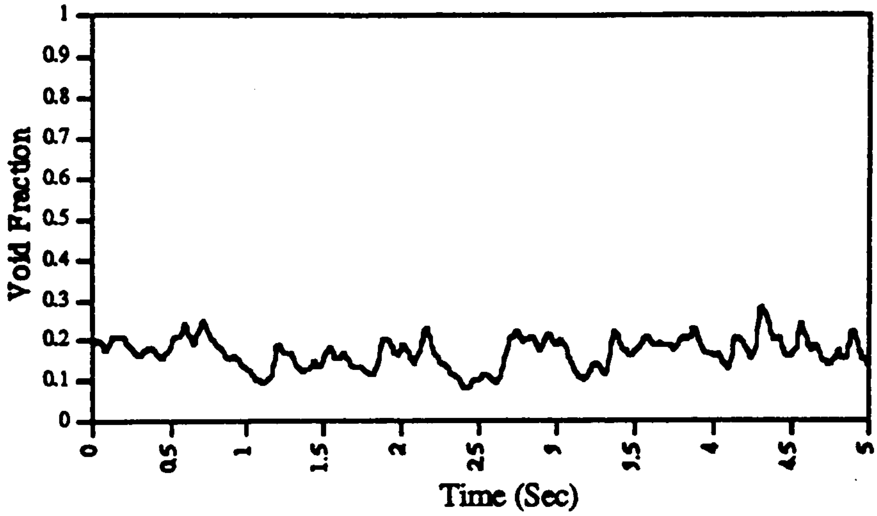

(a)

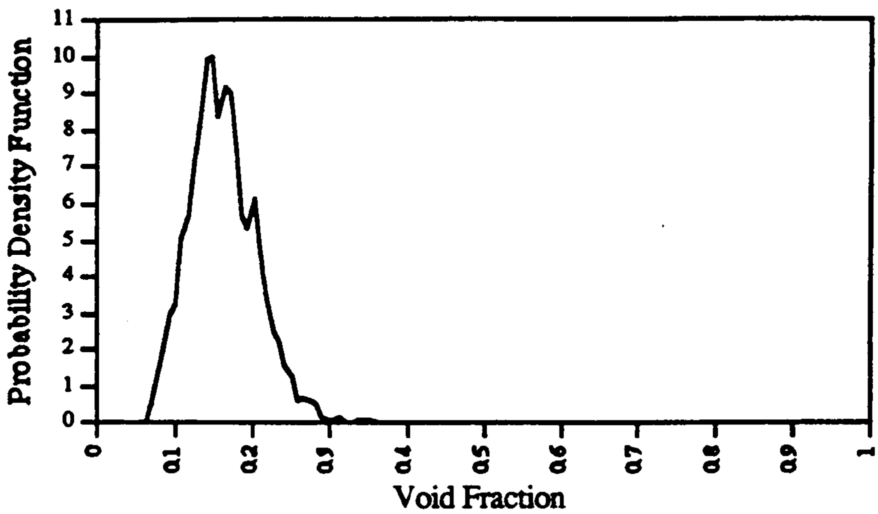

(b)

Figure 4.8: Flow Regime at Probe II: (a) Void Fraction Time Series, (b) Probability Density Function.

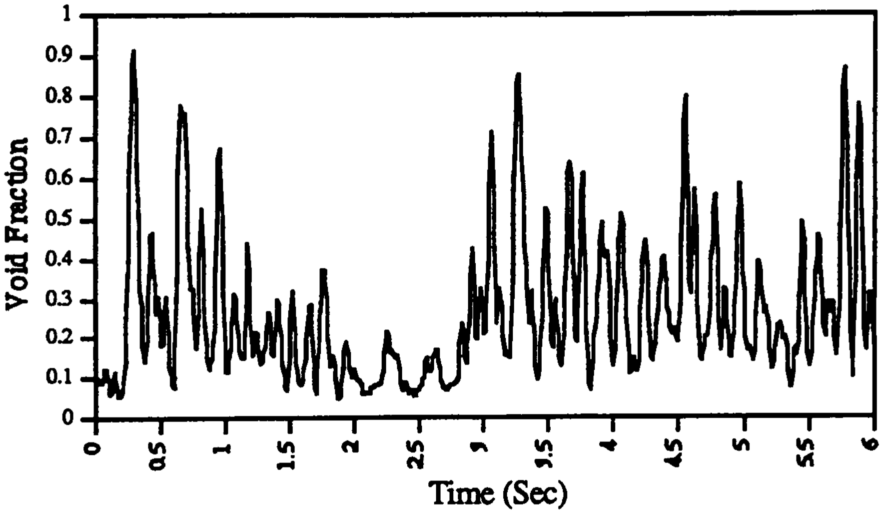

(a)

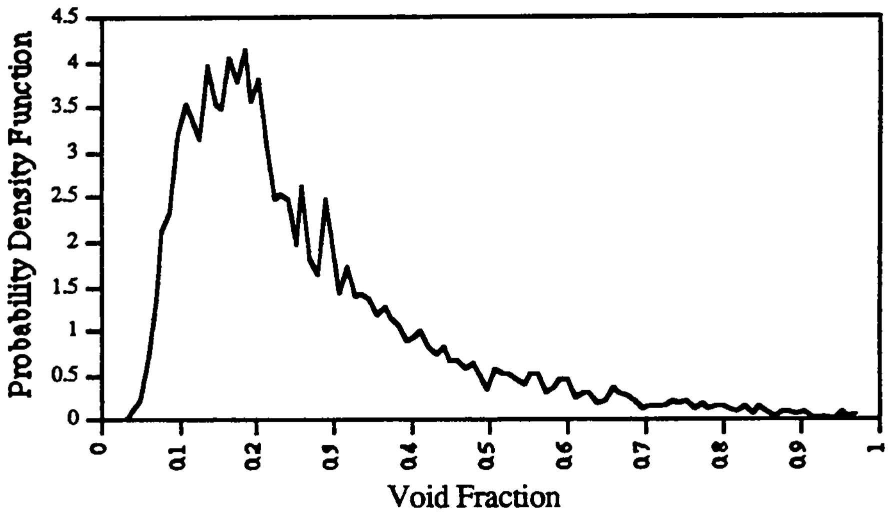

(b)

Figure 4.9: Flow Regime at Probe III : (a) Void Fraction Time Series, (b) Probabilty Density Function.

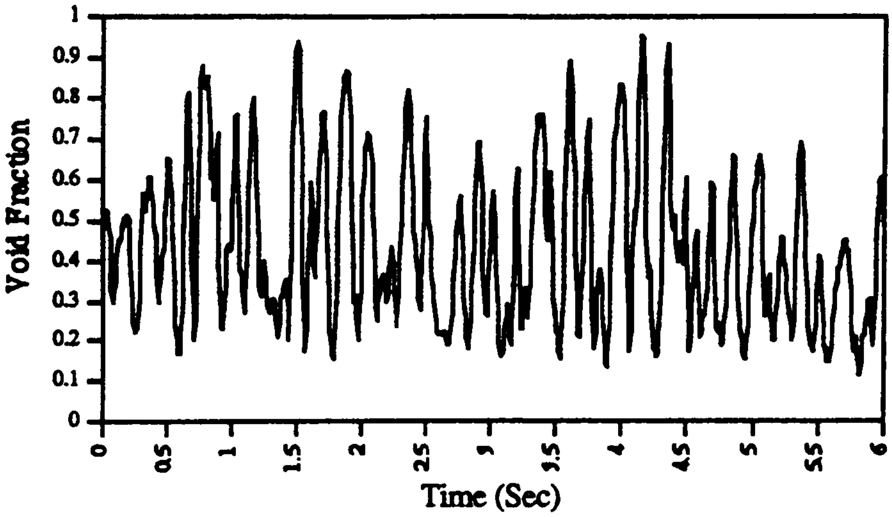

(a)

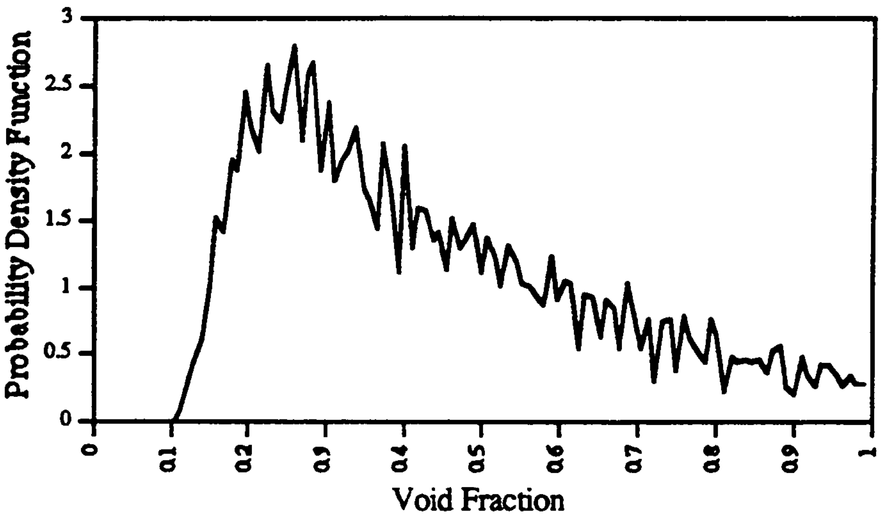

(b)

Figure 4.10: Flow Regime at Probe IV: (a) Void Fraction Time Series, (b) Probability Density Function.

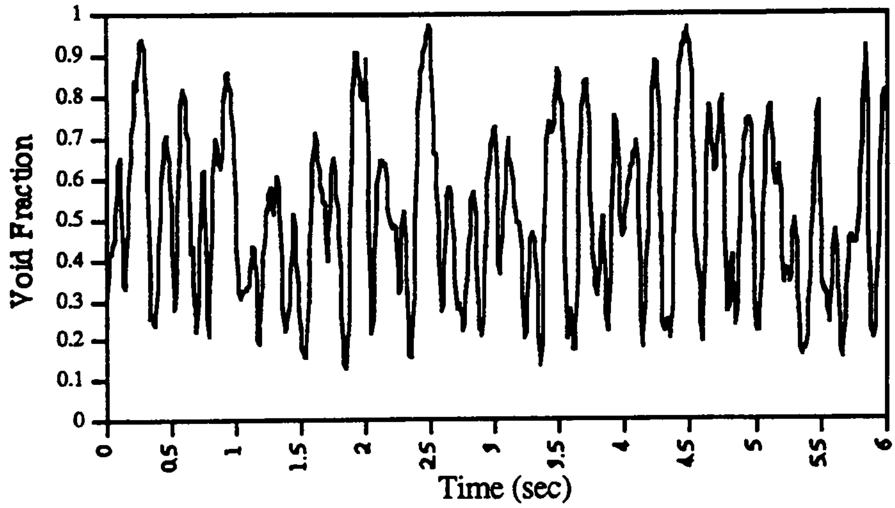

(a)

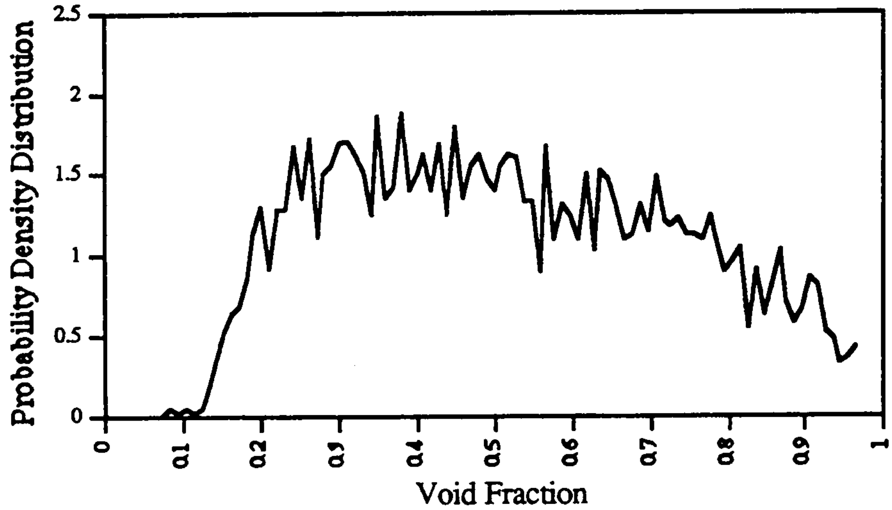

(b)

Figure 4.11: Flow Regime at Probe V: (a) Void Fraction Time Series, (b) Probability Density Function.

By plotting the PDFs of the four probes in Figure 4.12, the transition from bubbly to churn is seen as a shift in the PDF curve. The bubbly regime at probe II represents the highest distribution at low void fraction. In addition, the churn flow regime is characterized by a broadened spectrum.

4.5.3.2 High Frequency Contribution Fraction Analysis

The High Frequency Contribution Fraction was developed by Wang et al. [35,36] in order to set some criteria for the different flow patterns. The HFCF criteria depends on the experimental conditions and the type of sensor that has been used to record the void fluctuations. In the present study, the HFCF method is used to identify the flow regimes. For bubbly flow regime, the HFCF was found to be higher than 0.3. In addition, the HFCF for the churn flow is between 0.25 and 0.3. These criteria are different from the results obtained by Wang et al. who used an impedance probe with an arc geometry. Note also that Wang et al. performed their studies in an air water section with a co-current up flow while the present study is performed in a heated channel.

4.5.3.3 Power Spectral Density Analysis

A typical power spectral density of the void fraction fluctuation from the top four probes is shown in Figures 4.13 and 4.14, respectively. The power spectral density is computed using 10,000

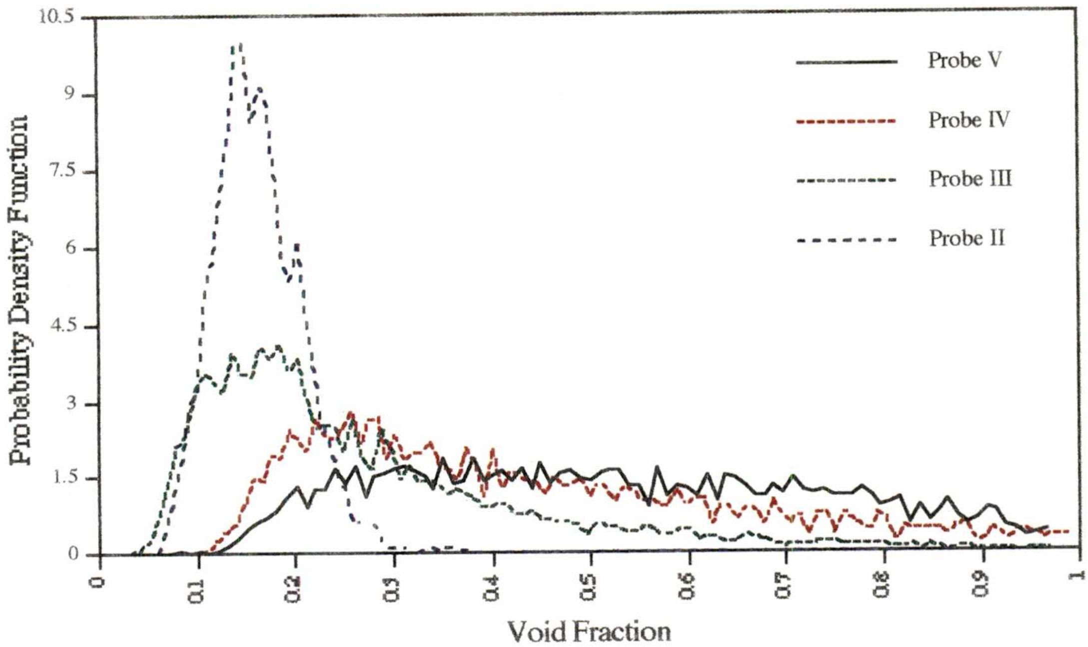

Figure 4.12 : Transition of Flow Regime in the Scaled Model Boiling Water Reactor

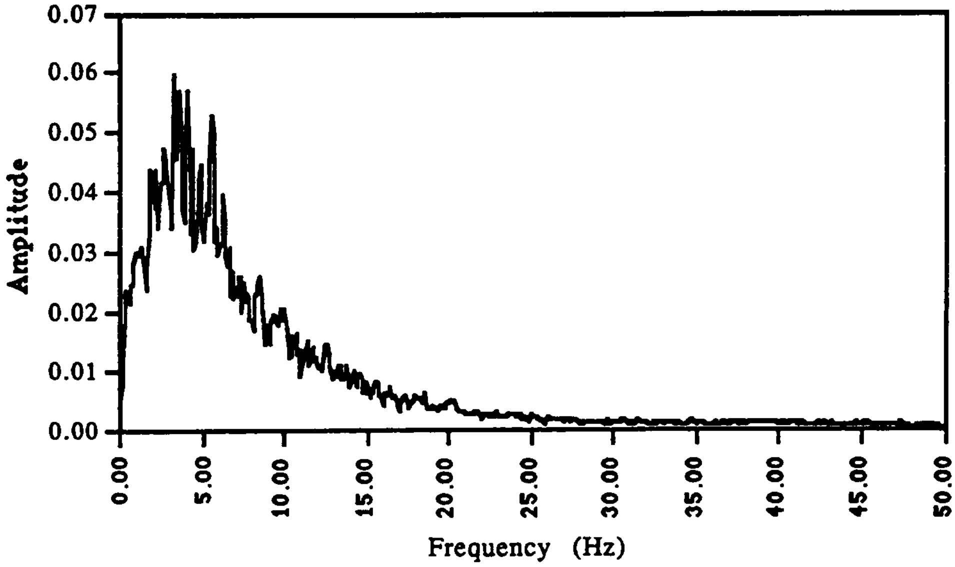

(a)

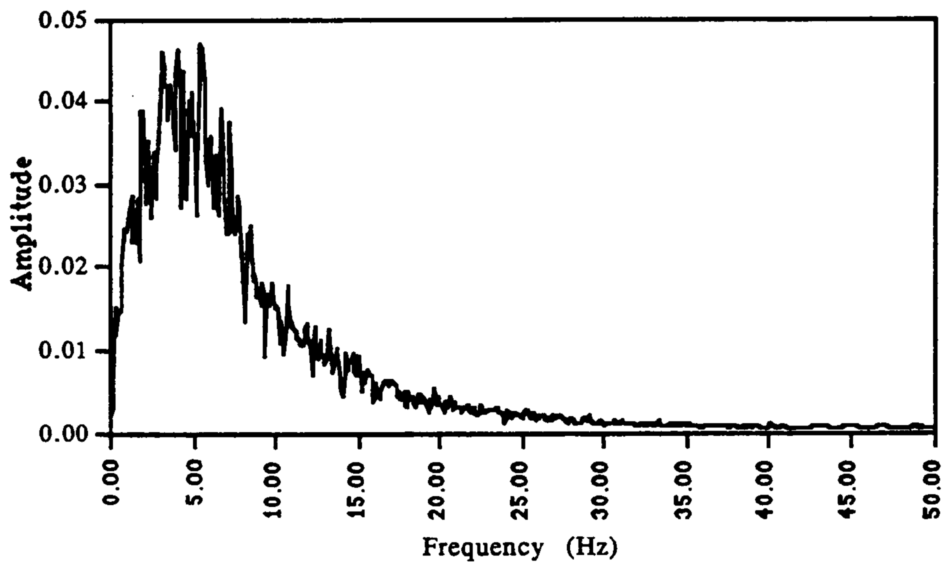

(b)

Figure 4.13: Void Fraction Power Spectral Density at: (a) Probe V; (b)Probe IV.

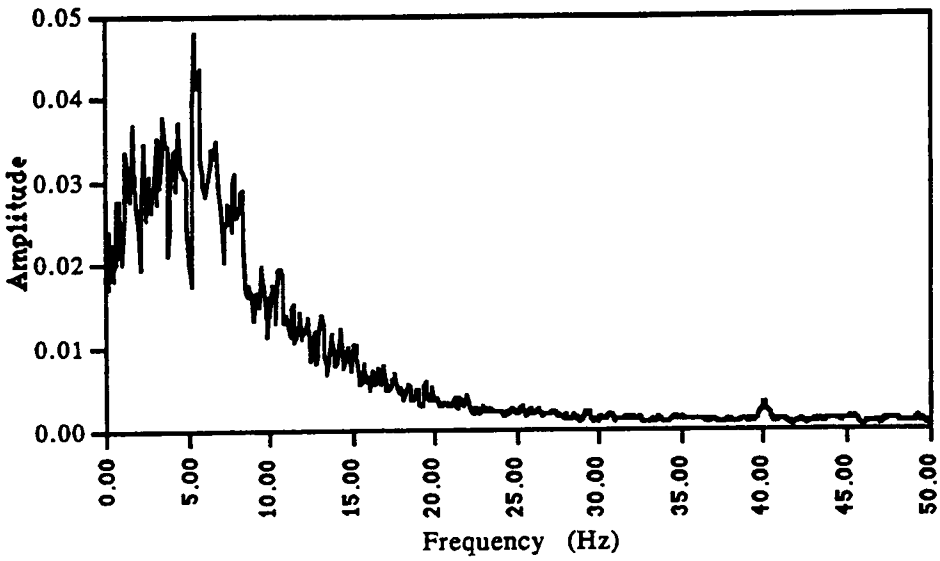

(a)

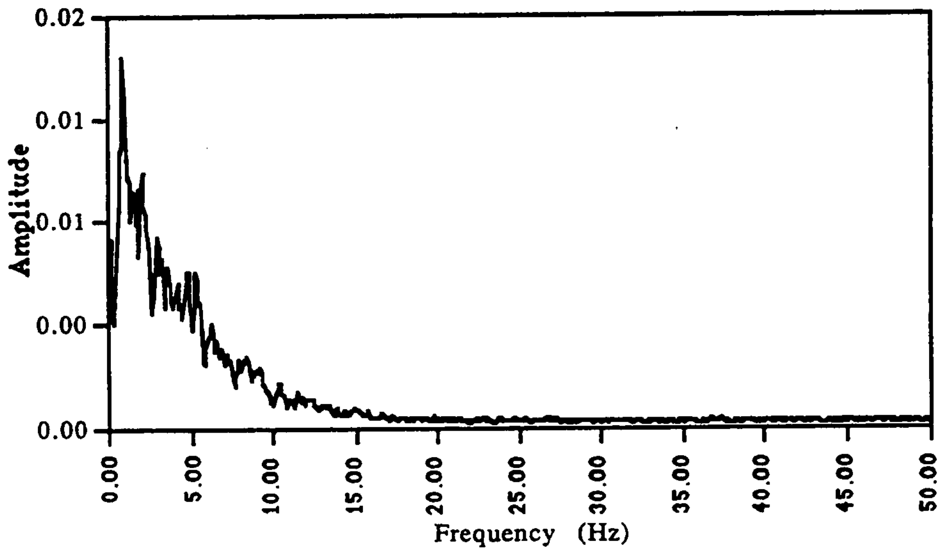

(b)

Figure 4.14: Typical Void Fraction Power Spectral Density at : (a) Probe III; (b) Probe II.

samples and Hanning windowing, whose size is set to 1024 points per block.

Figure 4.13.a shows the power spectral density of the void fluctuation at probe V, which represents the churn flow. The power spectrum exhibits multiple peaks with no clearly distinct frequency peak. The power spectrum is also broad in shape, which is a characteristic of chaotic behavior. This is reported by many authors as one of the properties of a chaotic system [2,42].

Figures 4.13.b and 4.14.a represent the power spectral densities of probes IV and III, respectively. These spectral densities have similar characteristics as that of probe V, whose power spectral density differs only in its high energy content. Figure 4.14.b shows the power spectral density for probe II, which is totally different from that of the other three spectra previously mentioned. In Figure 4.14.a, there is a shift of the spectrum to the left .

By analyzing the four power spectral densities of the four different probes, one can delineate between the churn flow regime and a bubbly regime with small vapor bubbles. However, this distinction becomes more difficult when the bubbly regime changes some of its characteristics, such as bubble velocity and size, as indicated by the response of probe III. As a result, it is suggested to look into other analysis techniques such as the Wavelet transforms to extract more information from the void signal

4.5.4 Identification of the Slug Flow Regime for Air-Water Flow in the SMBWR Channel

In this experiment, air was injected from the inlet feedwater line into the channel of the Scaled Model Boiling Water Reactor. The inlet air flow rate is set in a way that the slug regime is induced with the appearance of regular air plugs in the water channel.

The time series of the void fluctuation of the slug regime is shown in Figure 4.15.a. This figure is characterized by regular humps, which indicate the passage of big air bubbles across the sensor probe. The PDF is presented in Figure 4.15.b, which exhibits two peaks at high and low void fractions, respectively. The appearance of this so called double-humped PDF versus void profile is a distinctive characteristics for slug regime and it is reported in several studies [34,41,43]. In addition, this double-peak in the PDF distribution can be explained by the fact that the slug regime is a combination of bubbly and annular flow regimes. In the present study the annular regime was not observed in the air-water system. This is due to the fact that this regime requires very high air flow, which is not attained in the present system because of safety related operating limitations.

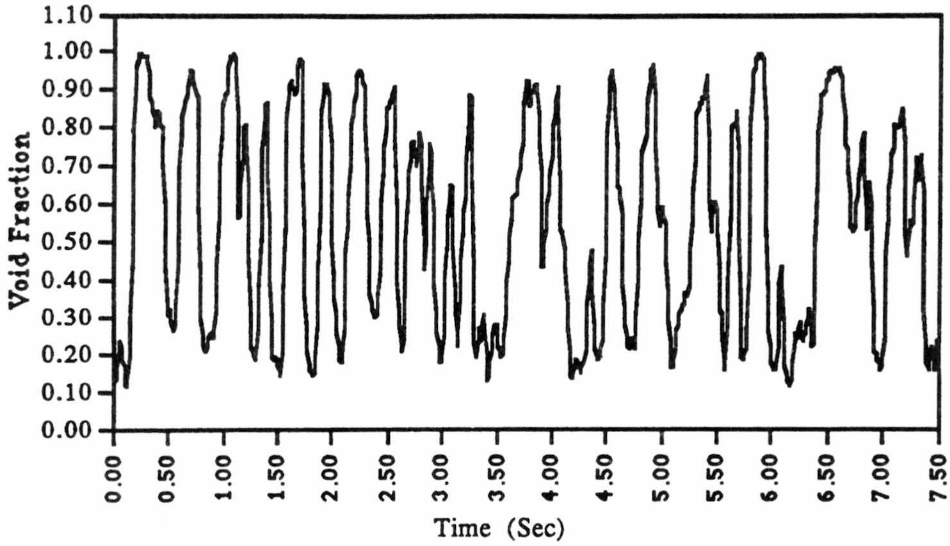

(a)

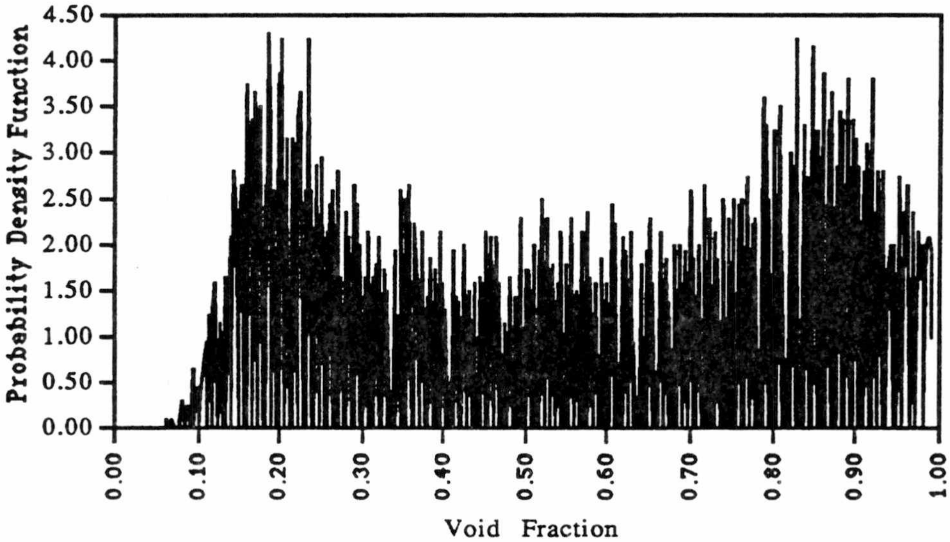

(b)

Figure 4.15: Slug Flow Regime at Probe V: (a) Void Fraction Time Series, (b) Probability Density Function.

4.6 Measurement of the Vapor Velocity in the Scaled Model Boiling Water Reactor

The objective of this section is to measure the vapor velocity in the boiling water channel. This analysis will enhance our understanding of the two-phase flow characteristics in the Scaled Model Boiling Water Reactor. The fluctuation of the void fraction signals are processed using the signal processing techniques discussed earlier in section 4.3.

4.6.1 Test conditions and Procedures

The void fraction signals were collected from the five void sensor probes in the boiling water channel, using the same methodology discussed in section 4.2. The five probes were each separated by a distance of 76.2 mm. In measuring the vapor velocity, two different methods are employed. In the first method, the basic concept of the cross-correlation function is applied to determine the delay time between two void signals, coming from adjacent void sensors. In the second method, the cross-spectral density is used. In this method the spectral density of each void signal is computed. This allows the relevant frequency range to be located. Then the cross-power spectral densities are determined between two adjacent probes. This gives the magnitude and the phase. The coherence function of each signal is determined to indicate the frequency range that the signals are correlated. Finally, the slope from the cross-phase curve is used in the region of high coherence to determine the time delay using Equation 4.13.

In this analysis, each data set consists of 5000 points. In addition, the Hanning window size used to compute the spectral estimates is fixed to 256 points per block, which represent a window of 2.5 seconds. This allows for enough time for the vapor bubbles to pass two neighboring probes in order to calculate the delay time. Furthermore, vapor velocity is determined by correlating signals from adjacent probes, which helps to get high coherence between the two signals.

4.6.2 Results and Discussions

The void signals from the top three probes (III, IV, V) are analyzed in order to determine the vapor velocity in the SMBWR.

4.6.2.1 Vapor Velocity Between Probes IV and V

Figure 4.16.a shows a typical cross correlation function for probes IV and V. The cross correlation curve has a negative correlation, which indicates that while one probe is covered with water liquid, the other probe is in the vapor region. This shape is charateristic of the slug and churn regimes as reported by Van Der Hagen [8]. The time delay, determined from the cross correlation

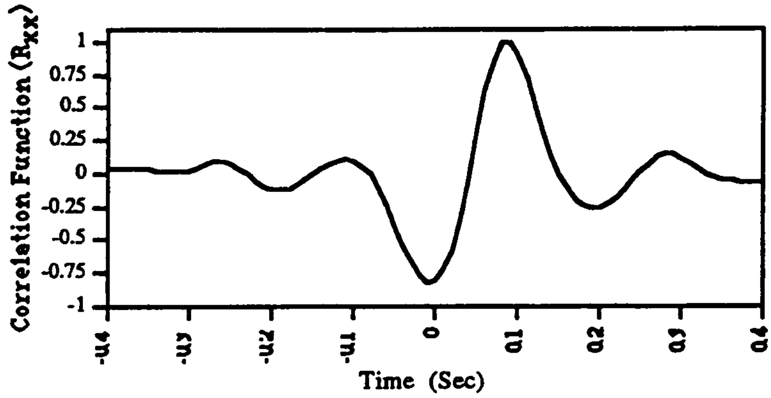

(a)

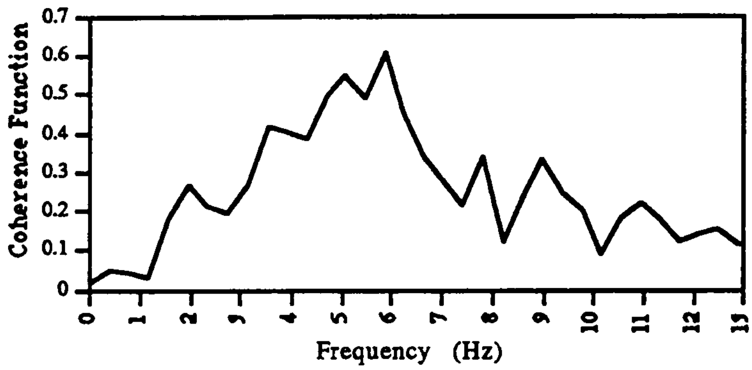

(b)

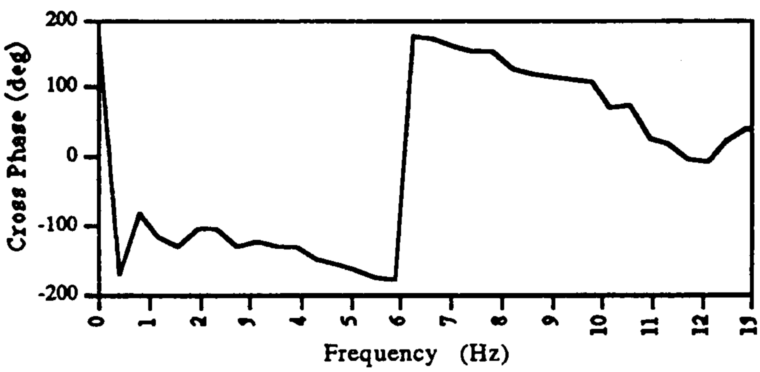

(c)

Figure 4.16: Measurement of the Vapor Velocity Between Probes IV and V: (a) Signals Cross Correlation, (b) Coherence Function, (c) Cross Phase.

curve is found to be between 0.08 and 0.09 sec, which gives a vapor velocity range of 0.95 and 0.85 m/sec. Next, the delay time is also determined from the cross power spectral density. A typical coherence function is shown in Figure 4.16.b. In this study the coherence function is found to be between 30% to 60%, which indicates that there is a good correlation between the signals of probes IV and V. The-cross phase is also given in Figure 4.16.c, which shows a linear function between the frequency and the phase for two particular frequency ranges. In addition, the cross phase plot exhibits a sudden change in the slope, which most probably refers to the reversal of flow in the system The vapor velocity is found to vary between 0.9 and 1.3 m/sec.

The present results are consistent with previous studies [44,45] since the churn regime is the dominant regime along the top three probes. Collins [44] investigated bubble velocities in the slug regime, formed by injecting air into a water channel. The slug bubble velocity was found to vary from 0.80 to 0.84 m/sec for a void fraction of 45%.

4.6.2.2 Vapor Velocity Between Probes III and IV

Figure 4.17 shows a typical correlation function, coherence and the cross phase for probes III and IV. The analysis of the cross correlation function gives a time delay 'between 0.8 and 0.9 sec. On the other hand, the time delay from the cross phase varies between

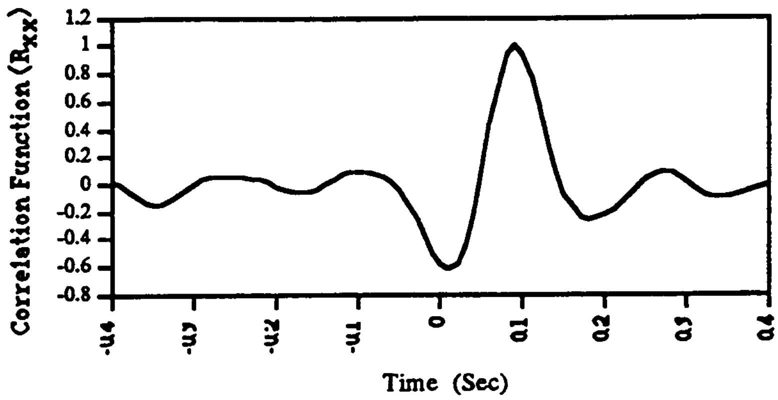

(a)

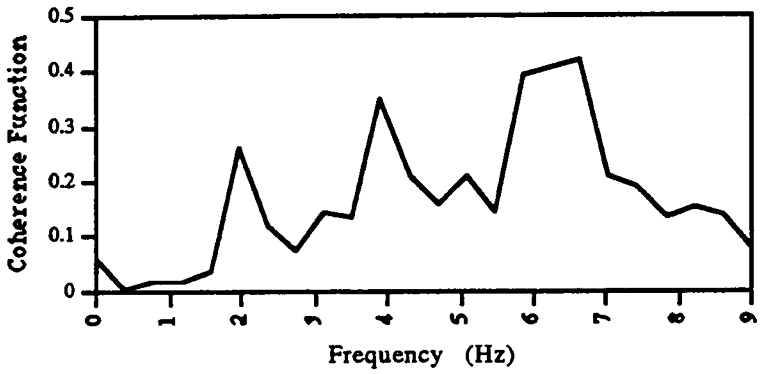

(b)

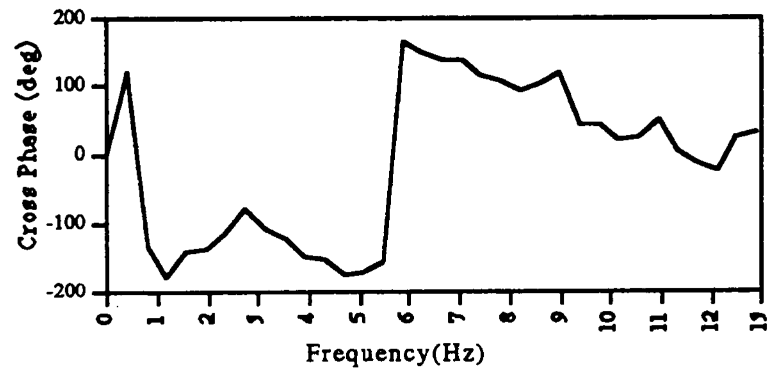

(c)

Figure 4.17: Vapor Velocity Measurement Between Probes III and IV : (a) Cross Correlation, (b) Coherence Function, (c) Cross Phase Angle

0.1016 sec and 0.084 sec , which yield a vapor velocity between 0.75 m/sec and 0.9 m/sec, depending on the particular experiment. In addition, the coherence function is not strong between the two probe signals, as shown in Figure 4.17.b.

The vapor velocity in the heated channel varies in time and with void size as the cross phase and the cross correlation function indicate. This study has shown that the void fraction sensor installed in the SMBWR, provides information on the behavior of the spatial and temporal void fraction fluctuations which provides a unique opportunity to explore the behavior of a heated channel.

CHAPTER 5

IMPLEMENTATION OF VOID-REACTIVITY FEEDBACK IN THE SCALED MODEL BOILING WATER REACTOR

5.1 Introduction

In commercial boiling water reactors, water boils inside the core to generate the steam used to produce electricity. The coolant is used both to produce vapor and to moderate fast neutrons to the thermal range in order to induce fission. Therefore, as the vapor content increases, most of the fast neutrons will not be moderated and hence will not initiate fission. This will result in a power reduction.

The void reactivity, which is defined as the change in reactivity produced by a unit change in void fraction, is the most important nuclear feedback parameter in a boiling water reactor. For example, the void reactivity in a conventional GE BWR is -1.0×10^{-3}, which is one order of magnitude larger than the moderator coefficient of reactivity (-1.0×10^{-4}) and 100 times larger than the doppler coefficient of reactivity (-1.0×10^{-5}) [46]. These reactivity feedback mechanisms also have different time delays. For example, a step increase in the reactor power will result in an increase in the fuel temperature with a time delay of 5 to 6 seconds. This delay is due to heat conduction through the gap and cladding of the fuel rods. The increase in the moderator temperature and core vapor content will follow within 2 to 3 seconds [9].

This chapter investigates the dynamic response of the Scaled Boiling Water Reactor Model with void reactivity feedback. The channel time-space averaged void fraction is obtained and coupled with a simple point kinetics model that is used to modulate the power in the system. In this section different aspects of the system response are presented, including the system behavior with and without void reactivity feedback.

5.2 Sensor Calibration in the SMBWR Channel

The installation of the void fraction sensor in the Scaled Model Boiling Water Reactor requires a liquid conductivity reference, determined by probe I. In the present setup the electronic circuits of the four top probes are calibrated using the circuit of probe I. The differences in the reading in the five electronic circuits are due to the use of variable resistors in the circuit design, which is required to increase the measurement range (see Figure 3.5).

The electronic circuit calibrations are performed by measuring different resistances. A calibration curve is generated for the four circuits as a function of the reading of circuit of probe I. This circuit correction is implemented in a LabVIEW Sub-Vi Program, shown in Figure 5.1.

During operation of the Scaled Boiling Water Reactor Model, the void fraction is measured only when the boiling length lies between probes I and II. This ensures that the liquid temperature at probe I is near saturation temperature.

5.3 Space and Time-Averaged Void Fraction

The void fraction fluctuation in the Scaled Model Boiling Water Reactor is characterized by its chaotic and turbulent behavior; and even at steady state the local void fraction component fluctuates in time. Therefore, it is useful to introduce some averaging operators that can be used to perform both space and time void fraction averaging. The instantaneous space-averaged void fraction, $\langle \alpha_v \rangle$ defined over a control volume V, occupied by the vapor phase, is written as [47,48]:

$$\langle \alpha_v \rangle = \frac{1}{V} \iiint_V \alpha_v dV = \frac{V_v}{V} = \frac{V_v}{V_v + V_l} \tag{5.1}$$

Similarly the liquid volume fraction is written as:

$$\langle \alpha_l \rangle = \langle 1 - \alpha_v \rangle \tag{5.2}$$

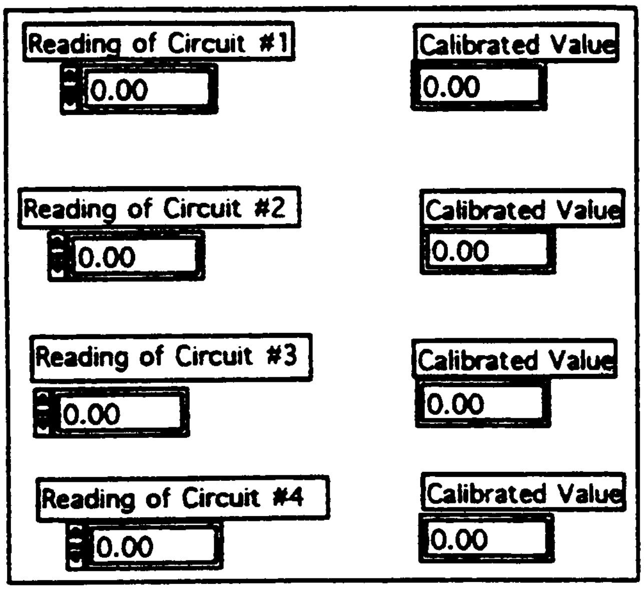

(a)

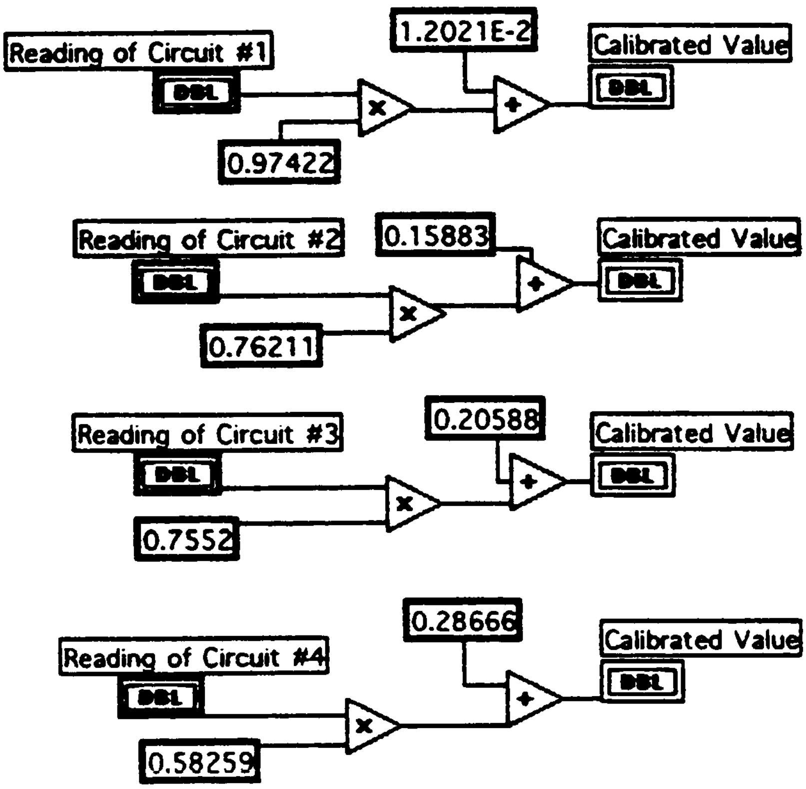

(b)

Figure 5.1 : Calibration of the Sensor Circuits

The space averaged void fraction is also determined in terms of the area average void fraction. The area average void fraction is given by

$$\{\alpha_v\} = \frac{1}{A_v}\iint_A \alpha_v dA \tag{5.3}$$

In addition, The local time-averaged void fraction is determined as:

$$\tilde{\alpha}_v = \frac{1}{\Delta t^*}\int_{t-\Delta t^*/2}^{t+\Delta t^*/2} \alpha_v dt \tag{5.4}$$

Where Δt^* is the time interval over which the averaging is taking place. The choice of the time interval is critical to obtain a reliable measurement of the void fraction. The duration of the time interval should be large enough to provide a meaningful average, but also short enough to allow detection of transients in the system. Next, the time and the volume-average void fraction can be defined as:

$$\langle\tilde{\alpha}\rangle = \frac{1}{\Delta t^*}\int_{t-\Delta t^*/2}^{t+\Delta t^*/2} \langle\alpha_v\rangle dt \tag{5.5}$$

In the Scaled Boiling Water Reactor Model the channel average void fraction is needed as a control input to modulate the power and to simulate the void-reactivity feedback. The void fraction is acquired at a rate of 100 samples per second using a Lab-View program, which is explained later. The void fraction from the top four probes is averaged in both the time and space domains. The time average void fraction signal from each probe is obtained by averaging 25 points each 0.25 sec. The space average void fraction is computed by averaging the four timed-averaged void fraction signals from the top four probes. The time-space averaged void fraction signal is then divided by the liquid reference conductivity at probe I. This conductivity ratio is then passed to the calibration curve to obtain the channel average void fraction.

5.4 Power Modulation in the Scaled Model Boiling Water Reactor

5.4.1 Overview of a Simple Point Kinetics Model in a BWR

In boiling water reactors the time behavior of the neutron flux in the reactor core can be approximated using the point kinetics equations with one delayed neutron group. This can be written as:

$$\frac{dn}{dt} = \frac{\rho(t) - \beta}{\Lambda} n(t) + \lambda c(t) \qquad (5.6)$$

and

$$\frac{dc}{dt} = \frac{\beta}{\Lambda} n(t) - \lambda c(t) \qquad (5.7)$$

Where,

n(t) is the neutrons density

β is the effective delayed neutrons fraction

$\rho(t)$ is the reactor total reactivity

Λ is the mean neutron generation time

λ is the average decay constant

C(t) is the neutron precursor concentration

The point kinetics equations are derived using a one group diffusion model [49]. Basically, this model assumes that the neutron transport in the core is governed by the diffusion process in which the neutrons diffuse from regions of high neutron density to regions of low density. In deriving the point kinetics equations, one is assuming that all the neutrons have the same energy and a uniform transport velocity. In addition, the spatial variation of the neutron flux in time is neglected.

The point kinetics equations can be rewritten in terms of the reactor power by assuming that the neutron variation in the core is proportional to the power. For a given control volume V, the reaction rate is expressed as:

$$R = \Sigma_f \Phi = (N\sigma_f)(nv) \tag{5.8}$$

Where,

Σ_f is the macroscopic fission cross section

Φ is the neutron flux

N is the target nuclei density, $\#/cm^3$.

σ_f is the microscopic fission cross section, neutron/cm^2

n is neutron density, neutrons/cm^3

v is the average neutron velocity, cm/sec

The reactor power in the reactor core of volume V can be written as:

$$P = (NV)\sigma_f(nv)p \tag{5.9}$$

Where, p is the energy produced per fission. Therefore the power behavior in the reactor core can be written as:

$$\frac{dP}{dt} = \frac{\rho(t) - \beta}{\Lambda} P(t) + \lambda C(t) \tag{5.10}$$

and

$$\frac{dC}{dt} = \frac{\beta}{\Lambda} P(t) - \lambda C(t) \tag{5.11}$$

The study of the point kinetics equations indicates that the reactor power is influenced by two neutronic effects. First, most of the neutron fission appears within 10^{-14} sec of the fission event. These neutrons are referred to as prompt neutrons. Second, 1% of the neutron population appears with an appreciable time delay that ranges from 0.6 to 80 seconds [49]. These delayed neutrons are mainly produced from the decay of radioactive fission products. Even though these delayed neutrons are a small fraction, they contribute in increasing the effective neutron life time to $l_f \approx 0.1\text{sec}$ for a commercial reactor, which allows for control of the fission chain reaction.

5.4.2 Prompt Jump Approximation

In studying the point kinetics equations, one can notice that any step change in the reactivity results in transient behavior in the time scale of the prompt neutron life. This behavior is then followed by a more slowly varying response governed by the delayed neutrons. Therefore, the point kinetics equations can be simplified by eliminating the rapid transient and taking the neutron lifetime to be zero by setting the term $\frac{dP}{dt}=0$. This approximation is called prompt jump approximation and it is frequently used in numerical studies to eliminate the very short time scale, represented in Λ, which unnecessarily complicates the analysis when slower phenomena are of interest. The response time scale of the void feedback mechanism, $\tau_{delay} \approx 5$ to 10 sec, is slow relative to both prompt and the delayed neutron groups. Therefore, the prompt jump approximation is a good approximation of the point kinetics equations, which can be reduced to [49]:

$$[\rho(t)-\beta]\frac{dP}{dt}+\left[\frac{d\rho}{dt}+\lambda\rho(t)\right]P(t)=0 \qquad (5.12)$$

Using LabVIEW, This equation is utilized in the SMBWR where the power is coupled to the total reactivity $\rho(t)$, which can be written as:

$$\rho(t)=\rho_{ext}+\alpha_v<\overline{\alpha}> \qquad (5.12)$$

Where,

ρ_{ext} is the external reactivity

α_v is the void fraction coefficient of reactivity

$<\overline{\alpha}>$ is the channel average void fraction.

5.5 Implementation of the Void Reactivity Feedback in LabVIEW Program

The LabVIEW program, developed to simulate the void reactivity feedback in the Scaled Boiling Water Reactor Model, is called System with Void Reactivity. This program implements the prompt jump approximation, discussed earlier. In addition, this program monitors the system pressures, temperatures and channel exit and average void fraction. The main functions of the program are shown in Figure 5.2.

5.5.1 Front Panel

The front panel gives the user a monitoring window where virtual instruments, such as pressure transducers and thermometers are shown. In the front panel the user monitors the system pressure, temperature, void fraction, and power variation in the boiling channel. Figure 5.2.a shows the general layout of the front panel.

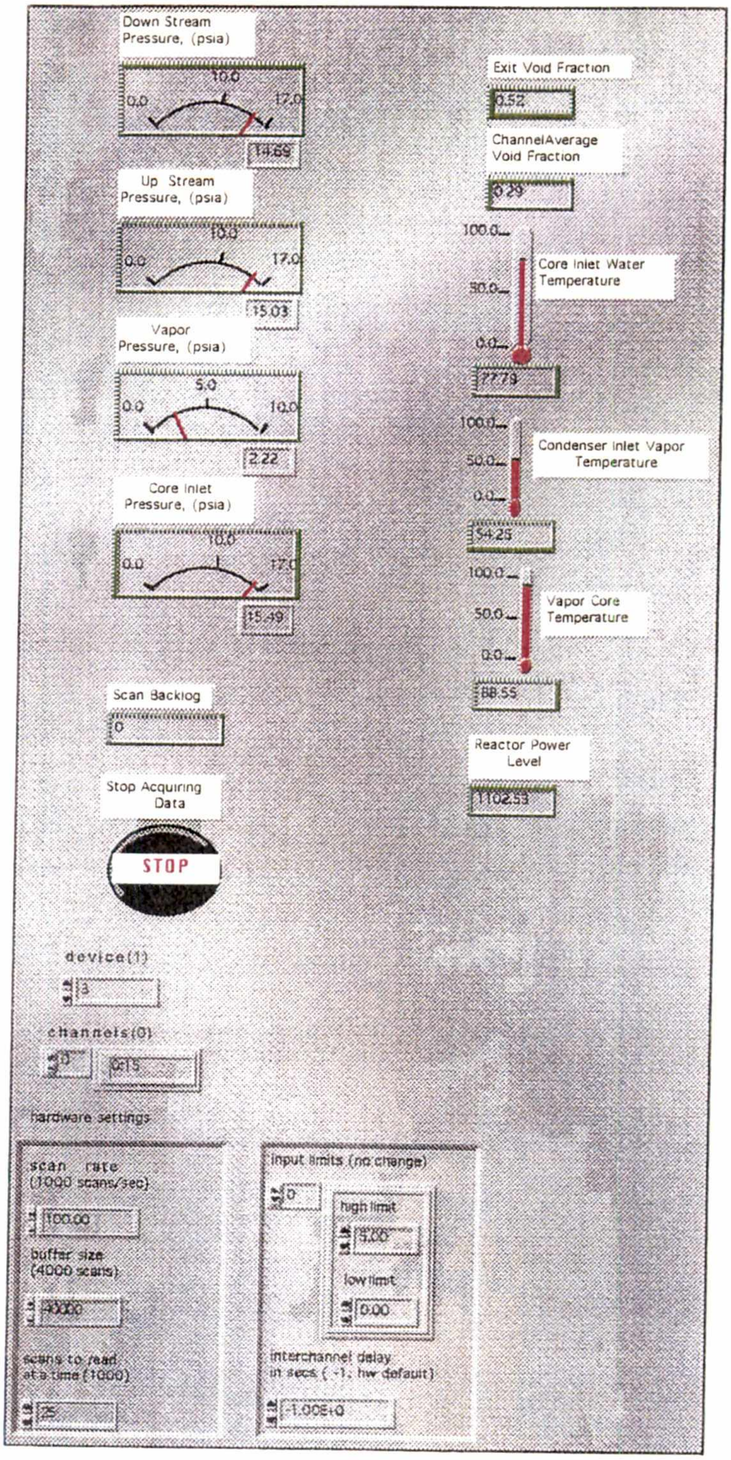

(a)

Figure 5.2: LabVIEW Program for the System Model with Void Reactivity Feedback: (a) Front Panel, (b) Block Diagram

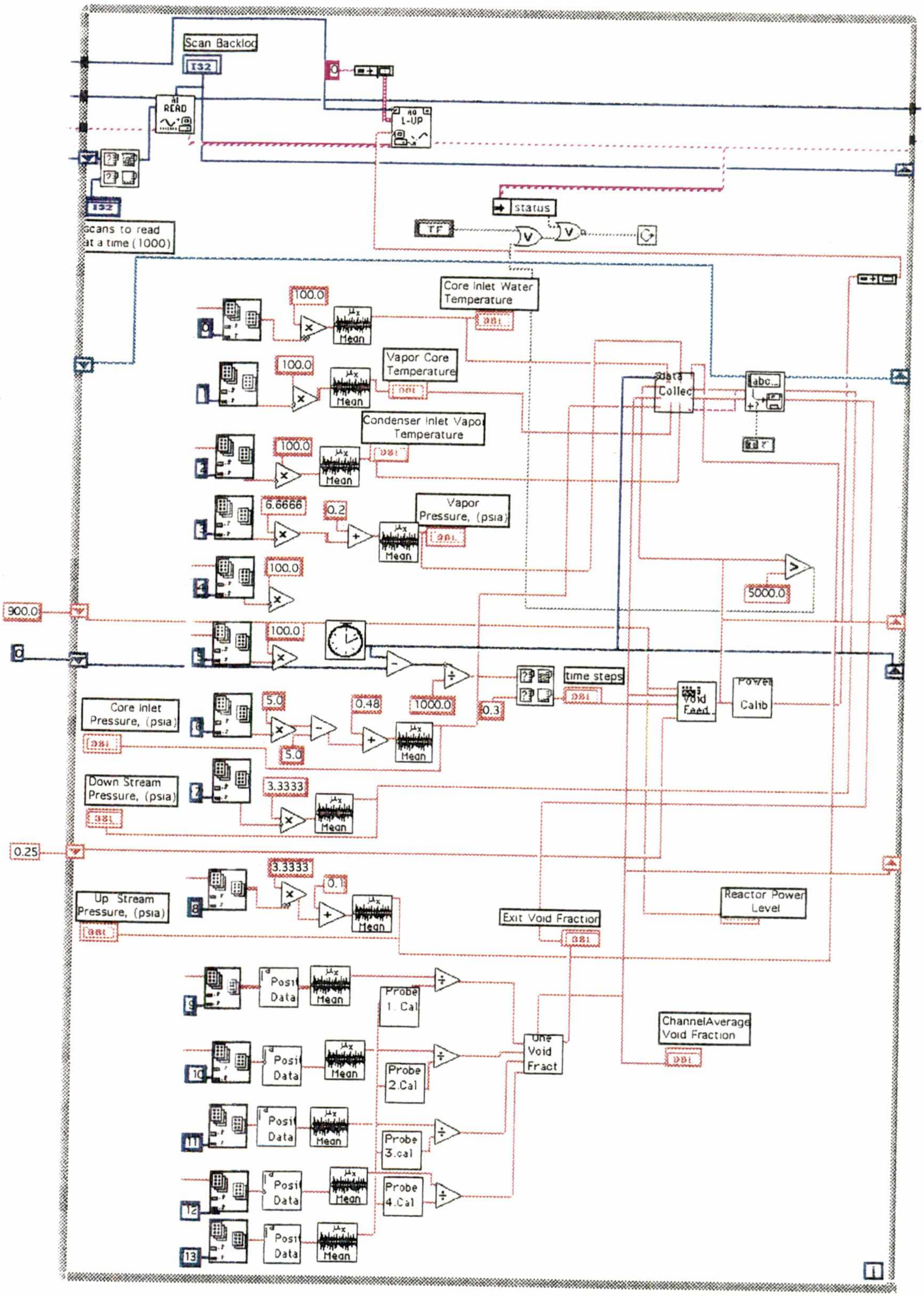

(b)

Figure 5.2 : (Continued)

5.5.2 Block Diagram

The block diagram is considered as the source code for the program. The initial conditions for the power and the average void fraction are set outside the While Loop, shown in Figure 5.2.b. The channel average void fraction is calculated from the void fraction signal that is acquired at a rate of 100 points per second. This rate is controlled in the front panel using the scan rate command. In each acquisition, a set of 25 points of the void signal is passed to the loop. This set of data is screened in order to eliminate spurious negative voltage values, caused by the power controller. This is accomplished by a Sub-Vi program called Positive Data, whose front panel and block diagram are shown in Figures 5.3.a and 5.3.b, respectively. The void signal data is then averaged by a Sub-Vi program called Mean. The Mean program is provided in the LabVIEW library functions. Next, the averaged signal is divided by the reference liquid conductivity voltage of probe 5. The Conductivity ratio of the top four probes are then used to determine the channel average and exit void fraction. This is accomplished in a Sub-Vi program called Void Fraction (see Figure 5.4), which employs the void fraction calibration curve discussed in chapter 3. The average void fraction is then passed to Void-Reactivity Sub-Vi program to compute the appropriate value for the channel power using the prompt jump approximation. This program is shown in Figure 5.5. This power is converted to a voltage value and sent to the power controller. Finally,

(a)

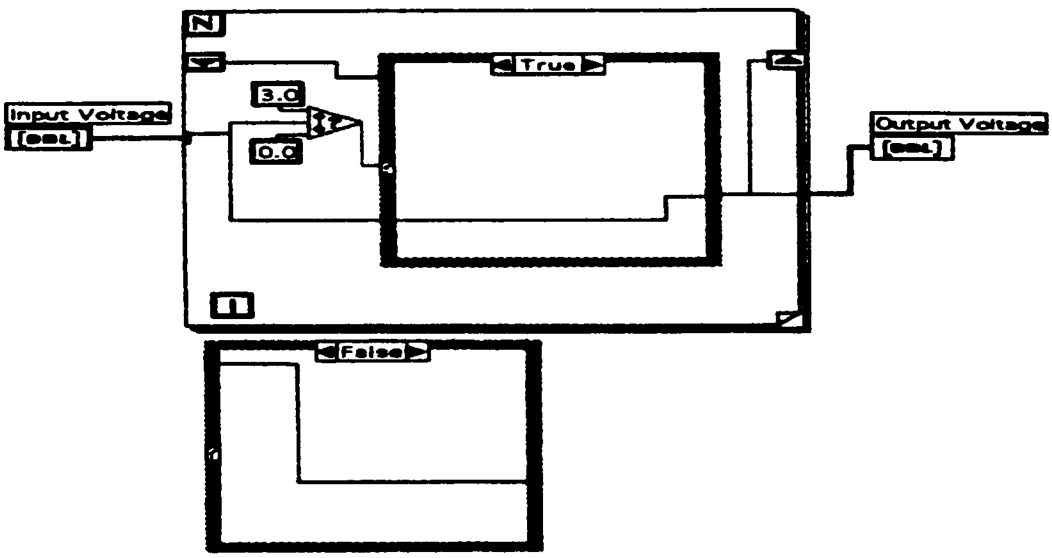

(b)

Figure 5.3: Positive Data LabVIEW Program: (a) Front Panel, (b) Block Diagram.

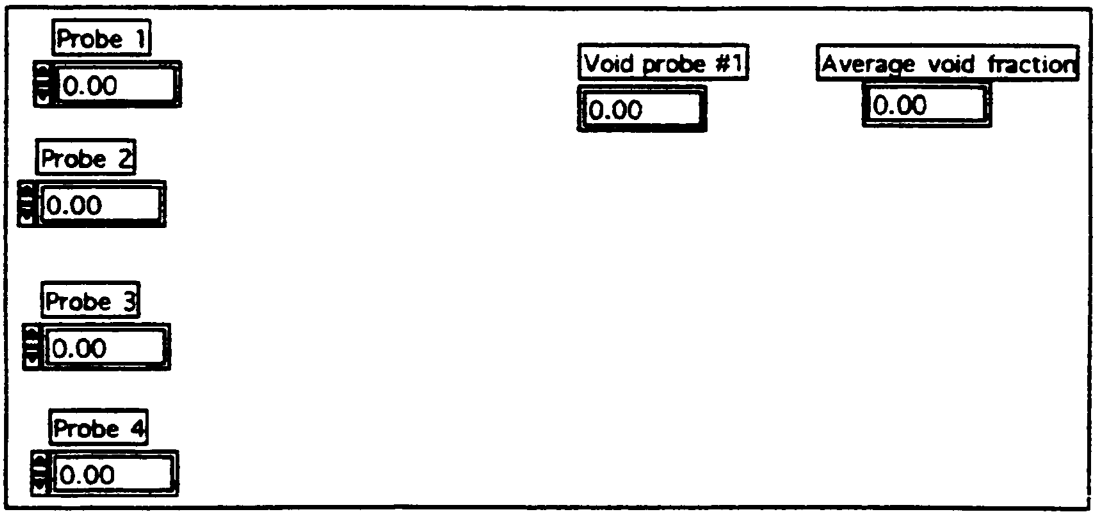

(a)

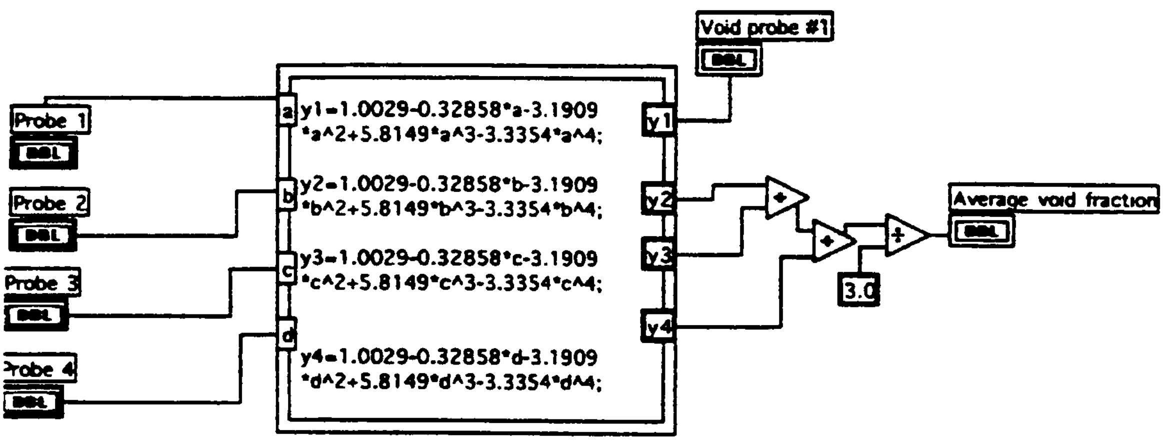

(b)

Figure 5.4: Void Fraction Calibration Curve LabVIEW Program: (a) Front Panel, (b) Block Diagram.

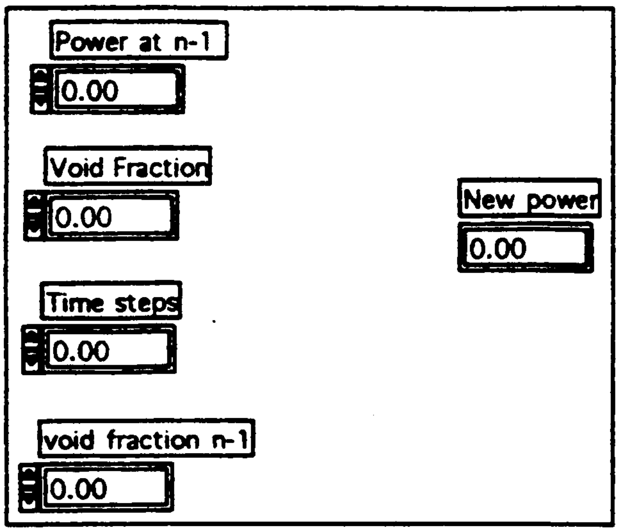

(a)

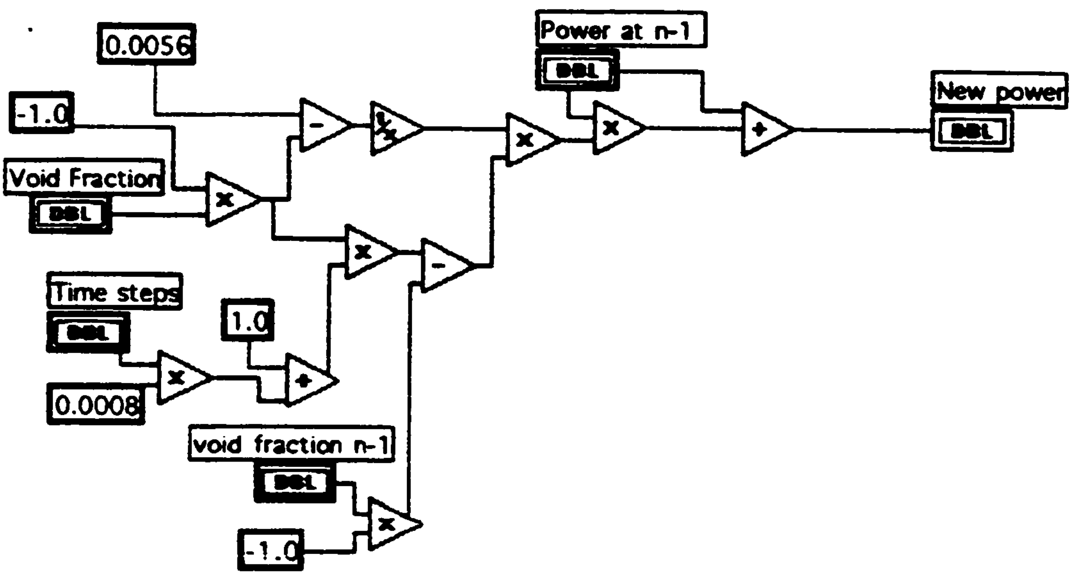

(b)

Figure 5.5: Void Reactivity LabVIEW Program: (a) Front Panel, (b) Block Diagram

the data are recorded in a spread sheet file using a Sub-Vi program called DATA.

5.6 Steady State Condition

In each test run, the Scaled Model Boiling Water Reactor is brought to steady state before any transient case is performed. The steady condition is achieved by draining the core channel and the condenser of used water. This ensures that water ionization will not build up in the system. A vacuum pressure is applied on the system to an absolute pressure of 25 in of mercury and the manual control valve is closed. The channel core and the condenser are filled with fresh water. The water level in the core should cover the heaters and the condenser should be filled to a 2 in height. The power of 500 W is applied and the system pressure is allowed to build up to 9 Psia. The manual control valve is slowly opened to allow steam into the condenser. The condenser cooling water is turned on. The power is then increased to 900 W and the feed water pump is turned on. The manual control valve is adjusted until the boiling channel is stable at 12 Psia. Steady state is achieved.

Figure 5.6 shows the vapor pressure, vapor temperature, channel average void fraction, inlet core pressure, inlet water temperature and condenser inlet pressure at the steady state condition. The system parameters are at constant operating conditions except the inlet condenser pressure. The variation in

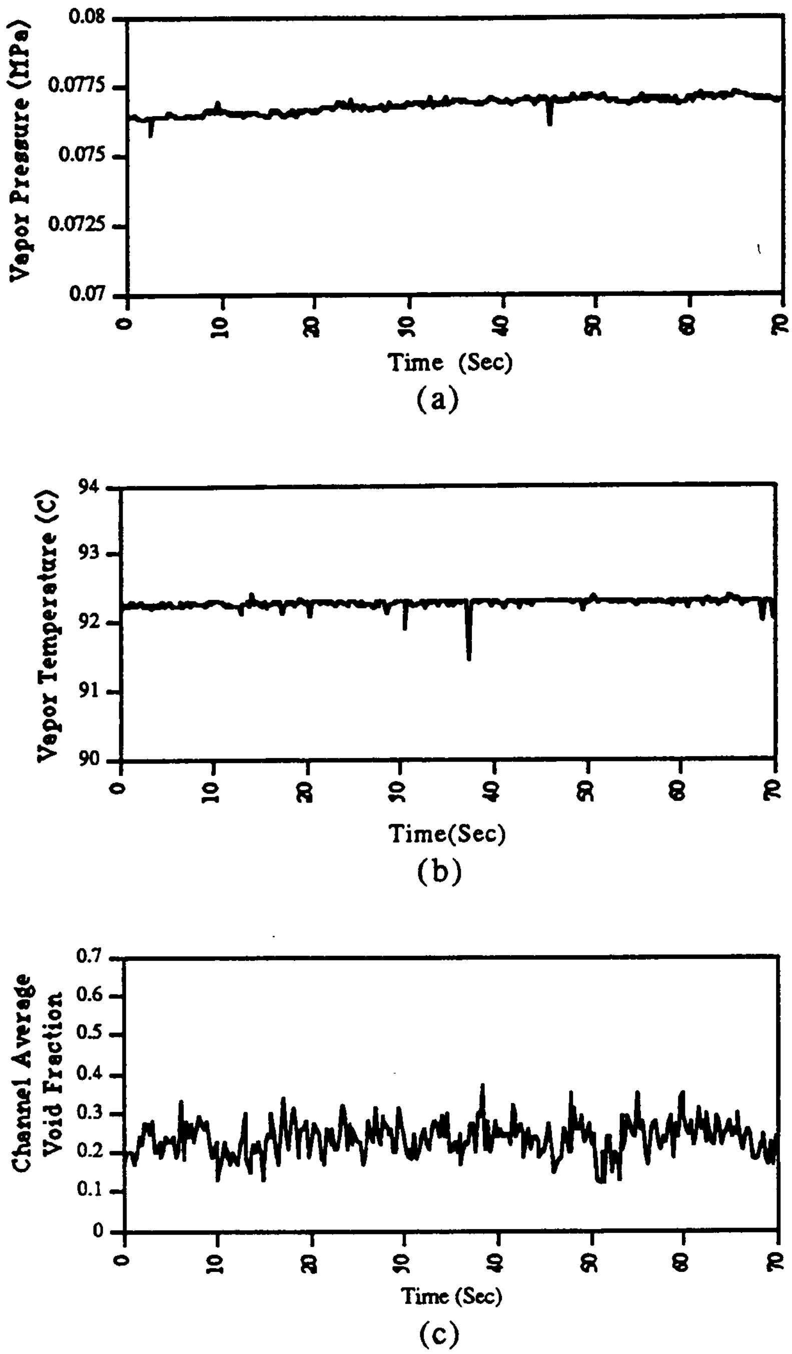

Figure 5.6: Steady State Conditions of the SMBWR: (a) Vapor Pressure, (b) Vapor Temperature, (c) Channel Average Void Fraction, (d) Inlet Core Pressure, (e) Inlet Water Temperature, (f) Inlet Condenser Pressure.

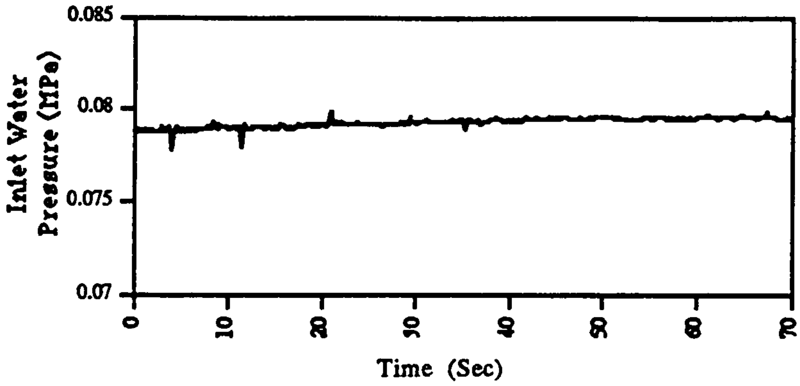

(d)

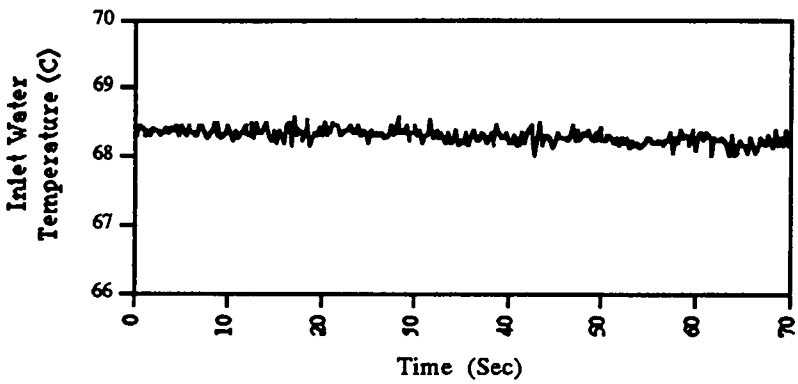

(e)

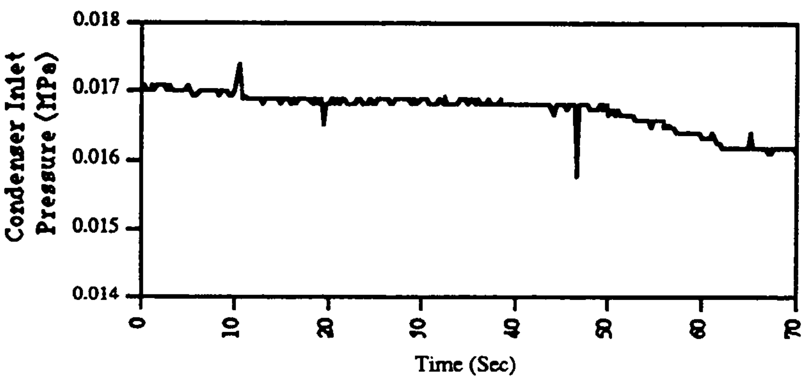

(f)

Figure 5.6: (Continued)

condenser pressure is due to the charging and discharging of the compressor supplying in the air inductor. Figure 5.7 shows the effect of the compressor charging and discharging on the inlet condenser pressure and temperature without operating the reactor model. As one can see the pressure oscillation has period of 300 sec; and the oscillation amplitude is around 0.002 MPa. These oscillations do not effect the behavior of the boiling channel since the manual control valve is always choked.

5.7 Results and Discussion

The objective of this section is to investigate the effect of void reactivity feedback on the system response. This shows the differences between a simple heated channel and that with void reactivity feedback. Next, the effect of the void reactivity coefficients on the response of the Scaled Model Boiling Water Reactor is presented. In this study several experiments are conducted at different operating conditions during steady-state and transient conditions. In the transient cases the system is brought to steady-state and then a step increase in the power or steam flow is effected. The step increase in the steam flow is accomplished by closing the control valve near the condenser. The step increase in the power is performed by changing the power set-point in the LabVIEW program used to control the power to the heaters. Also, the Scaled Boiling Water Reactor Model is run at steady state conditions for 9 minutes,

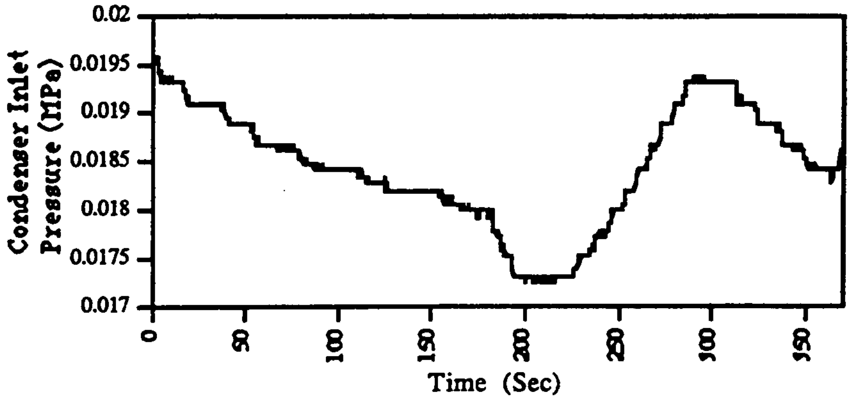

(a)

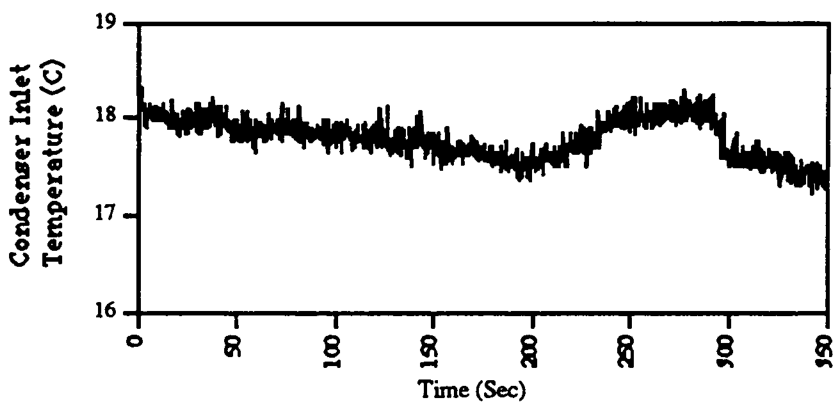

(b)

Figure 5.7: Effect of the Compressor operation on the Inlet Condenser Pressure and Temperature: (a)Condenser Inlet Pressure, (b) Condenser Inlet Temperature.

with and without void reactivity feedback, in order to determine the effect of the power coupling on the temporal behavior of the channel average void fraction.

5.7.1 Step Power Change

For a simple heated channel without void reactivity feedback, the step change in the power level results in a change in the system operating conditions, which can lead to either a stable or unstable system. To illustrate, the heater power is increased stepwise from 700 to 900 Watts with a constant inlet feedwater flow rate of 19.5 ml per minute. This results in a change in the system parameters. Figure 5.8 shows these changes. The step power increase puts more heat into the boiling water channel. This results in an increase in the vapor pressure, temperature and the channel average void fraction, as shown in Figures 5.8.a, 5.8.b, 5.8.c, respectively. The power increase also effects the inlet feedwater temperature due to the increased recirculation. This can be seen in Figure 5.8.d, which shows the temperature history of the inlet water temperature. This figure indicates that the inlet water temperature has first increased due to the power change and then decreased because of the increase in the feedwater inlet flow.

The implementation of the void reactivity feedback changes the system response as shown in Figure 5.9, which shows the change of the power level, average void fraction and the vapor pressure,

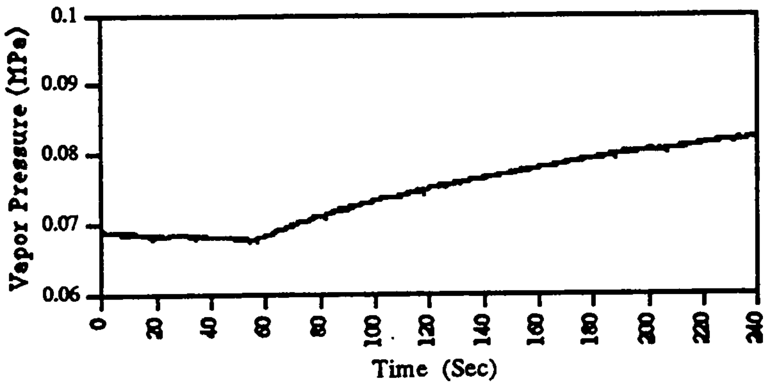

(a)

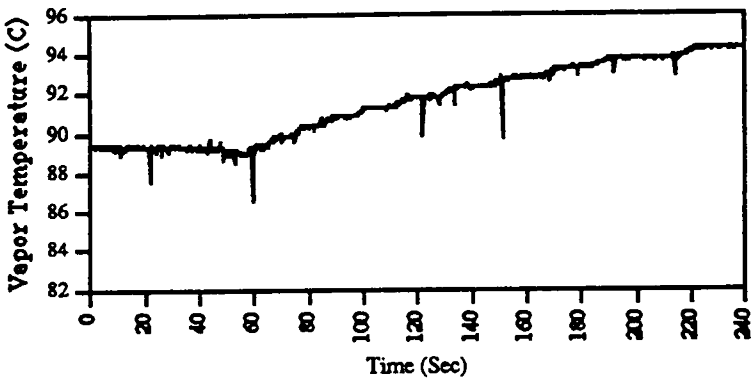

(b)

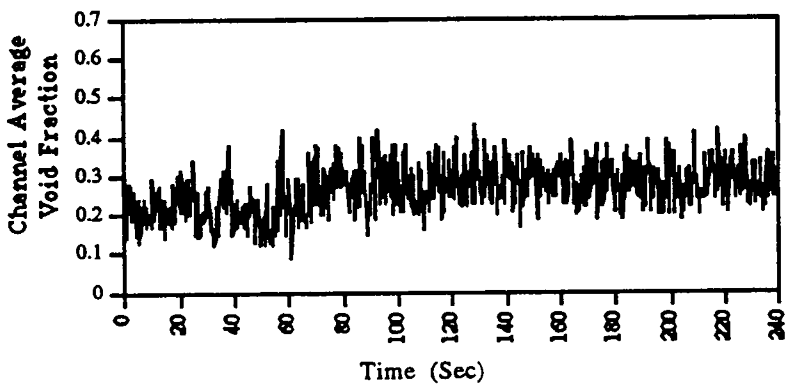

(c)

Figure 5.8: System Response for a Power Step Change from 700 to 900 W : (a) Vapor Pressure, (b) Vapor Temperature, (c) Channel Average Void Fraction, (d) Inlet Core Temperature, (e) Inlet water Temperature, (f) Condenser Inlet Pressure

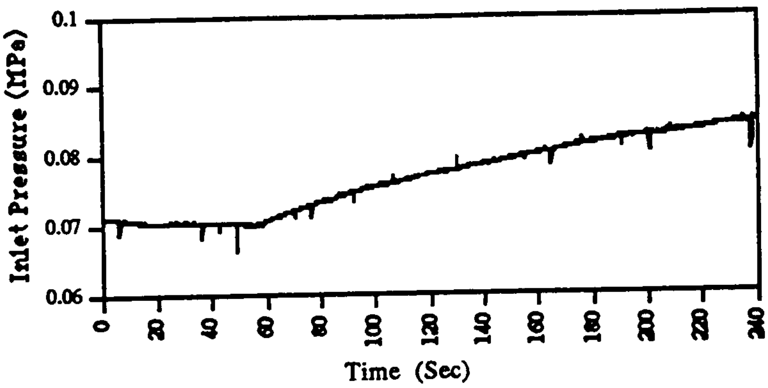

(d)

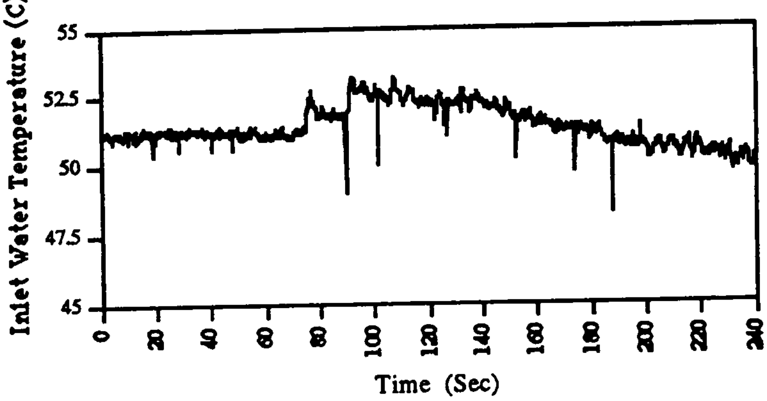

(e)

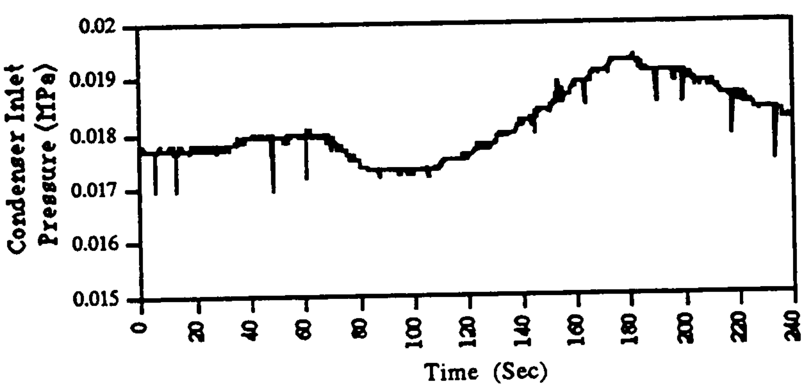

(f)

Figure 5.8 : (Continued)

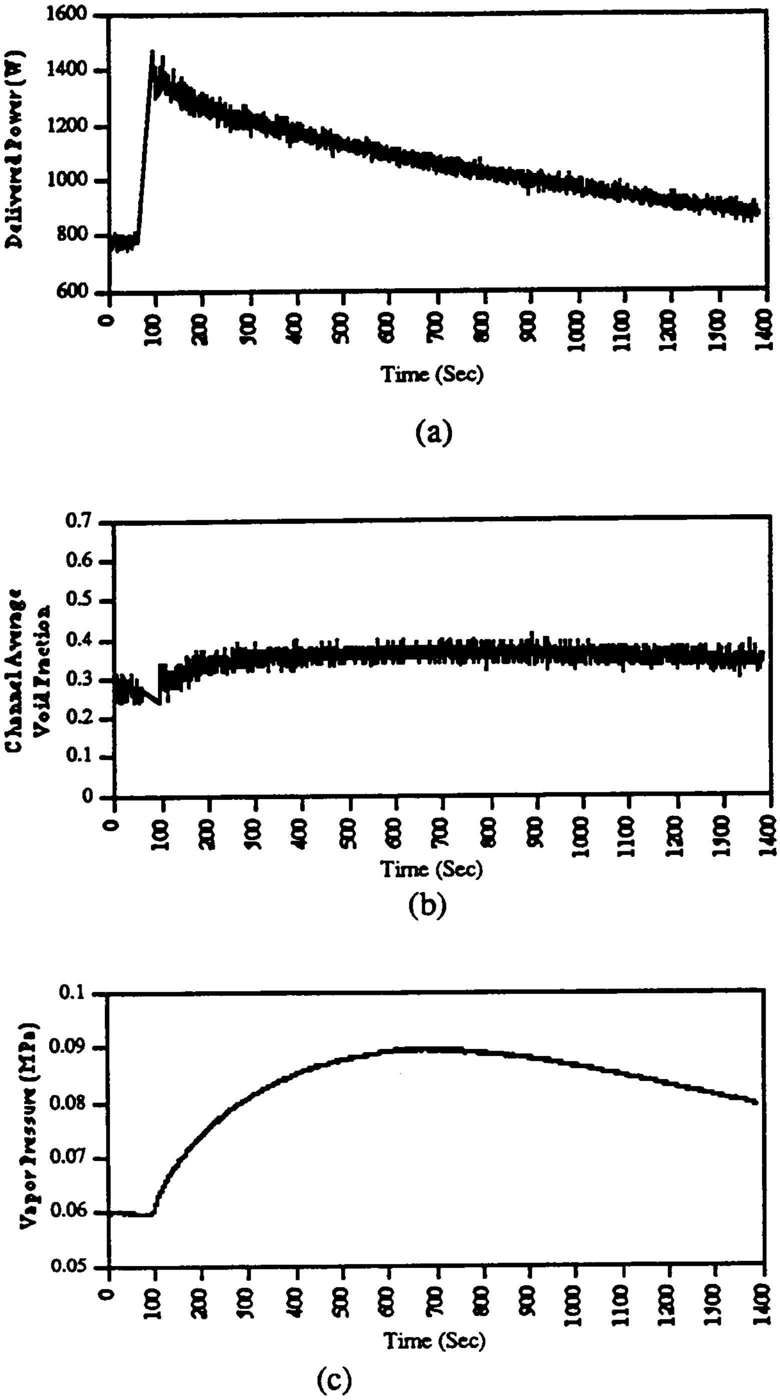

Figure 5.9 : System Response to a Step Change in the Power Level with a Negative Reactivity Coefficient of -0.01: (a) Power Level Change; (b) Channel Average Void Fraction; (c) Vapor Pressure.

respectively, for a reactivity coefficient of minus 0.01. The step increase in the power level causes the channel average void fraction and the system pressure to increase. The increase of the channel average void fraction causes the power to decrease due to the negative reactivity feedback. This process continues until the system reaches a stable condition.

For a positive reactivity coefficient of 0.0001, the step change in the power level increases the channel average void fraction and the vapor pressure. Because of the positive reactivity the system pressure increases monotonically, as shown in Figure 5.10. However, the rate of change of both the power and channel average void fraction is relatively slow. This is due to the relationship between the system pressure and the steam enthalpy, and also it is a result of the increase in vapor slip for $\alpha > 60\%$, which allows the flow quality to increase without significant increase in the vapor volume fraction.

5.7.2 Steam Flow Step Change

In this case the control manual valve is suddenly closed and the system response is recorded. For a simple heated channel, the closing of the manual valve increases the system pressure. Figures 5.11.a and 5.11.b show respectively the time history of the vapor pressure and temperature, which starts to increase as the valve is closed. This has resulted in a decrease in the channel average void fraction, shown in Figure 5.11.c. The inlet water pressure is presented in

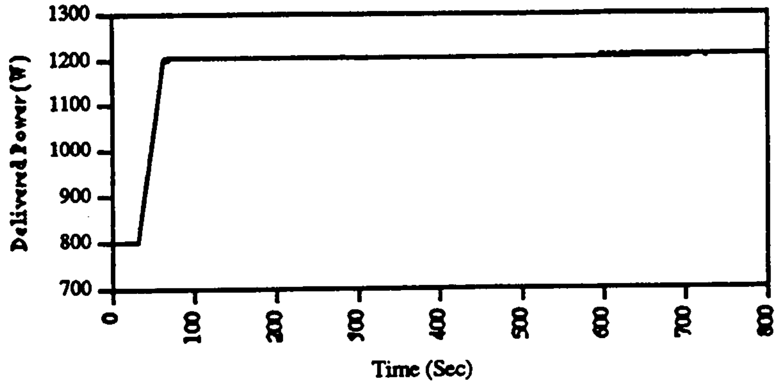

(a)

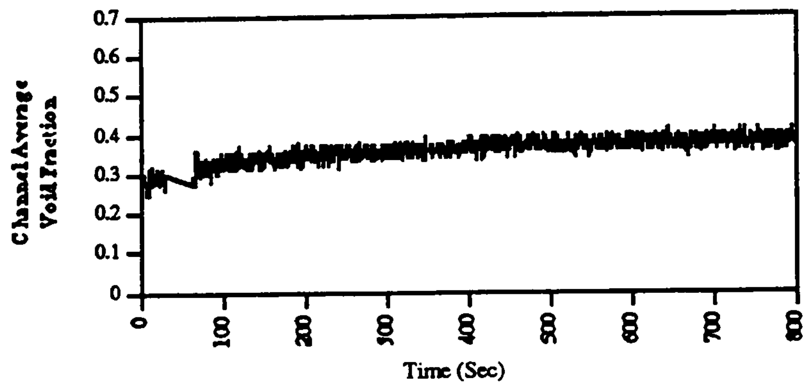

(b)

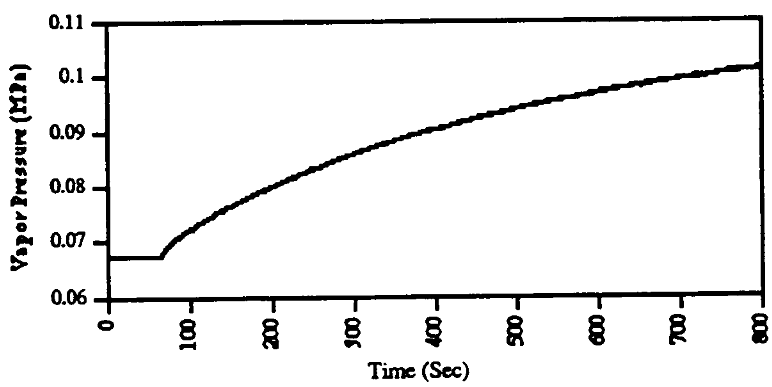

(c)

Figure 5.10: System Response for a Step Power Change with a Positive Reactivity Coefficient of 0.0001: (a) Power level; (b) Channel Average Void Fraction; (c) Vapor Pressure.

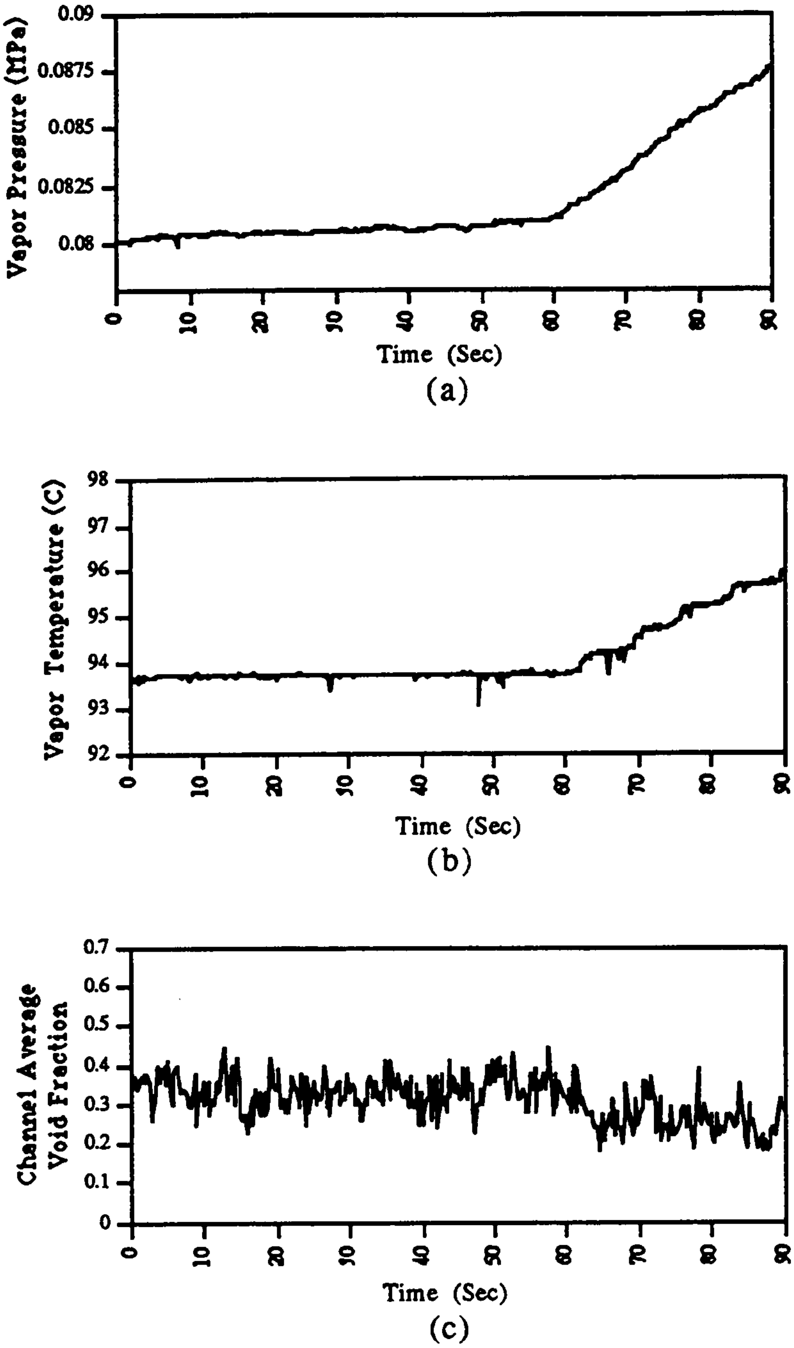

Figure 5.11: System Response for a Pressure Step Change in a Simple Heated Channel: (a) Vapor Pressure; (b) ` Vapor Temperature; (c) Channel Average Void Fraction; (d) Inlet Water Pressure; (e) Inlet Water Temperature; (f) Inlet Condenser Pressure.

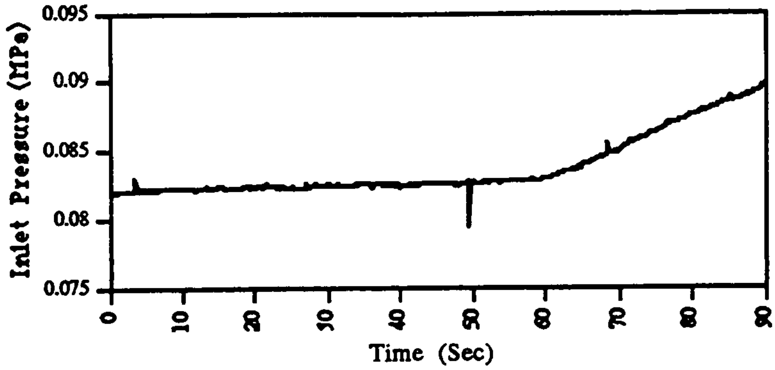

(d)

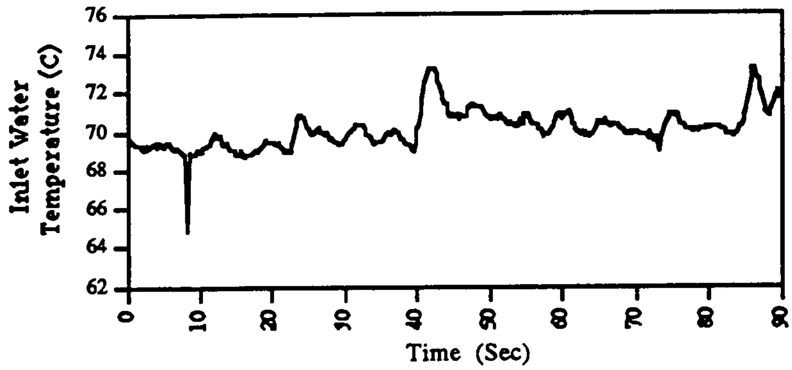

(e)

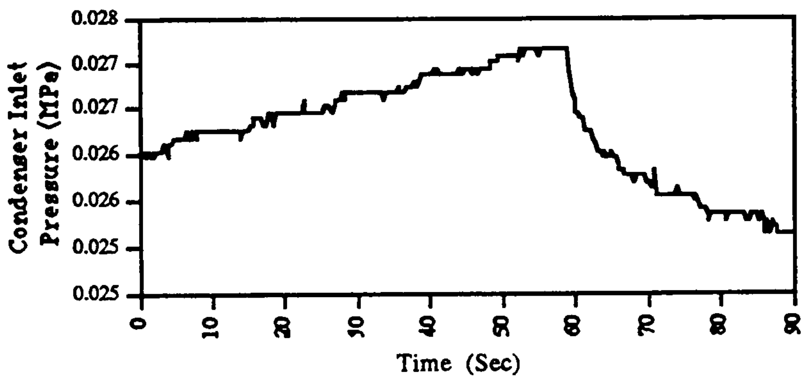

(f)

Figure 5.11: (Continued)

Figure 5.11.d whose trend resembles that of the vapor pressure. The inlet water temperature (Figure 5.11.e), still in the subcooled region, decreases slightly during the transient. In addition, the water temperature exhibits small fluctuations about its mean. Next, Figure 5.11.f shows the behavior of the inlet condenser pressure, which decreases due to the stoppage of the vapor inflow.

The coupling between the heater power and the channel thermalhydraulic behavior via void-reactivity feedback has changed the system response during the pressure transient. By closing the manual valve, the system pressure increases. This is shown in Figures 5.12.a and 5.12.e, which represent the vapor pressure and inlet water pressures, respectively. This pressure increase causes the channel average void fraction to decrease, as shown in Figure 5.12.c. As a result, the heater power increases because of the negative reactivity feedback loop. This induces a further increase in the pressure rate, which leads to a pressure excursion. Figure 5.12.f shows the behavior of the inlet water temperature, which decreases during the pressure transient. The inlet water temperature fluctuates during the steady state condition due to incomplete fluid mixing in the lower plenum

5.7.3 Effect of Varying the Coefficient of Reactivity Feedback

The effect of varying the void reactivity feedback coefficient on the system behavior is evaluated in this section. This study includes

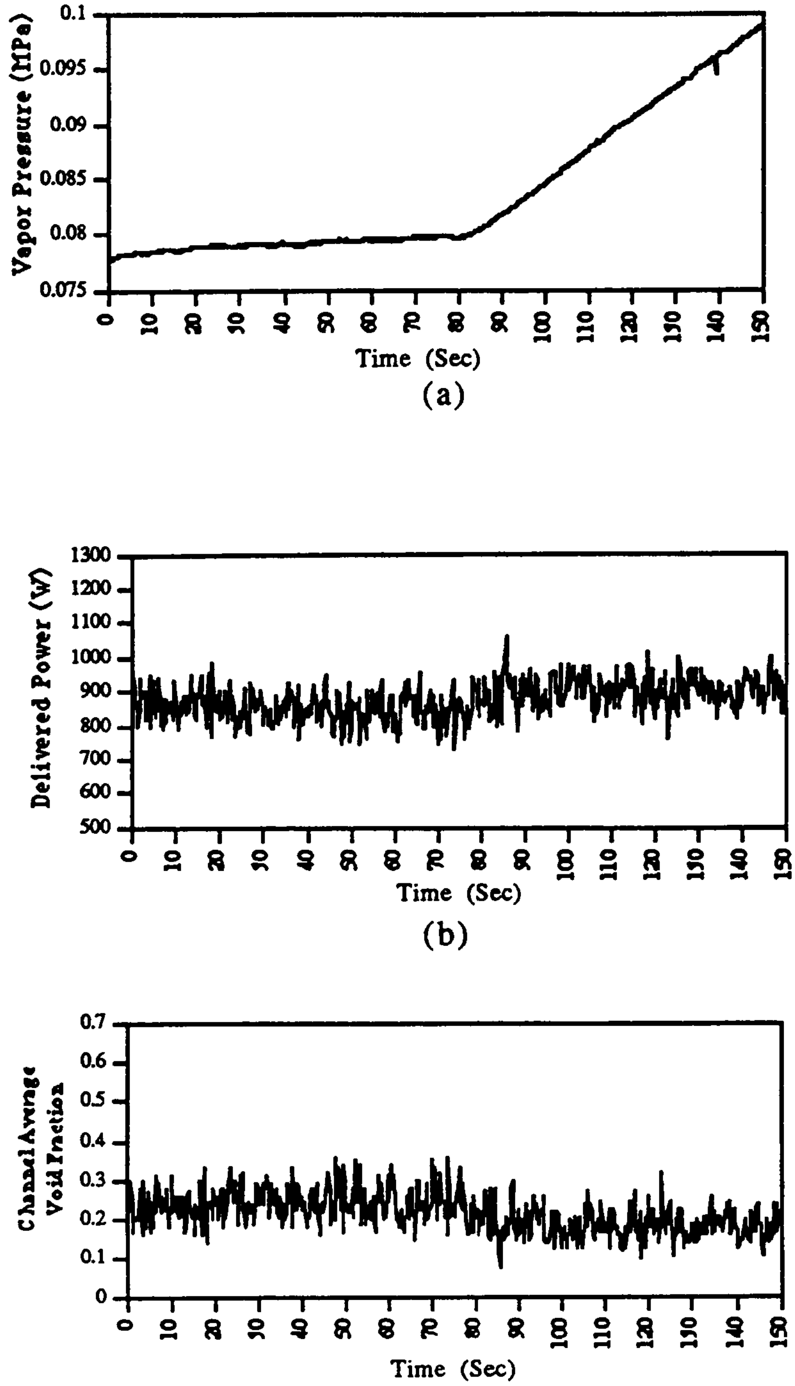

(a)

(b)

(c)

Figure 5.12: Effect of Void Reactivity Feedback on the System Response during a pressure Transient: (a) Vapor Pressure; (b) Power Level; (c) Average Void Fraction; (d) Vapor Temperature (e) Inlet Water Pressure; (f) Inlet Water Temperature.

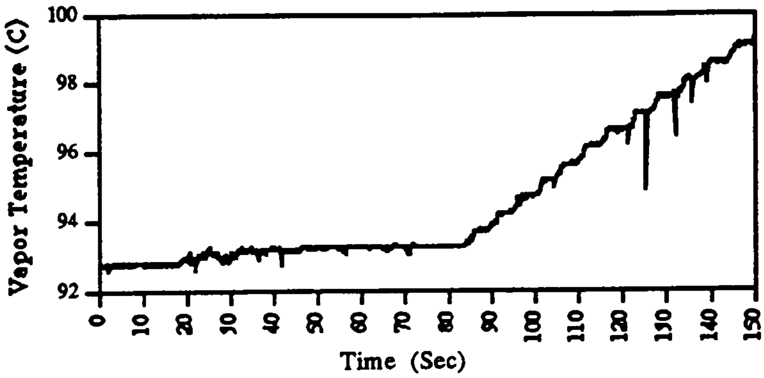

(d)

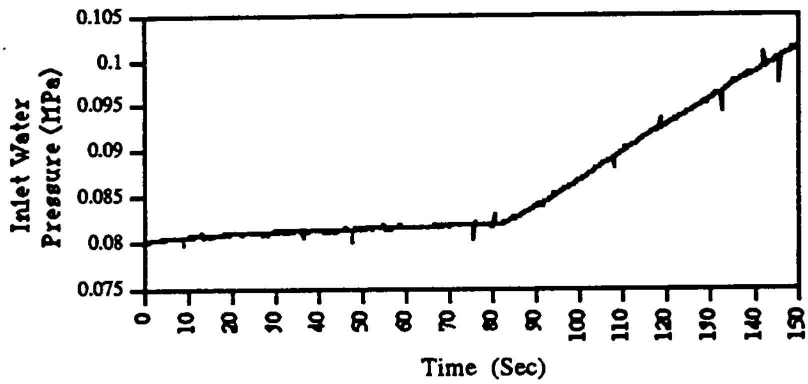

(e)

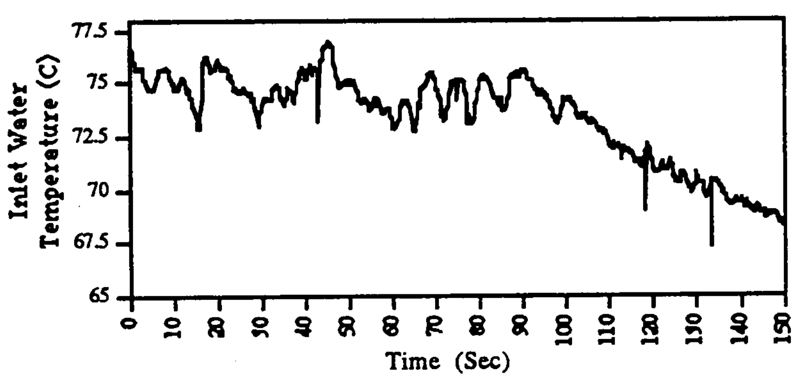

(f)

Figure 5.12: (Continued)

the transient and steady state conditions. As mentioned earlier, the void coefficient of reactivity, α_v, can be varied in the Sub-Vi program, called Void Reactivity. The main features of the effect of void reactivity feedback can be investigated by performing several experiments during steady state and transient conditions with different void coefficients of reactivity. The transient experiments are performed using pressure step increases by closing the manual valve. The void coefficients of reactivity, varied in these experiments, from: -0.01, -10.0, -100 and -1000. For the steady state condition the procedures of section 5.6 are followed.

5.7.3.1 Transient Response

For α_v=-0.01, the system response to a pressure transient is shown in Figure 5.13, which presents the time history of the vapor pressure, delivered power and channel average void fraction, respectively. The system power and channel average void fraction follow a first order behavior during the transition from steady state to transient. the power amplitude is relatively small. The increase of the void reactivity coefficient to -10.0 increases the amplitude of the power fluctuations, as seen in Figure 5.14. For α_v=-100.0, the power is more sensitive to the fluctuation of the void fraction, especially during the transient, as shown in Figure 5.15. Next, for α_v=-1000.00, the amplitude of the power varies greatly for small changes in the void fraction as shown in Figure 5.16.

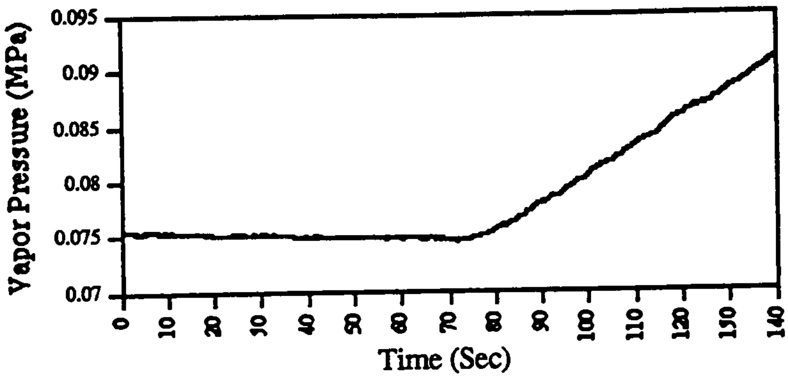

(a)

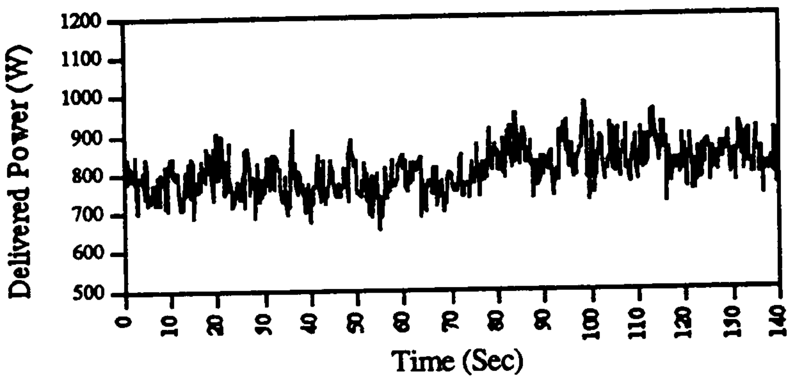

(b)

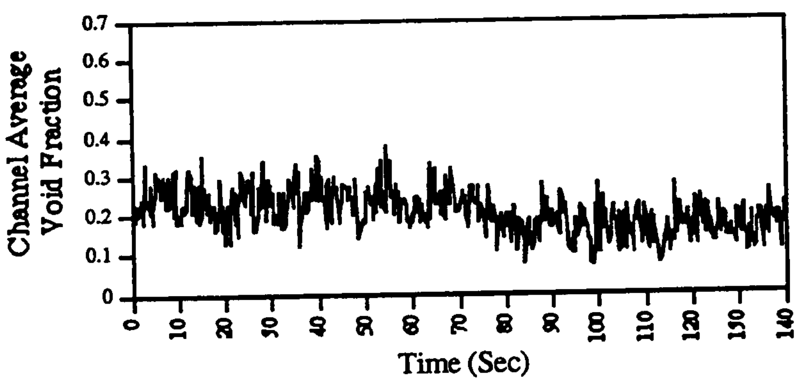

(c)

Figure 5.13: System Response For a Pressure Transient for α_v=-0.01 (a) Vapor Pressure; (b) Power Level; (c) Channel Average Void Fraction.

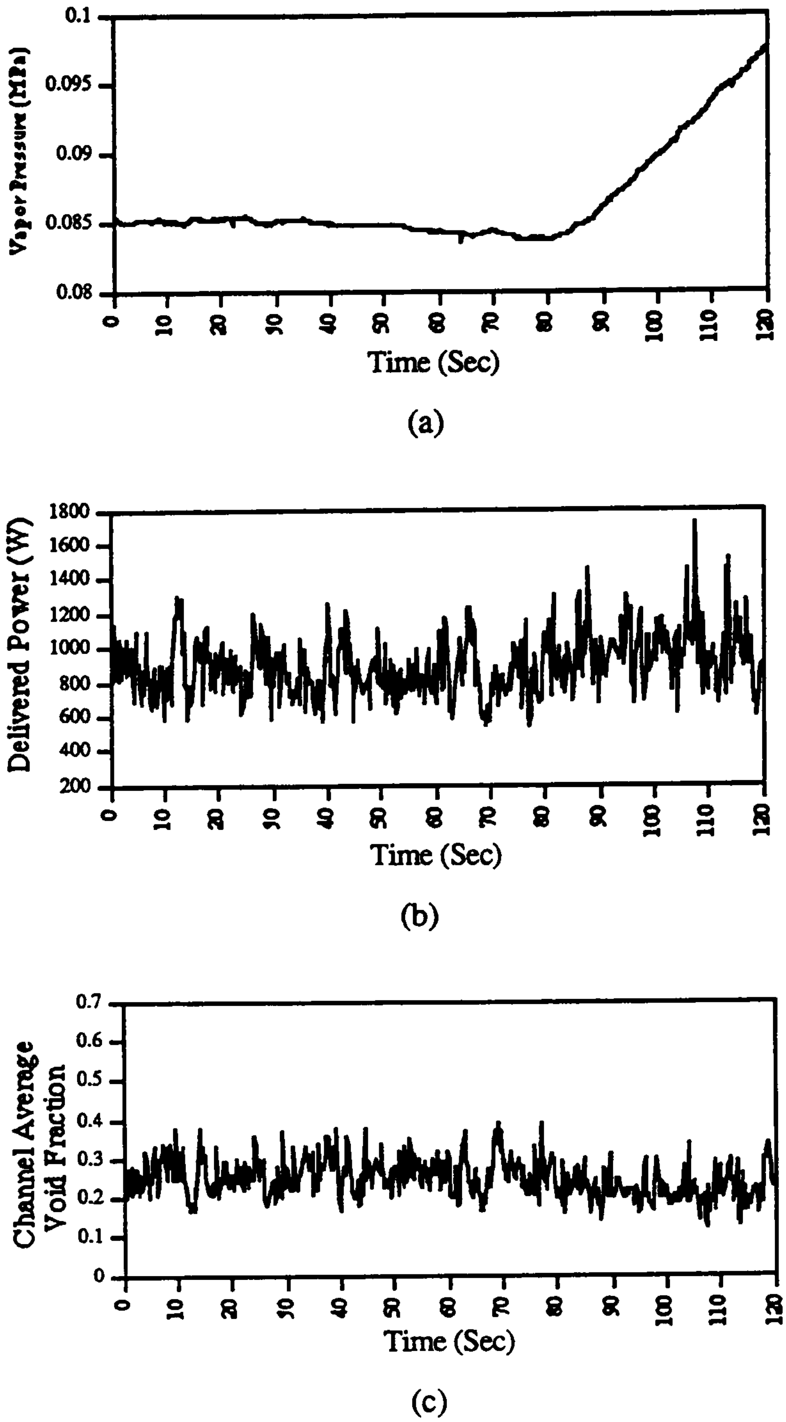

Figure 5.14:System Response For a Pressure Transient for α_v=-10.0 (a) Vapor Pressure; (b) Power Level; (c) Channel Average Void Fraction.

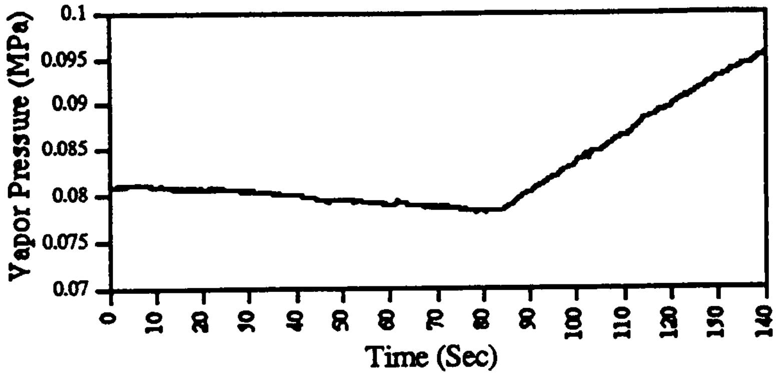

(a)

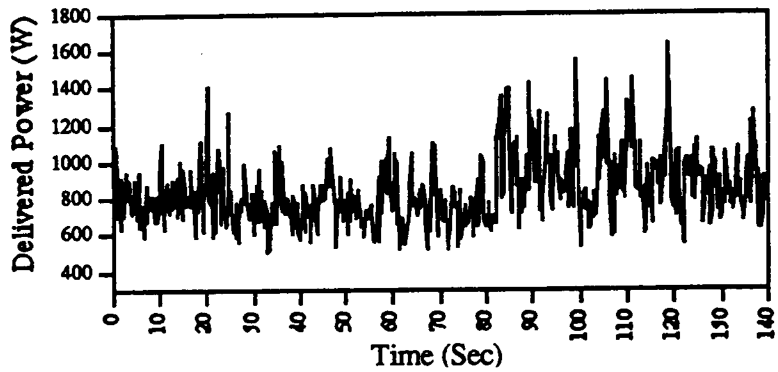

(b)

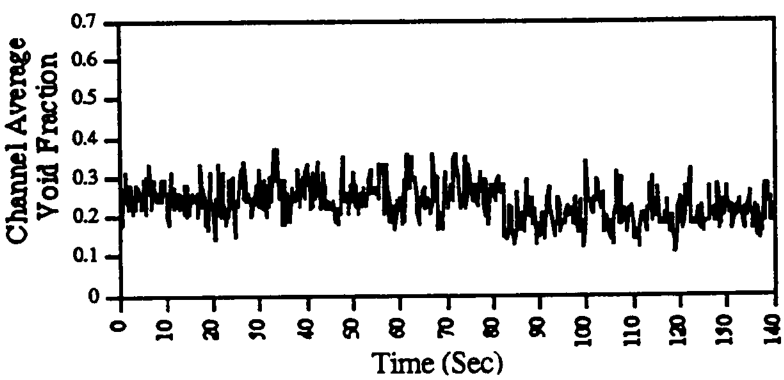

(c)

Figure 5.15: System Response For a Pressure Transient for α_v=-100.0: (a) Vapor Pressure; (b) Power Level; (c) Channel Average Void Fraction.

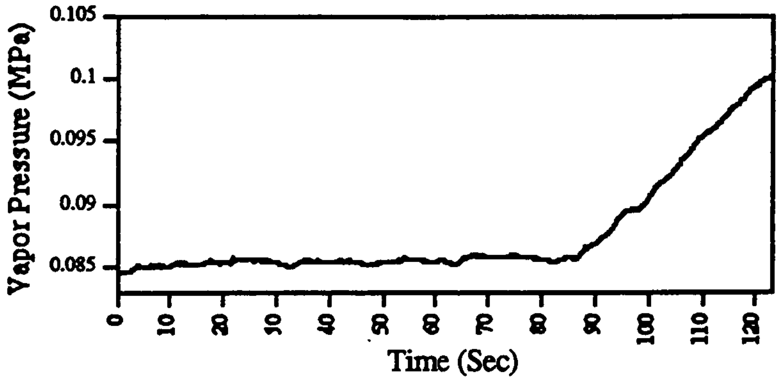

(a)

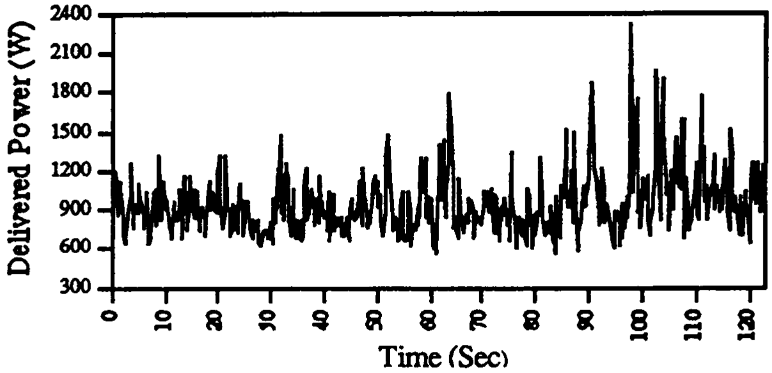

(b)

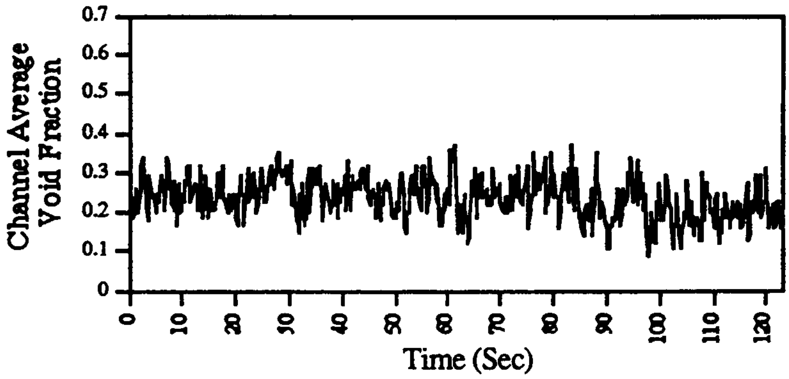

(c)

Figure 5.16: System Response For a Pressure Transient for α_v=-1000.0 (a) Vapor Pressure; (b) Power Level; (c) Channel Average Void Fraction.

The effect of void reactivity feedback is seen as a variation of the sensitivity of the power toward the void fraction fluctuation. For high negative void reactivity coefficients the power has very high fluctuating amplitudes. However, this variation does not induce any significant global temporal oscillation in the system parameters such as pressure or temperature.

5.7.3.2 Steady State Analysis

The objective of this section is to identify the power coupling effect on the system behavior. This is determined by comparing the system behavior at steady state conditions with and without void reactivity feedback.

The Scaled Boiling Water Reactor is brought to a steady state condition and data are collected in two different cases by operating the channel as a simple heated channel and with a closed feedback loop between the power and void fraction. The void reactivity coefficient is varied in order to investigate the system behavior at different reactivity coefficients, which include: -0.1, -10.0, -100.0, -1000.0, respectively.

For a simple heated channel, the steady state operation of the Scaled Boiling Water Reactor is shown in Figure 5.17. The vapor pressure and temperature exhibits some small fluctuations, as can be seen in Figures 5.17.a and 5.17.b, respectively. The channel average void fraction is presented in Figure 5.17.c, which shows the

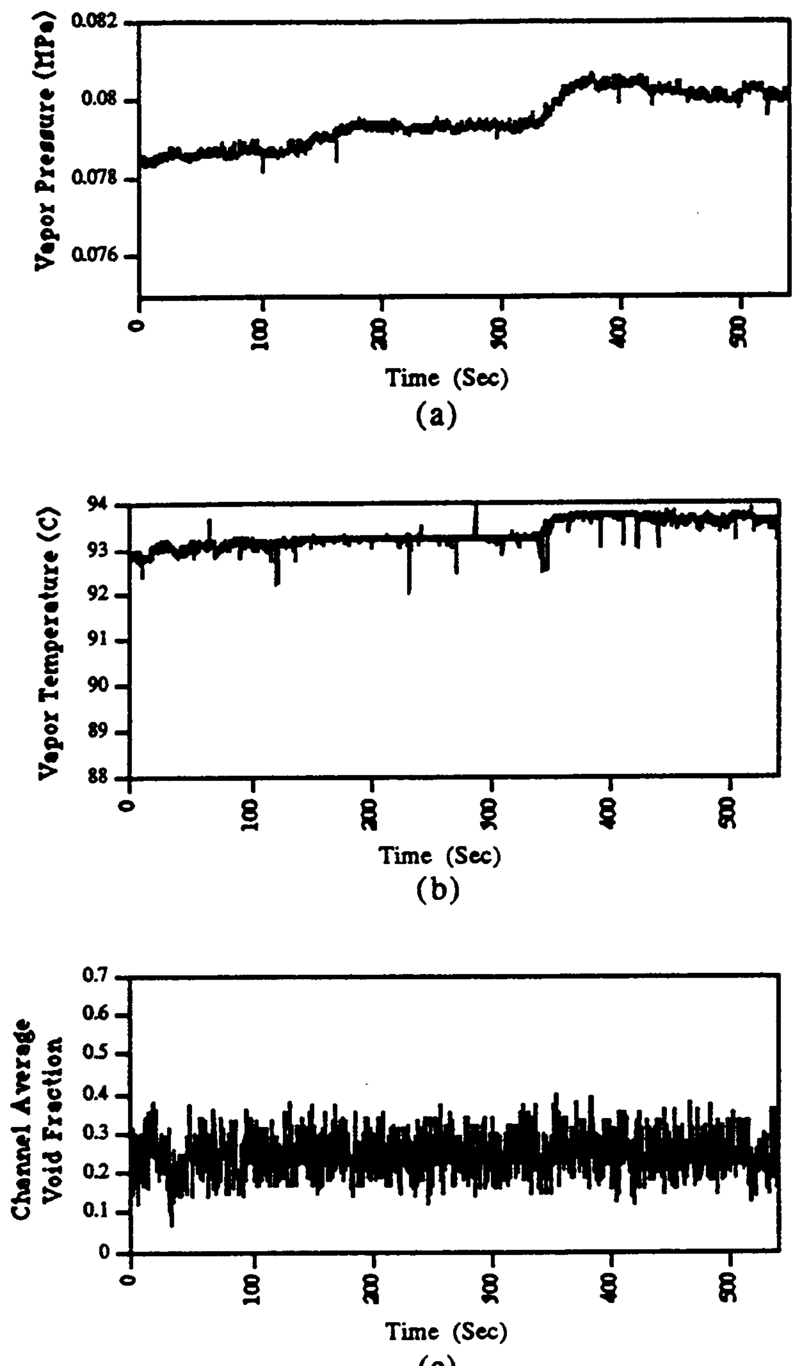

Figure 5.17: Steady State Operation of the Simple Heated Channel: (a) Vapor Pressure; (b) Vapor Temperature; (c) Average Void Fraction; (d) Inlet Core Pressure; (e) Inlet Water Temperature; (f) Inlet Condenser Temperature.

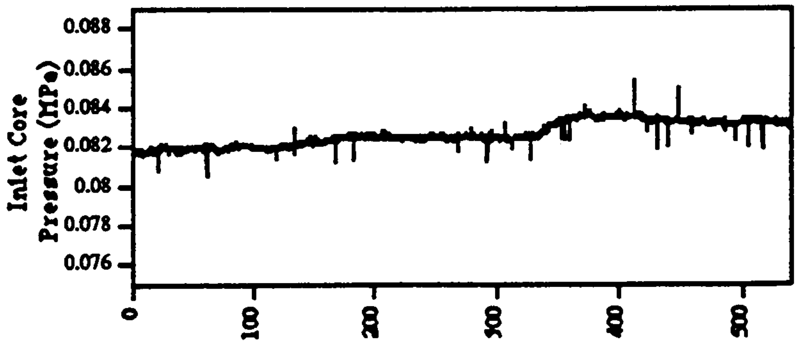

(d)

(e)

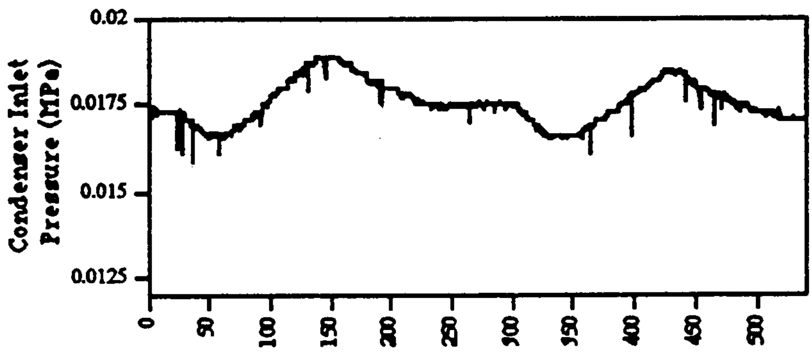

(f)

Figure 5.17: (Continued)

fluctuating nature of the void in the boiling water channel. Next, the inlet water pressure is shown in Figure 5.17.d, and it represents the same trend as that of the vapor pressure. The inlet water temperature, shown in Figure 5.17.e, is slightly decreasing.

By implementing the void reactivity feedback, the operation of the Scaled Boiling Water Reactor Model depends mainly on the coefficient of reactivity used in the power kinetic equation. The use of a small coefficient of reactivity makes the range of the power fluctuation small. On the other hand, for a large negative coefficient of reactivity (e.g., α_v=-1000.0) the delivered power fluctuates with large amplitudes. Figure 5.18 shows the frequency response of the channel average void fraction at different void reactivity coefficients. This figure indicates that there is a frequency peak in the range of 0.1 and 0.14Hz, which appears only when void reactivity is incorporated and enhanced by high values of reactivity. This is consistent with the heater response time which is in the range of 8 to 1 sec.

In the present study flow oscillations were not observed in the simple heated channel nor in the channel with void reactivity feedback. In the case of the simple heated channel, the system was observed to be very stable at low pressure and the system behaves in a first order fashion during transients, as shown in this chapter. The system is characterized by the flow reversal and chugging, typical of low pressure flows. The shortness of the test section has prevents observation of density wave oscillations. In the case of the

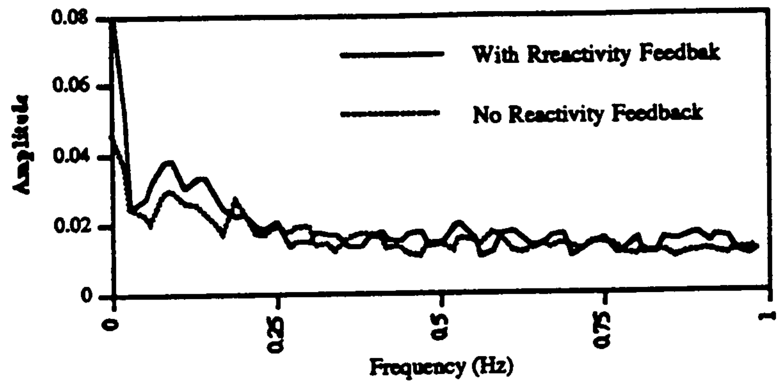

(a)

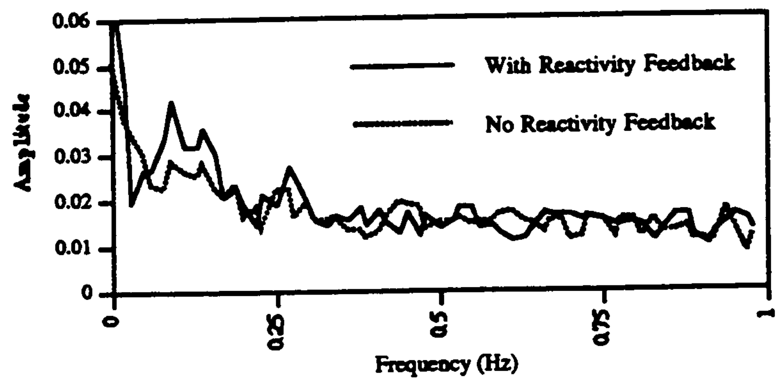

(b)

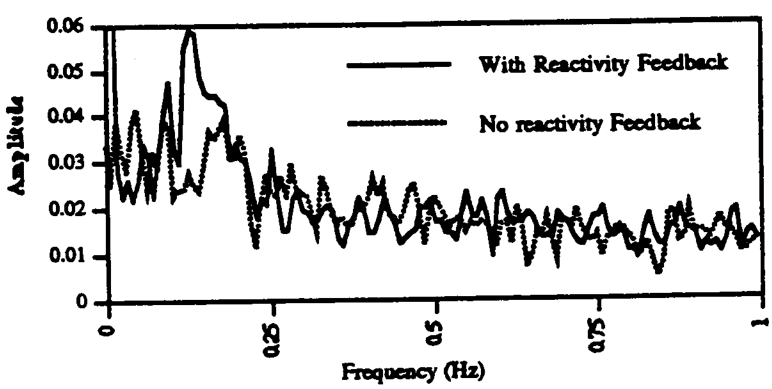

(c)

Figure 5.18: Effect of Void Reactivity Feedback on the System Response for : (a) Reactivity Coefficient of -10; (b) Reactivity Coefficient of -100; (c) Reactivity Coefficient of -1000.

heated channel with void reactivity feedback, the increase of the void reactivity coefficient has increased the sensitivity of the power toward the variation in the void fraction. However, the slow response of the heater has prevented the appearance of flow instability such as thermal instability. Therefore, the existing heaters must be replaced with those of faster response if flow instability is to be observed and studied.

CHAPTER 6

CONCLUSIONS AND RECOMMENDATIONS FOR FUTURE WORK

6.1 Summary and Conclusions

The objective of this research is to investigate the effect of the void reactivity feedback on the dynamic behavior of the Scaled Model Boiling Water Reactor. A void fraction sensor is designed, constructed and installed in the boiling water channel to facilitate this task.

The calibration curve of the void sensor is compared with Maxwell's theoretical curve. For low void fraction (bubbly regime), the experimental data correlates well with the Maxwellian curve as expected. Agreement with the Maxwell curve persists to void fraction of 20%. As the void fraction increases in the channel, the calibration curve deviates from the Maxwell curve due to the transition from bubbly to churn flow regimes. The effect of the initial water conductivity on the void fraction measurement is established and a method for *in-situ* compensation for changing liquid conductivity is implemented.

The void fraction is analyzed in order to determine the flow regimes using the probability density function distribution, the power spectral density and the High Frequency Contribution Fraction (HFCF), which was recently developed by Wong et al. In addition, the high speed camera along with visual observation is employed to correlate flow behavior. The Scaled Model Boiling Water Reactor Model exhibits bubbly and churn regimes in the heated channel. By using the PDF technique the bubbly regime is characterized by a sharp peak with a narrow band at low void fraction. As the void fraction increases the PDF starts to widen and shifts to the left. The PDF analyses give us an opportunity to see how the transition occurs from the bubbly to the churn regime. The slug regime is also identified in an air water system in order to further investigate the sensor performance. The PDF of the slug regime is characterized by double humped-peaks, which indicates that the slug regime is a combination of the bubbly regime and the annular regime. Furthermore, the High Frequency Contribution Fraction (HFCF) was used to characterize the flow regimes. For bubbly regime the HFCF was found to be higher than 0.30, whereas the HFCF for the churn flow was found to be between 0.25 and 0.30. Next, the use of the power spectral density of the void fraction signal shows that there is a difference in the spectrum shape between the bubbly regime with low velocity and the churn regime. This distinction becomes more difficult as the bubbles increase their convected velocity and size.

The void fraction is also analyzed to determine the vapor velocity in the heated channel. This analysis is performed by analyzing signals from adjacent probes using the cross correlation function and the cross power spectral density. In this study the vapor velocity was found to vary between 0.7 and 1.3 m/sec along the boiling water channel. The cross correlation function indicates the flow reversal by the presence of two delay times in the cross correlation curve. The cross phase curve also shows the flow reversal by the sudden change in the phase angle slope.

The dynamic response of the Scaled Model Boiling Water Reactor with void reactivity feedback is investigated. The average channel void fraction is measured and coupled with the heater power using the prompt jump approximation of the power kinetics. The system response was studied during transient cases and steady state. For a step power increase the system pressure, temperature and void fraction increase; however, the negative reactivity coefficient acts to decrease the power. This feedback continues until the system reaches a stable condition. System steam flow decrease transients cause the void fraction to decrease which increases the power.

The increase in the void reactivity coefficient increases the sensitivity of the power to the void fluctuation. This sensitivity may create instability in the system behavior; however, the slow response of the heater has prevented such instability. The frequency analysis has shown that the heater response time is between 8 and 10 Sec.

6.2 Recommendations for Future Work

The installation of the void fraction sensor has provided useful information on the behavior of the two-phase flow characteristics in the boiling channel. In this study the analysis of the void fraction was limited to the determination of the flow regimes and the vapor velocity. However, the void fraction signal can be further explored in order to determine other two-phase flow characteristics such as bubble size and void wave propagation characteristics. Therefore, it is recommended to use more sophisticated techniques such as the Wavelet transform in order to explore and better analyze the void fraction signal. The chaotic behavior of the void fraction signal was clearly shown in the power spectral density. This feature should be further studied using fractal analysis, which will give insight into the system behavior.

REFERENCES

1. M. Z. Podowski, "Instabilities in Two-Phase Systems", Modern Developments and Advances in Boiling Heat Transfer, Elsevier Science Publisher, pp 271-316, 1992

2. J.H. Kim, and John Stringer, "Applied chaos", John Wiley & sons, Inc, 1992

3. Rizwan-uddin and Dorning J. J., "Nonlinear Dynamics of Nuclear Coupled Density-Wave Oscillations", Tran. Am. Nucl. Soc. Vol 59, pp 165-166, 1986

4. S. Kakac and T. N. Vezoruglu, "A Review of Two Phase Flow Instabilities",

5. M. M., Padki , K. Palmer, S. Kakac and T. N. Veziroglu " Bifurcation Analysis of Pressure-Drop Oscillations and the Ledinegg Instability", Nuclear science and Engineering, Vol 32, PP 525-531, 1991.

6. K. Whitfield and R. P. Roy, "Boiling Flow Through a Rod-Bundle Channel: Steady States and Dynamic Instabilities", Int. J. Heat Mass Transfer, Vol 38, No 8, pp 1409-1425, 1995.

7. T. H. J. J. Van Der Hagen, "Stability Monitoring of a Natural-Circulated-Cooled Boiling Water Reactor", Ph.D. Dissertation, Proefschrift Delft.- Met lit. opg., 1989.

8. Rizwan-uddin and Dorning, J. J., "The Nonlinear Dynamics of Two-Phase Flow in a Simple Heated loop", Chem. Engr. Comm. Vol 87, pp 1-19, 1990

9. J. March-Leuba, "Dynamic Behavior of Boiling Water reactor", Ph.D., Dissertation, University of Tennessee, Knoxville, December 1984

10. B. G. Bergdahl, F. Reisch, R. Oguma, J. Lorenzen and F. Akerhielm, "BWR Stability Investigation at Forsmark 1", Am. Nucl. Energy, Vol 16, No 10, pp 509-520, 1989.

11. G. F. Hewitt, "Measurement of Two Phase Flow Parameters", Academic Press, 47-128, 1978

12. J. C. Micaelli, "Propagation D' Ondes Dans les Ecoulements Diphasique a Bulles a deux Constituants. Etudes Theorique et Experimentale", Dissertation Thesis USMG-INPG, December 1982

13. A. Tournaire, "Detection et Etudes des Ondes de Taux de Vide en Ecoulement Diphasique A Bulles Jusqua' a la Tranmsition Bulles-Bouchons", Dissertation Thesis , L' Institut National Ploytechnique de Grenoble, March 1987

14. H. V. Kok, "Capacitive Measurement Technique for Void Fraction Measurement in a Rod Bundle Geometry", Graduation Report, Interfacultair Reactor Instituut, 1993.

15. W. C. Hereens, "Application of Capacitance Techniques in Sensor Design", Journal. Phys. E: Sci.Instrum, Vol 19, 897-906, 1986.

16. A. E. Ruggles, D. Kenna, K. Meftah and U. Mertuyurek, "A Conceptual Design for the Scaled Model Boiling Water Reactor", Departmental Report, University of Tennessee, 1994.

17. D. Kenna, "Boiling Water Reactor Model- Engineering Design, analysis and Construction", Master Thesis, University of Tennessee of Knoxville, 1996

18. LAB-VIEW Manual, National Instruments, 1994

19. G. F. Hewitt, "Measurement of Void Fraction" Handbook of Multiphase Systems, McGraw Hill, 1982.

20. M. Merillo, R. L. Dechene, and W. M. Cichowlas, "Void Fraction Measurement With a Rotating Electric Field Conductance Gauge", Transactions of the ASME Journal of Heat Transfer, Vol 99, pp 330-332, 1977.

21. Conductivity Measurement Manual, Fisher-Rosemount Co., 1994

22. L. Cimorelli, A. Premoli, "Measurement of Void Fraction with Impedance Gauge Technique", Energia Nucleare, Vol 13, pp 12-23, 1966.

23. J. C. Maxwell, "A Treatise on Electricity And Magentism", Claredon Press Oxford (1881).

24. D. A. G. Burgeman, "Berechnung Verschnung Physikalischer Konstaten von Heteregonen Substanzen", Annal Physics, Leipzig, Vol-24, P 636, 1935.

25. D. J. Jeffery, Proc R. Soc. Lon. A335-355, 1965.

26. R. Cimorelli and R. Evangelisti, "The Application of he Capacitance Method for Void Fraction Measurement in Bulk Boiling Conditions", Journal of Heat Transfer, Vol 10. pp 277-288, 1966.

27. Power Control Concepts Manual, Power Concepts, 1994

28. J. S. Bendat and A. G. Piersol, "Random Data, Analysis and Measurement Procedures", Wiley-Interscience, New York, 1971

29. J. S. Bendat and A. G. Piersol, "Engineering Application of Correlation and Spectral analysis", Wiley-Interscience, New York, 1980.

30. B. R. Upadhyaya, "Experimental Methods in Reactor dynamics ", Graduate Course, University of Tennessee, 1994.

31. S. Z. Rouhani and M. S. Sohal, "Two-Phase Flow Patterns: a Review of Research Results", Progress in Nuclear Energy, Vol 11, pp 219-260.

32. J. M. Delhaye, M. Giot and M. L. Riethmuller, "Thermohydraullics of Two-Phase Flow Systems for Industrial Design and Nuclear Enigineering", Hemisphere Publishing Corporation, 1981

33. A. E. Duckler and Y. Taitel, "Flow regime transitions for vertical upward gas liquid flow: A preliminary approach through physical modeling," NUREG-0162, progress report No. 1, University of Houston, 1980.

34. O. C. Jones and N. Zuber, "The interrelation Between Void Fraction Fluctuations and Flow Patterns in Two-Phase Flow", International Journal of Multiphase Flow, Vol 3, PP 273-306, 1975

35. Y. W. Wang, B. S. Pei and W. K. Lin, "Verification of Using A Single Void Fraction Sensor to Identify Two-Phase Flow Patterns", Journal of Nuclear Technology, Vol 95, pp 87-95, 1991

36. Y. W. Wang, C. H. King and B. S. Pei, "Identification of Two-Phase Flow Patterns in a Nuclear Reactor by High-Frequency Contribution Fraction", Journal Nuclear Technology, Vol 89, P 217, 1990.

37. B. R. Upadhyaya "Information Processing Techniques" Graduate Course, university of Tennessee, 1996.

38. C. H. King, M. S. Ouyang, B. S. Pei and S. C. Lee, "Identification of Two-Phase Flow Regimes by Neutron Noise Analysis", Nuclear Technology, Vol. 86, pp 70-86, 1989

39. C. H. King, M. S. Ouyang, B. S. Pei and Y. W. Wang, "Identification of Two-Phase Flow Regimes by an Optimum Modeling Method", Nuclear Technology, Vol. 82, pp211-226, 1988

40. GLOBAL, Signal Processing Tool Box.

41. M. A. Vince and R. T. J. Lahey, "Flow Regime Identification and Void Fraction Measurement Techniques in Two-Phase Flow", NUREG/CR-1692, Rensselaer Polytechnique Institute, 1980

42. R. C. Hilborn, "Chaos and Nonlinear Dynamics", Oxford University Press, 1994

43. Y. Mi, L. H. Tsoukalas, M. Ishii, M. Li, and Z. Xiao, "Hybrid Fuzzy-Neural Flow Identification Methodology", Fifth IEEE International Conference on Fuzzy Systems, PP 1332-1338, 1996.

44. R. Collins, F. De Moras, J. F. Davidson and D. Harrison, "The Motion of a Large Gas Bubble Rising Through Liquid Flowing in a Tube", Journal of Fluid Mechanics, Vol 89, p. 497

45. R. C. Fernandes, R. Semiat, A. E. Dukler, "A Hydrodynamic Model for Gas Liquid Slug Flow in Vertical Tubes", AICHE J., Vol. 29, p. 981.

46. System Manual General Electric Technology, Nuclear Regulatory Commission, Vol 1, pp 1.7_3 - 1.7_7.

47. N. E. Todreas and M. S. Kazimi, "Nuclear system I: Thermal Hydraulic Fundamentals", Hemisphere Publishing Corporation, 1990

48. J. M. Delhaye, M. Giot and M. L. Riethmuller, "Thermohydraullics of Two-Phase Systems for Industrial Design and Nuclear Engineering", Hemisphere Publishing Corporation, 1981

49. J. J. Duderstadt and L. J. Hamilton, "Nuclear Reactor Analysis", John Wiley & Sons, Inc. 1976.

VITA

Khaled Meftah was born in Kairouan, Tunisia on April 17, 1966. He Graduated from Al-Mansoura High School in June 1986. Meftah was awarded a scholarship from the Tunisian Government to study in the U. S. He entered the University of Tennessee, Knoxville in the Spring of 1987. He received his bachelors degree in Mechanical Engineering with high honors in August of 1990. He continued his study at the University of Tennessee, Knoxville where he received his Master of Science in Mechanical Engineering in May of 1992 and a Ph. D. in Nuclear Engineering in May, 1997.